

Initiated Chemical Vapor Deposition of Polymeric Thin Films: Mechanism and Applications

by

Kelvin Chan

M.S. in Chemical Engineering Practice
Massachusetts Institute of Technology, 2003

B.S.E. in Chemical Engineering
The University of Michigan, Ann Arbor, 2000

Submitted to the Department of Chemical Engineering
in Partial Fulfillment of the Requirements for the Degree of

DOCTOR OF PHILOSOPHY IN CHEMICAL ENGINEERING
AT THE
MASSACHUSETTS INSTITUTE OF TECHNOLOGY

August 2005

[September 2005]

©2005 Massachusetts Institute of Technology. All Rights Reserved.

Signature of Author.....*[Handwritten Signature]*.....

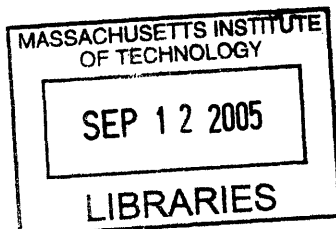
Department of Chemical Engineering
August 18, 2005

Certified by*[Handwritten Signature]*.....

Karen K. Gleason
Professor of Chemical Engineering
Thesis Supervisor

Accepted by.....*[Handwritten Signature]*.....

Daniel Blankschtein
Professor of Chemical Engineering
Chairman, Committee for Graduate Students



ARCHIVES

Initiated Chemical Vapor Deposition of Polymeric Thin Films: Mechanism and Applications

By

Kelvin Chan

Submitted to the Department of Chemical Engineering
on the 18th of August, 2005, in Partial Fulfillment of the
Requirements for the Degree of
Doctor of Philosophy in Chemical Engineering

ABSTRACT

Initiated chemical vapor deposition (iCVD) is a novel technique for depositing polymeric thin films. It is able to deposit thin films of application-specific polymers in one step without using any solvents. Its uniqueness of *in situ* surface polymer synthesis distinguishes iCVD from conventional processes such as spin-on deposition and plasma-enhanced chemical vapor deposition. It allows engineering polymers to be made with specific microscale properties translating to well-defined macroscale behaviors. In this thesis work, two application-specific polymers based on poly(2-hydroxyethyl methacrylate) (PHEMA) and poly(cyclohexyl methacrylate) (PCHMA) were synthesized using iCVD. PHEMA thin films with specific degrees of cross-linking leading to well-defined structural, thermal, wetting, and swelling properties were made in a single vacuum step by simply adjusting chamber conditions. Cross-linked PCHMA thin films were synthesized for use as sacrificial layers for microfabrication. Such films of engineering polymers cannot be made using conventional methods. A study of the polymerization mechanism was included to serve as a groundwork for increased understanding of iCVD as a thin-film deposition method. Growth rates and molecular weights, crucial parameters for polymeric thin films, were found to be highly dependent on the surface concentrations of monomers, leading to the conclusion that polymer formation occurs predominantly on the surface of the substrate. This conclusion also infers that controlling the surface concentrations of monomers can lead to copolymers/terpolymers with well-defined compositions, which was demonstrated in the iCVD of PHEMA-based thin films. iCVD therefore can be extended to

complex polymer systems with multiple monomeric building blocks. Photo-initiated chemical vapor deposition (piCVD) using a volatile photoinitiator is introduced for the first time in this thesis. piCVD possesses all the benefits of iCVD over conventional processes but uses a photochemical initiation mechanism that simplifies chamber design and potentially allows self-patterning during deposition.

Thesis Supervisor: Karen K. Gleason

Title: Professor of Chemical Engineering

Dedicated to the memory of

my grandmother

and

my father

Acknowledgments

First I need to thank Karen for giving me a chance to work in her lab and for being so patient. She has given me the greatest amount of freedom and allowed me to explore with few boundaries. Thanks for believing in me, Karen! I appreciate every bit of your guidance and confidence in me throughout these few years.

Special thanks to Professors Paula Hammond and Herb Sawin for serving on my committee and for the helpful discussions and ideas.

My friends in the Gleason Lab have also provided much support and, most importantly, fun. I thank Leslie for showing me around in my first year and Ken, who knows pretty much everything, for all the technical assistance. I am glad to have known Tom, who would never hesitate to provide help when I needed it. I thank Jessie for assuring me everything would work out. I also thank Tyler, who never hesitates to discuss with me my research and introduced me to the world of tennis, and Shannan, whose attitudes toward life and work have taught me great lessons. I am especially grateful to have known John and April, who were great companions through some of my toughest times in the journey that appeared to be neverending. I thank John for all the good times in the Muddy and for introducing me to many new things and people. I thank April for becoming an excellent Big-2 player, for being a late-night lab buddy on many occasions, and for all the late rides home. Through preaching the gospel of Big 2 to the Gleason Lab, I too have refined my skills. Thanks!

I thank Theresa for sticking with me, a graduate student who at times loses his mind and cannot be reasoned with, even though sometimes it really does not justify doing so.

It took almost 28 years for me to come to this point. There have been many good times and bad times. Some bad times were so bad that even I gave up on myself, but one or more of the following people picked me up every single time. All of them made decisions and took actions to help me become what I am. It is because of them that I am able to make the most out of myself. I deeply regret that I did not take the chance to thank my grandmother, who received no formal education at all, for repeatedly reminding me the importance of learning. I also thank my parents, who have supported me both spiritually and financially throughout all these years. I am most indebted to mom, who never ever foregoes any opportunity to better my life. I thank my sister for being such a great friend and for all the love.

And finally, yes, I did it, father. I finally did something that you really wanted me to do. Now you have one fewer thing to worry about and can leave all the worrying to me. I will take care of things from now on.

TABLE OF CONTENTS

Abstract	2
Dedication	4
Acknowledgments	5
List of Figures	9
List of Tables	14
List of Abbreviations, Acronyms, and Symbols	15

CHAPTER ONE _____ 17

Introduction

1.1	Background	18
1.2	Chemical Vapor Deposition	19
1.3	Initiated Chemical Vapor Deposition	23
1.4	Scope of Thesis	23
	References	26

CHAPTER TWO _____ 29

Initiated Chemical Vapor Deposition of Linear and Cross-linked Poly(2-hydroxyethyl methacrylate) for Use as Thin-Film Hydrogels

	Abstract	30
2.1	Introduction	32
2.2	Experimental Methods	36
2.3	iCVD of Poly(2-hydroxyethyl methacrylate) Homopolymer	40
	2.3.1 Fourier-Transform Infrared Spectroscopy	40
	2.3.2 X-Ray Photoelectron Spectroscopy	41
	2.3.3 Deposition Rate	42
2.4	iCVD of Cross-linked Poly(2-hydroxyethyl methacrylate)	45
	2.4.1 Fourier-Transform Infrared Spectroscopy	45
	2.4.2 X-Ray Photoelectron Spectroscopy	47
	2.4.3 Thermal Properties	50
	2.4.4 Contact-Angle Measurements	53
	2.4.5 Degree of Swelling and Water Content	56
2.5	Conclusions	58
	References	61

CHAPTER THREE _____ **65**

Air-Gap Fabrication Using a Sacrificial Polymeric Thin Film Synthesized via Initiated Chemical Vapor Deposition

	Abstract	66
3.1	Introduction	67
3.2	Experimental Methods	71
3.3	iCVD Polymer Film Properties	76
3.4	Single-Level Air-Gap Fabrication	81
3.5	Conclusions	84
	References	86

CHAPTER FOUR _____ **89**

A Mechanistic Study of Initiated Chemical Vapor Deposition: Analyses of Deposition Rate and Molecular Weight

	Abstract	90
4.1	Introduction	91
4.2	Experimental Methods	93
	4.2.1 iCVD Experiments	93
	4.2.2 Quartz-Crystal Microbalance Measurements	96
4.3	Results and Discussion	98
	4.3.1 Effects of Surface Temperature on Dep. Rate and Molecular Weight	98
	4.3.2 Modeling iCVD Polymerization	103
	4.3.3 Effects of Monomer Partial Pressure on Dep. Rate and Mol. Weight	107
4.4	Conclusions	110
	References	111

CHAPTER FIVE _____ **112**

Photo-Initiated Chemical Vapor Deposition of Polymeric Thin Films Using a Volatile Photoinitiator

	Abstract	113
5.1	Introduction	115
5.2	Experimental Methods	118
5.3	Results and Discussion	122
	5.3.1 Fourier-Transform Infrared Spectroscopy	122
	5.3.2 X-Ray Photoelectron Spectroscopy	124
	5.3.3 Molecular-Weight Control	125
	5.3.4 Rate Enhancement due to Initiator	128
	5.3.5 Comparison between piCVD and iCVD	131

5.4	Conclusions	134
	References	137

CHAPTER SIX _____ **139**

Initiated Chemical Vapor Deposition of Poly(methyl methacrylate) Thin Films

	Abstract	140
6.1	Introduction	141
6.2	Experimental Methods	144
6.3	Results and Discussion	145
	6.3.1 X-Ray Photoelectron Spectroscopy	146
	6.3.2 Fourier-Transform Infrared Spectroscopy	150
	6.3.3 Proton Nuclear Magnetic Resonance Spectroscopy	154
6.4	Conclusions	156
	References	159

CHAPTER SEVEN _____ **162**

Conclusions and Future Directions

7.1	Conclusions	163
7.2	Future Directions	164

List of Figures

CHAPTER ONE

Figure 1-1: Schematic of CVD Chamber.

Figure 1-2: Hot-Filament CVD Chamber.

CHAPTER TWO

Figure 2-1: Precursor species being introduced into the vacuum chamber. HEMA is the monomer, EGDA is the cross-linking agent, and TBPO is the initiator.

Figure 2-2: FTIR absorbance spectra of (a) PHEMA film synthesized from iCVD (Sample L3) and (b) spin-cast PHEMA standard obtained from Aldrich. The wide band centered at $\sim 3450\text{ cm}^{-1}$ indicates the retention of hydroxyl groups in the iCVD process. Baseline correction and thickness normalization were the only processing done on these spectra.

Figure 2-3: Deposition rate as a function of partial pressure of HEMA in the chamber. The nonlinearity has two likely origins: multilayer adsorption of HEMA on the surface and primary termination of chains.

Figure 2-4: FTIR hydroxyl (top) and carbonyl stretching (bottom) absorbances normalized for film thickness as a function of the partial pressure of HEMA in the chamber. The hydroxyl intensity decreases and the carbonyl intensity increases with increasing EGDA partial pressure.

Figure 2-5: XPS high resolution scans of (top) the homopolymer film, Sample X1, and (bottom) the most cross-linked film, Sample X5. The intensity of Peak 2 that refers to the O*-H oxygen decreases with increasing degree of cross-linking.

Figure 2-6: EGDA/HEMA ratio in iCVD films as a function of the partial pressure of EGDA in the chamber. More EGDA units are incorporated as the EGDA partial pressure increases.

Figure 2–7: Percent thickness removal and onset temperature of decomposition as functions of EGDA/HEMA ratio in iCVD film.

Figure 2–8: Advancing and receding contact angles as functions of the droplet volume. The film with more incorporation of EGDA has higher advancing and receding angles. The inset picture depicts the receding contact angle of 17° at the end of the advancing/receding cycle (ultimate receding angle) measured on Sample X2.

Figure 2–9: Changes in film thickness and refractive index of swollen film as functions of the EGDA/HEMA ratio in the film.

Figure 2–10: Water content of swollen film as a function of the EGDA/HEMA ratio in the film.

CHAPTER THREE

Figure 3–1: Scheme of using a sacrificial material to make a simple void structure. In the final step, the sacrificial material decomposes to form small molecules capable of diffusing through the top cover layer.

Figure 3–2: Species used in the iCVD synthesis of sacrificial polymer.

Figure 3–3: Fabrication scheme used to make a single-level air-gap prototype. The topography after PECVD is not explicitly represented.

Figure 3–4: Absorbance infrared spectrum of iCVD P(CHMA-co-EGDMA).

Figure 3–5: Details of the unzipping mechanism involving the cross-linker EGDMA. Main-chain scission results in depropagation by release of CHMA units. The cross-linker EGDMA is eventually released when the chains with which it is associated have both unzipped through the point of cross-linking.

Figure 3–6: FTIR spectra of (a) iCVD cross-linked PCHMA, (b) air-gap structure before annealing comprised of PECVD SiO₂ on top of iCVD cross-linked PCHMA, (c) PECVD SiO₂, and (d) air-gap structure after annealing. The absence of the C–H stretching bands (3050–2800

cm⁻¹) and the C=O stretching band (centered at 1726 cm⁻¹) in (d) indicates removal of cross-linked PCHMA during annealing.

Figure 3-7: Cross-sectional scanning electron micrograph depicting the single-level air-gap structure.

CHAPTER FOUR

Figure 4-1: Free-radical polymerization scheme. I_2 = initiator; $I\cdot$ = initiating radical; M = monomer; $IM_x\cdot$ = growing radical chain (where x is any integer).

Figure 4-2: Monomers and initiator used in this work.

Figure 4-3: Equilibrium monomer surface concentration as a function of surface temperature as measured by the quartz-crystal microbalance (QCM). The partial pressure of GMA was fixed at 208 mTorr for the experiment, while that of CHMA was set at 167 mTorr.

Figure 4-4: Deposition rate as a function of substrate temperature. The partial pressure of GMA was fixed at 208 mTorr, while that of CHMA was maintained at 167 mTorr.

Figure 4-5: Number-average molecular weight as a function of substrate temperature. The partial pressures of GMA and CHMA were set at 208 and 167 mTorr, respectively.

Figure 4-6: Plot of deposition rate data from iCVD experiments against equilibrium surface concentration data from QCM measurements. For each of the monomers, the iCVD and the QCM data were collected at the same monomer partial pressure.

Figure 4-7: Plot of number-average molecular weight from GPC measurements on dissolved iCVD polymer films against equilibrium surface concentration data from QCM measurements. The iCVD and the QCM experiments had matching monomer partial pressures.

Figure 4–8: Normalized surface concentration as a function of monomer partial pressure. Both sets of measurements were performed at a crystal temperature of 35 °C.

Figure 4–9: Deposition rate from iCVD experiments as a function of normalized surface concentration from QCM measurements.

Figure 4–10: Number-average molecular weight as a function of monomer partial pressure.

CHAPTER FIVE

Figure 5–1: Schematic of the vacuum chamber (not to scale).

Figure 5–2: FTIR spectra of (a) piCVD PGMA film, (b) iCVD PGMA film, and (c) spin-cast PGMA obtained from Polymer Source. The absorption peaks at 907, 848, and 760 cm^{-1} are assigned to the characteristic absorption bands of the epoxide group.

Figure 5–3: Number-average (M_n) and weight-average (M_w) molecular weights as functions of the monomer-to-initiator ratio. Both increase with increasing M/I ratio.

Figure 5–4: Deposition rate as a function of the lamp power. The increase in rate can be attributed to the increase in the concentration of initiating radicals with increasing lamp power.

Figure 5–5: Postulated free-radical polymerization mechanism in the piCVD process using 2,2'-azobis(2-methylpropane) as the photoinitiator.

Figure 5–6: Number-average and weight-average molecular weights as functions of the lamp power. The numbers in parentheses are the respective polydispersity indices (PDI) of the piCVD PGMA films made at different lamp powers.

CHAPTER SIX

Figure 6–1: XPS survey scans of a) film deposited from 30 sccm MMA and b) film deposited from 9 sccm MMA. The peaks at 531 eV, 402 eV, and 287

eV correspond to O 1s, N 1s, and C 1s photoelectrons, respectively. The ratios between the carbon and the oxygen atoms are 2.52 and 2.71 for Samples a) and b), respectively. The ideal ratio for standard PMMA is 2.50.

Figure 6–2: High-resolution C 1s (left) and O 1s (right) XPS scans of iCVD films. The spectra on the top are from the 30-sccm sample; those on the bottom are from the 9-sccm sample. Peak X in the bottom right spectrum is an unidentified impurity peak.

Figure 6–3: FTIR spectra of a) PMMA standard obtained from Alfa Aesar, b) iCVD film deposited from 30 sccm MMA, and c) iCVD film deposited from 9 sccm MMA.

Figure 6–4: Details of the C–H stretching (left) and the C–H bending (right) regions showing the structural similarity between a) the 30-sccm iCVD sample and b) the standard.

Figure 6–5: NMR spectrum of iCVD PMMA deposited from 30 sccm MMA. The inset details the β -methylene proton region. The peak assignments are based on those from the literature.

List of Tables

CHAPTER TWO

Table 2-1: Details of experimental runs.

Table 2-2: High-resolution XPS scan data of the iCVD PHEMA film (Sample L3). The literature values are from Ref. 50.

Table 2-3: Summary of advancing and ultimate receding angles of sessile contact angle measurements on iCVD films.

CHAPTER FOUR

Table 4-1: Details of iCVD experiments.

CHAPTER FIVE

Table 5-1: Details of experimental runs.

Table 5-2: High-resolution XPS scan data of the piCVD PGMA film.

CHAPTER SIX

Table 6-1: High-resolution XPS scan data of the PMMA film deposited from iCVD.

Table 6-2: FTIR assignments from the literature.

Table 6-3: Literature assignments of PMMA proton peaks.

List of Abbreviations, Acronyms, and Symbols

^1H	Proton
ABMP	2,2'-Azobis(2-methylpropane)
ARROW	Antiresonant Reflecting Optical Waveguides
C	Carbon
C	Capacitance
CDCl_3	Chloroform- <i>d</i>
CHMA	Cyclohexyl Methacrylate
Cr	Chromium
CVD	Chemical Vapor Deposition
e	Electron
EGDA	Ethylene Glycol Diacrylate
EGDMA	Ethylene Glycol Dimethacrylate
EMA	Effective Medium Approximation
IC	Integrated Circuit
iCVD	Initiated Chemical Vapor Deposition
ITS	Interferometry for Thermal Stability
FTIR	Fourier-Transform Infrared Spectroscopy
GMA	Glycidyl Methacrylate
HEMA	2-Hydroxyethyl Methacrylate
HFCVD	Hot-Filament Chemical Vapor Deposition
Hg	Mercury
HMDS	Hexamethyldisilazane
HPLC	High-Performance Liquid Chromatography
k	Dielectric Constant
k_i	Initiation Rate Constant
k_c	Mass-Transfer Coefficient Based on Concentration
k_d	Initiator Decomposition Rate Constant
k_p	Propagation Rate Constant
k_t	Termination Rate Constant
[M]	(Surface) Monomer Concentration
[I]	Initiator Concentration
[I·]	(Surface) Concentration of Initiation Radicals
[IM _x ·]	Surface Concentration of Unterminated, Growing Radicals
<i>m</i>	Meso
MA	Methyl Acrylate
MEMS	Microelectromechanical System
MFC	Mass-Flow Controller
M/I	Monomer-to-Initiator Ratio
MMA	Methyl Methacrylate
MOCVD	Metal-Organic Chemical Vapor Deposition
n	Refractive Index
N ₂	Nitrogen
Ni	Nickel
NMR	Nuclear Magnetic Resonance
O	Oxygen
O ₂	Oxygen
OSG	Organosilicate Glass
PCHMA	Poly(cyclohexyl methacrylate)

PDI	Polydispersity Index
PECVD	Plasma-Enhanced Chemical Vapor Deposition
PGMA	Poly(glycidyl methacrylate)
PHEMA	Poly(2-hydroxyethyl methacrylate)
$p_{l,0}$	Partial Pressure of Radicals in Gas Phase in Close Proximity to Surface
$p_{l,\infty}$	Partial Pressure of Radicals in Gas Phase Far Away from Surface
piCVD	Photo-Initiated Chemical Vapor Deposition
PLP-SEC	Pulsed Laser Polymerization-Size Exclusion Chromatography
PMMA	Poly(methyl methacrylate)
POM	Polyoxymethylene
PPECVD	Pulsed Plasma-Enhanced Chemical Vapor Deposition
PR	Photoresist
PTFE	Poly(tetrafluoroethylene)
QCM	Quartz-Crystal Microbalance
r	Racemo
R	Resistance
R	Universal Gas Constant
RIE	Reactive-Ion Etching
RSF	Relative Sensitivity Factor
sccm	Standard Cubic Centimeters per Minute
Si	Silicon
SiO ₂	Silicon Dioxide
SOD	Spin-On Deposition
T	Temperature
T ₀	Surface Temperature
T _∞	Temperature of Gas Far Away from Surface
TBPO	<i>tert</i> -Butyl Peroxide
TEA	Triethylamine
THF	Tetrahydrofuran
VASE	Variable-Angle Spectroscopic Ellipsometry
XPS	X-Ray Photoelectron Spectroscopy



CHAPTER ONE

INTRODUCTION

1.1 BACKGROUND

Polymer thin films have a wide range of uses in both the industry and the research community. They are used for surface coating,^{1,2} surface modification,³ species adhesion or adsorption,⁴⁻⁸ species sensing,⁹⁻¹² separation,^{1,2,10,13-16} lithographic imaging,¹⁷⁻²⁴ photonics,²⁵⁻²⁷ microfabrication,^{1,2,28} etc. The prominent methods of polymer thin-film deposition are spin-on deposition (SOD) and chemical vapor deposition (CVD). SOD involves spinning of a polymer solution on a substrate to make a thin film. It therefore can be applied to many dissolvable polymers. CVD builds polymers on substrates *in situ* from their monomeric building blocks and involves no solvents. The trivial difference—the use of solvents—translates to many differences between the applicability and the characteristics of the two processes. The polymers for use in SOD are pre-made, and therefore the chemical structures and the properties of the polymers are independent of the actual spinning but instead rely on the polymerization processes that were used to synthesize the polymers. Bulk- and solution-phase polymerizations are well studied and characterized, so polymers with specific functional groups, chemical structures, and molecular weight distributions can be deposited using SOD. The use of solvents, however, increases workers' exposure to chemicals and also requires that the polymers be soluble. CVD, on the other hand, do not have these shortcomings. It can be used to deposit polymers for which no practical solvents exist. Thickness control is excellent, as films are grown *in situ* in a bottom-up manner. It is able to produce films of nanoscale thicknesses on a wide variety of substrates with macroscale uniformity. Non-uniform wetting and surface-tension effects associated with SOD are nonexistent for CVD, so

uniform coatings on complex geometries can be made.²⁹ CVD also offers environmental benefits by mitigating the use of solvents.

1.2 CHEMICAL VAPOR DEPOSITION ---

Most CVD processes are performed under vacuum in a chamber equipped with peripheral equipment. Figure 1-1 is a schematic of a vacuum CVD chamber. CVD is a continuous process in which one or more species are fed into the chamber through the inlet and gases or vapors are pumped out through the exhaust. The vacuum pump downstream maintains the vacuum inside the chamber, whereas the butterfly valve controls the pressure of the reactor. The pressure sensor, typically a diaphragm gauge, senses the pressure and routes a signal to the pressure controller, which controls the butterfly valve. The flow rates of precursor species are controlled by mass-flow controllers (MFC), which accurately control the mass flow rate of species, typically in units of standard cubic centimeters per minute (sccm). The stage on which the substrate is placed is temperature-controlled by either an electric heater or a cooling coil. A typical deposition is specified by its chamber pressure, substrate temperature, energy input, and species flow rates.

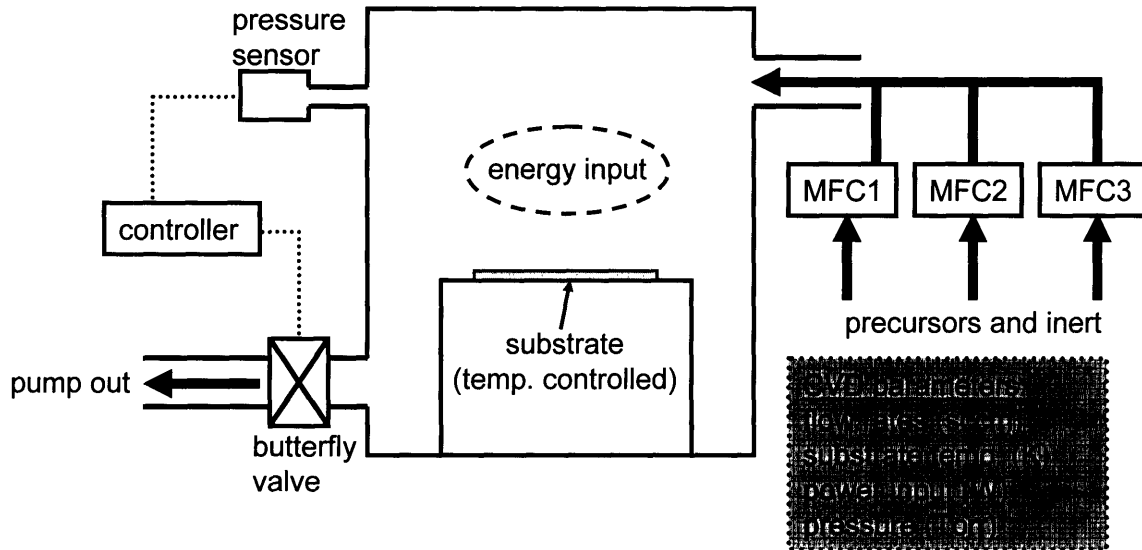


Figure 1-1. Schematic of CVD Chamber.

The parameter that differentiates one CVD technique from another is the type of energy input. CVD is a chemical synthesis that involves chemical reactions, so an energy input is usually needed to initiate them. Plasma-enhanced CVD (PECVD) uses an electric discharge as the energy input into the gas within the chamber to create radicals, ions, and excited neutrals.^{1,2,30,31} These energetic species are responsible for film growth on the substrate. A radio-frequency or microwave excitation excites the gas between the electrodes of which one is usually the grounded stage on which the substrate is placed.

Hot-filament CVD (HFCVD) is another polymer CVD technique and uses heat as the energy input. Unlike thermal CVD³²⁻³⁵ and metal-organic CVD (MOCVD),³⁶ which are rarely used for depositing polymers, the heat is not imposed onto the substrate but is rather input into the chamber separately through the use of thin filament wires. This setting is analogous to that of parylene deposition,³⁷⁻⁴⁰ in which a separate entity (e.g., a furnace) upstream is thermal energy source. HFCVD eliminates the need of an upstream furnace by incorporating the heat source inside the deposition chamber. The resistively-heated wires in HFCVD heat the gas but

not the substrate, which is backside-cooled to promote adsorption of species. The thermal breakdown of species creates radicals responsible for film growth. As seen in Figure 1-2, an HFCVD chamber is no different from an ordinary CVD chamber, except that a filament array is suspended above the substrate. The filament temperature and the total power input are important HFCVD parameters.

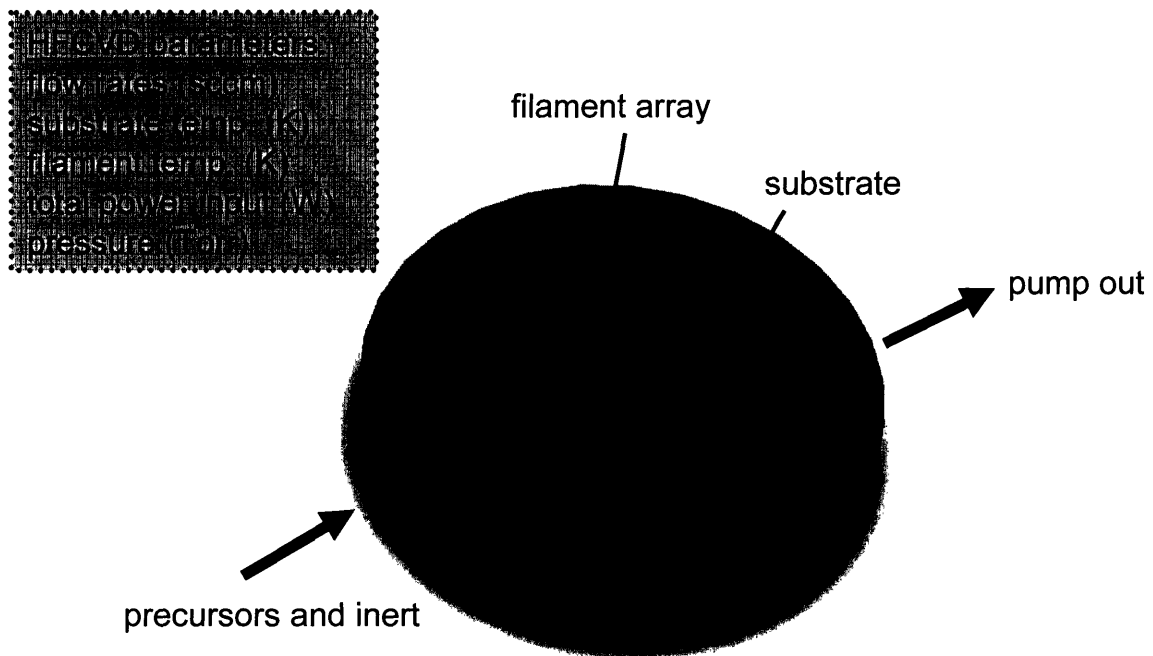


Figure 1-2. Hot-Filament CVD Chamber.

Although PECVD is able to synthesize a wide variety of polymers from both saturated and unsaturated precursors, its major problem lies with the use of a nonselective energy source for excitation. The electric discharge within the chamber fragments molecules in a nonselective way such that undesirable bond breaking often occurs. The lack of selectivity often results in polymers that do not have well-defined chemical structures. PECVD seldom makes polymers that resemble their traditionally-polymerized counterparts in terms of structural and physical properties. Loss of functional groups (or side groups) and unintended

cross-linking are usual characteristics of PECVD polymer films. The loss of functional groups during PECVD is bound to affect the functionality of the resulting polymer. Pulsed-PECVD (PPECVD) has therefore been implemented to counter PECVD's shortcomings. PPECVD, like PECVD, also uses an electric discharge, but the discharge is not on at all times. The plasma is turned on and off in a distinctive pattern to reduce exposure of species to electric discharge and thereby nonselective fragmentation. However, due to the reduced power input, deposition rate is significantly reduced, although the technique has been shown to produce polymers with improved structural integrity.⁴¹⁻⁴³

HFCVD was designed to address PECVD's problems. The use of thermal energy allows selective chemistries to occur inside the chamber, so that only certain chemical reactions can happen. As chemical reactions are activated processes, the filament temperature controls which of these reactions can proceed. Although the plasma power can be adjusted in PECVD and PPECVD, the electric discharge is still nonselective regardless of how low the plasma power is. Owing to the selectivity of HFCVD, it has been shown to produce poly(tetrafluoroethylene) (PTFE),⁴⁴ polyoxymethylene,⁴⁵ organosilicate glass,⁴⁶ fluorocarbon-organosilicon copolymer⁴⁷ thin films with high structural integrity. For instance, the comparison between films deposited from hexafluoropropylene oxide using PECVD and HFCVD clearly shows that HFCVD is able to produce films that are spectroscopically indistinguishable from conventional PTFE.⁴⁴

1.3 INITIATED CHEMICAL VAPOR DEPOSITION

Initiated CVD (iCVD) extends HFCVD's capability to produce structurally well-defined polymer through the use of an initiator. Like the initiators used in traditional free-radical polymerization, the initiators in iCVD are thermally-labile species that fragment to form radicals at moderate temperatures. The introduction of an initiator to HFCVD allows lower filament temperatures to be used than with no initiator because higher temperatures are needed to fragment the precursor species to create radicals. For example, in the iCVD of poly(glycidyl methacrylate) (PGMA) from glycidyl methacrylate (GMA),⁴⁸ the use of *tert*-butyl peroxide (TBPO) as an initiator allowed warm filament temperatures (180–250 °C) to be used to obtain high deposition rates. The same setting without TBPO resulted in a significantly lower deposition rate because the bonds in GMA are much stronger than the peroxy bond in TBPO. The immediate advantage of iCVD is that the lower filament temperatures guarantee that the precursor species stay intact throughout the process, eliminating chances of loss of functional groups. Such an improvement further differentiates the thermal process from PECVD. Not only are lower filament temperatures allowed, the introduction of initiators also accelerates film growth and simultaneously allows molecular-weight control.⁴⁸⁻⁵⁰

1.4 SCOPE OF THESIS

This thesis aims at further investigating the capability of iCVD and at the same time understanding the process from a reaction engineering standpoint. It intends to broaden the horizon of iCVD from homopolymers to application-specific polymer systems with well-defined microscale and macroscale properties. Each

chapter in this thesis is self-contained and can be read as a stand-alone document, as it is formatted as a manuscript for submission to a journal.

CHAPTER TWO reports the iCVD of linear and cross-linked poly(2-hydroxyethyl methacrylate) (PHEMA) for use as thin-film hydrogels. PHEMA is a widely-used biopolymer whose thin films have a broad spectrum of applications ranging from adsorption of cells and proteins to drug delivery. It is the first report of its kind to show systematic control of cross-linking in a CVD manner to result in well-defined thermal, wetting, and swelling properties. SOD is inherently incapable of producing as-deposited, cross-linked polymer, and PECVD has not demonstrated systematic control of cross-linking. Not only does iCVD demonstrate a drastic improvement over PECVD in terms of structural integrity and deposition rate, it also shows that polymer engineering is possible with iCVD. Films with specific microscale properties that translate to macroscale functionalities can be synthesized by adjusting chamber conditions.

CHAPTER THREE reports the iCVD of cross-linked poly(cyclohexyl methacrylate) (PCHMA) for use as a sacrificial polymer. This work is yet another demonstration of the power of iCVD as a thin-film deposition technique. The uniqueness of iCVD allows cross-linked PCHMA to be made in one step with properties suited for the sacrificial purpose.

CHAPTER FOUR investigates the mechanism of iCVD and serves as a groundwork for increased understanding of the process. It relates concentrations of species inside the chamber to deposition rates and molecular weights and attempts to model the iCVD process with mathematical expressions.

CHAPTER FIVE introduces photo-initiated chemical vapor deposition (piCVD), a first attempt of its kind to combine the bond-breaking ability of UV irradiation

with iCVD. It uses a volatile photoinitiator as the initiator and eliminates the need of a hot-filament array. This elimination simplifies chamber design and allows applications in which the use of a hot-filament array is inconvenient. piCVD also allows potential photomasked deposition, which would combine deposition and patterning in one single step.

CHAPTER SIX reports the first CVD process that is capable of depositing poly(methyl methacrylate) (PMMA) thin films that spectroscopically resemble conventional PMMA. It has a detailed analysis of structural properties with respect to chamber conditions.

CHAPTER SEVEN includes some concluding remarks about the thesis work and potential future directions on iCVD research.

This thesis would not have been possible without the support of the National Science Foundation/Semiconductor Research Corporation (NSF/SRC) Engineering Research Center (ERC) for Environmentally Benign Semiconductor Manufacturing (EBSM) and the SRC International Fellowship. The thesis work made use of Materials Research Science and Engineering Centers Shared Facilities supported by the NSF under Grant DMR-9400334.

REFERENCES

- (1) Yasuda, H., Plasma Polymerization. In Academic: Orlando, FL, 1985.
- (2) Hollahan, J. R.; Bell, A. T., Techniques and Applications of Plasma Chemistry. In Wiley: New York, 1974.
- (3) Yang, G. H.; Kang, E. T.; Neoh, K. G. *J. Polym. Sci. Pol. Chem.* 2000, 38, 3498.
- (4) Harkes, G.; Feijen, J.; Dankert, J. *Biomaterials* 1991, 12, 853.
- (5) Guan, J. J.; Gao, G. Y.; Feng, L. X.; Sheng, J. C. *J. Biomater. Sci.-Polym. Ed.* 2000, 11, 523.
- (6) Morra, M.; Cassinelli, C. *J. Biomed. Mater. Res.* 1995, 29, 39.
- (7) Morra, M.; Cassinelli, C. *J. Biomed. Mater. Res.* 1996, 31, 149.
- (8) Osada, Y.; Iriyama, Y. *Thin Solid Films* 1984, 118, 197.
- (9) Ralston, A. R. K.; Tobin, J. A.; Bajikar, S. S.; Denton, D. D. *Sens. Actuator B-Chem.* 1994, 22, 139.
- (10) Russell, S. P.; Weinkauff, D. H. *Polymer* 2001, 42, 2827.
- (11) Capan, R.; Ray, A. K.; Hassan, A. K.; Tanrisever, T. *J. Phys. D-Appl. Phys.* 2003, 36, 1115.
- (12) Zhang, C.; Wyatt, J.; Weinkauff, D. H. *Polymer* 2004, 45, 7665.
- (13) Kramer, P. W.; Yeh, Y. S.; Yasuda, H. *J. Membr. Sci.* 1989, 46, 1.
- (14) Denizli, A.; Say, R.; Patir, S.; Arica, M. Y. *React. Funct. Polym.* 2000, 43, 17.
- (15) Ibrahim, E. H.; Denizli, A.; Bektas, S.; Genc, O.; Piskin, E. *J. Chromatogr. B* 1998, 720, 217.
- (16) Lee, W.; Oshikiri, T.; Saito, K.; Sugita, K.; Sugo, T. *Chem. Mat.* 1996, 8, 2618.
- (17) Tamano, J.; Hattori, S.; Morita, S.; Yoneda, K. *Plasma Chem. Plasma Proc.* 1981, 1, 261.
- (18) Morita, S.; Tamano, J.; Hattori, S.; Ieda, M. *J. Appl. Phys.* 1980, 51, 3938.
- (19) Yamada, M.; Tamano, J.; Yoneda, K.; Morita, S.; Hattori, S. *Jpn. J. Appl. Phys. Part 1 - Regul. Pap. Short Notes Rev. Pap.* 1982, 21, 768.
- (20) Martinu, L.; Biederman, H. *Vacuum* 1983, 33, 253.
- (21) Vasilopoulou, M.; Boyatzis, S.; Raptis, I.; Dimotikalli, D.; Argitis, P. *J. Mater. Chem.* 2004, 14, 3312.
- (22) Mao, Y.; Felix, N. M.; Nguyen, P. T.; Ober, C. K.; Gleason, K. K. *J. Vac. Sci. Technol. B* 2004, 22, 2473.
- (23) Thompson, L. F.; Willson, C. G.; Bowden, M. J. *Introduction to Microlithography*, 2nd ed.; American Chemical Society: Washington, DC, 1994.

- (24) Shirai, M.; Sumino, T.; Tsunooka, M. In *Polymeric Materials for Microelectronic Applications: Science and Technology*, Ito, H., Tagawa, S., Horie, K., Eds.; American Chemical Society: Washington, DC, 1994; p 185.
- (25) Li, G. F.; Tobin, J. A.; Denton, D. D. *Appl. Phys. Lett.* **1993**, *62*, 1582.
- (26) Tobin, J. A.; Denton, D. D. *Appl. Phys. Lett.* **1992**, *60*, 2595.
- (27) Zhao, Y.; Wang, F.; Cui, Z. C.; Zheng, J.; Zhang, H. M.; Zhang, D. M.; Liu, S. Y.; Yi, M. B. *Microelectron. J.* **2004**, *35*, 605.
- (28) Teh, W. H.; Liang, C. T.; Graham, M.; Smith, C. G. *J. Microelectromech. Syst.* **2003**, *12*, 641.
- (29) Pierson, H. O. *Handbook of Chemical Vapor Deposition*, 2nd ed.; Noyes Publications: Norwich, NY, 1999.
- (30) Inagaki, N., Plasma Surface Modification and Plasma Polymerization. In Technomic: Lancaster, PA, 1996.
- (31) Morosoff, N. In *Plasma Deposition, Treatment, and Etching of Polymers*; d'Agostino, R., Ed. Academic Press: Boston, MA, 1990.
- (32) Vossen, J. L.; Kern, W. *Thin Film Processes II*, Academic Press: Boston, MA, 1991.
- (33) Bunshah, R. F. *Handbook of Deposition Technologies for Films and Coatings: Science, Technology, and Applications*, 2nd ed.; Noyes Publications: Park Ridge, NJ, 1994.
- (34) Nishi, Y.; Doering, R. *Handbook of Semiconductor Manufacturing Technology*, Marcel Dekker: New York, 2000.
- (35) Sivaram, S. *Chemical Vapor Deposition: Thermal and Plasma Deposition of Electronic Materials*; Van Nostrand Reinhold: New York, 1995.
- (36) Stringfellow, G. B. *Organometallic Vapor Phase Epitaxy: Theory and Practice*; Academic Press: Boston, MA, 1989.
- (37) Rogojevic, S.; Moore, J. A.; Gill, W. N. *J. Vac. Sci. Technol. A-Vac. Surf. Films* **1999**, *17*, 266.
- (38) Lu, T. M.; Moore, J. A. *MRS Bull.* **1997**, *22*, 28.
- (39) Greiner, A. *Trends Polym. Sci.* **1997**, *5*, 12.
- (40) You, L.; Yang, G. R.; Lang, C. I.; Moore, J. A.; Wu, P.; McDonald, J. F.; Lu, T. M. *J. Vac. Sci. Technol. A-Vac. Surf. Films* **1993**, *11*, 3047.
- (41) Tarducci, C.; Schofield, W. C. E.; Badyal, J. P. S. *Chem. Mat.* **2002**, *14*, 2541.
- (42) Savage, C. R.; Timmons, R. B.; Lin, J. W. *Chem. Mater.* **1991**, *3*, 575.
- (43) Lau, K. K. S.; Gleason, K. K. *J. Phys. Chem. B* **1998**, *102*, 5977.
- (44) Lau, K. K. S.; Gleason, K. K. *J. Fluor. Chem.* **2000**, *104*, 119.
- (45) Loo, L. S.; Gleason, K. K. *Electrochem. Solid State Lett.* **2001**, *4*, G81.

- (46) Pryce Lewis, H. G.; Casserly, T. B.; Gleason, K. K. *J. Electrochem. Soc.* 2001, 148, F212.
- (47) Murthy, S. K.; Gleason, K. K. *Macromolecules* 2002, 35, 1967.
- (48) Mao, Y.; Gleason, K. K. *Langmuir* 2004, 20, 2484.
- (49) Murthy, S. K.; Olsen, B. D.; Gleason, K. K. *Langmuir* 2002, 18, 6424.
- (50) Pryce Lewis, H. G.; Caulfield, J. A.; Gleason, K. K. *Langmuir* 2001, 17, 7652.

CHAPTER TWO

INITIATED CHEMICAL VAPOR DEPOSITION OF LINEAR
AND CROSS-LINKED POLY(2-HYDROXYETHYL
METHACRYLATE) FOR USE AS THIN-FILM HYDROGELS

ABSTRACT

Initiated chemical vapor deposition (iCVD) is able to synthesize linear and cross-linked poly(2-hydroxyethyl methacrylate) (PHEMA) thin-films, in one step, from vapors of 2-hydroxyethyl methacrylate (HEMA), ethylene glycol diacrylate (EGDA), and *tert*-butyl peroxide (TBPO) without using any solvents. This all-dry technique also allows control of the cross-link density by adjusting the partial pressure of the cross-linking agent EGDA in the vapor phase. Films with specific cross-link densities and hence thermal, wetting, and swelling properties can be created in one single vacuum processing step. Through selective thermal decomposition of the initiator TBPO, films with well-defined chemical structures and full functionality retention can be deposited, which is evident in the Fourier-transform infrared (FTIR) and X-ray photoelectron spectroscopy (XPS) analyses. These spectroscopic methods also facilitate determination of EGDA incorporation in the cross-linked films based on the fact that HEMA contains a hydroxyl group but EGDA does not. For the linear PHEMA depositions, the growth rate was found to be nonlinear in the partial pressure of HEMA, possibly due to nonlinear multilayer adsorption and/or primary termination. The EGDA/HEMA ratio in the films systematically increased from 0.00 to 0.46 as the EGDA partial pressure was raised. The onset temperatures of decomposition were between 270 and 302 °C for the linear and the most cross-linked films, respectively. Thermal annealing at ~430 °C resulted in minuscule amounts of residue for all films, linear or cross-linked. The most cross-linked film had ~99.50% thickness removed after annealing. The contact angle was found to increase with increasing cross-link density. Significant contact-angle hysteresis was observed, indicating surface reconfiguration, and the lowest receding angle was 17° for the linear film. Swelling measurements using spectroscopic ellipsometry showed that the degree of swelling decreased with

increasing EGDA incorporation. The water content decreased from 35% (v/v) for the linear film to below 10% (v/v) for the most cross-linked film. These results show that iCVD is able to produce PHEMA thin films that function as hydrogels when soaked in water. The spectroscopic results, the contact-angle results, and the swelling analysis altogether prove the retention of the hydrophilic pendant groups in the iCVD process.

2.1 INTRODUCTION

Poly(2-hydroxyethyl methacrylate) (HEMA) and HEMA-based materials have been of great interest and importance since their discovery in 1960.¹ HEMA-based hydrogels have been widely researched and used in biomedical applications because of their non-toxicity, non-antigenic properties, and biocompatibility.² Since the ground-breaking demonstration of polymeric materials for sustained-release purposes,³ HEMA and HEMA-based materials have been investigated and used as carriers for controlled release of water-soluble drugs.⁴⁻¹² A number of these drug-delivery studies involved the use of HEMA and HEMA-based thin films. HEMA and HEMA-based surfaces have been used for cell adhesion,^{13,14} cell growth,¹⁴ protein adsorption,^{15,16} separation devices,^{17,18} biosensors,¹⁹ and metal-ion adsorption.²⁰ For micropatterning, HEMA thin films have been demonstrated as deep-UV and e-beam resists that are developable in aqueous solutions.²¹ Methacrylic polymers are also known to decompose thermally into small molecules,²²⁻²⁶ so thin-films of these materials may be used as sacrificial layers for microstructure fabrication for microelectronic and optical applications.

Although HEMA is not sufficiently hydrophilic to dissolve in water, cross-linking of the polymer is normally required to control its gel properties. For instance, the degree of cross-linking has been found to have a significant impact on the rate of drug release from HEMA-based hydrogels.^{4-7,10,11} The degree of swelling has been found to decrease^{5,27,28} and the mechanical properties have been found to increase²⁷ with increasing cross-link density. The ability to produce thin-films of well-defined cross-link densities is therefore crucial.

Thin films of HEMA and HEMA-based materials are normally prepared by solution-phase grafting,²⁹ casting from polymer solution,^{2,30} or confined solution-phase polymerization,³¹ all of which are wet processes. Solution-phase grafting is

a two-step process involving the creation of radicals on the surface followed by graft polymerization and requires a graftable surface. Casting requires that the polymer be soluble in a solvent, so post-treatment is necessary to create cross-links. Confined solution-phase polymerization is able to create a cross-linked polymer thin film in one polymerization step, but the technique requires a number of solution preparation steps and subsequent confinement of the solution to produce a thin film. Although this technique allows films of different cross-link densities to be made by preparing solutions of different compositions, it is time-consuming and has poor thickness control. In contrast to these wet techniques, an all-dry process can be used to produce thin-film coatings on materials that would otherwise dissolve in solvents used in wet processes (e.g. drug particles). A dry process also offer environmental benefits by mitigating the use of solvents (e.g. N,N-dimethylformamide) and avoiding potential retention of solvents in the films. The release of drugs from hydrogels in Ref. 4 to 12 typically involves gel formation in the presence of dissolved drugs in the polymerization solution or post-polymerization swelling of the gel to incorporate drugs within it. An all-dry process would allow coating of pre-manufactured drug particles for controlled release. Such a coating would act as a membrane that swells in water, and the diffusional transport of drugs would depend on the thickness and the cross-link density.

Chemical vapor deposition (CVD) is a one-step, vacuum process, involving no solvents or volatiles. Using CVD, monomers are converted directly to desired polymeric films without the need for purification, drying, or curing steps. Custom copolymers can be created simply by changing the ratio of feed gases to the CVD reactor.³² CVD allows films of nanoscale thicknesses with macroscale uniformity to be produced and can be applied to complex geometries.³³ It can be used to coat nanoscale features, as there are no surface tension and non-uniform wetting

effects typically associated with wet processes. Plasma-enhanced CVD (PECVD) is a proven method for producing PHEMA thin films.^{15,16,34} In particular, the pulsation of the plasma on the μs – ms time scale has been found to allow a high degree of retention of hydroxyl groups.³⁴ Systematic control of cross-link density, however, has not been demonstrated for PECVD.

The goal of this work is to use initiated CVD (iCVD) to produce thin films of linear PHEMA homopolymer and cross-linked PHEMA copolymers. iCVD can be positioned as a complementary method to PECVD in depositing PHEMA films with control of cross-link density. In contrast to PECVD, there is no plasma and hence no UV irradiation or ion bombardment during the iCVD process; the resulting films have lower densities of dangling bonds than films grown using plasma excitation.³⁵

The iCVD method is a subset of hot-filament CVD (HFCVD) in which selective thermal decomposition of species is achieved using resistively-heated filament wires. The substrates to be coated are backside-cooled to promote adsorption of growth species. iCVD differs from conventional HFCVD on one main count—an initiator in addition to the monomer is introduced into the vacuum chamber. Mao and Gleason³⁶ have demonstrated the iCVD of a methacrylic polymer from the same chemical family as PHEMA: poly(glycidyl methacrylate) (PGMA). Glycidyl methacrylate (GMA) was the monomer, and *tert*-butyl peroxide (TBPO) was the initiator. Due to the weakness of the peroxy bond in TBPO, very low filament temperatures (180–250 °C) are required to generate radicals for initiation. These radicals serve as starters of polymer chains to which multiple monomer units are added spontaneously. As a result of low temperatures, the bond-scission chemistry inside the chamber is limited to only the fragmentation of TBPO. The pendant epoxide groups are therefore preserved in the process, leading to high structural resemblance of iCVD PGMA to solution-polymerized PGMA. The use of an initiator not only allows control of chemistry but also accelerates film growth

and provides molecular-weight and rate control.³⁶⁻³⁸ The energy input is low because of the low filament temperatures (<50 mW/cm²) and the need to decompose only the initiator but not the monomer. Yet, high growth rates (>100 nm/min) were achieved in the iCVD of PGMA. All these benefits of iCVD position it as an improvement over conventional HFCVD, which already is a proven method for depositing poly(tetrafluoroethylene),³⁹ polyoxymethylene,⁴⁰ organosilicate glass,⁴¹ and fluorocarbon-organosilicon copolymer³² thin films. Radicals in iCVD processes are annihilated through termination. Both disproportionation and coupling reactions eliminate radicals and halt the addition of monomer units to the chains. The recombination of radicals avoids the presence of dangling-bond defects⁴² in the resulting polymeric film. In addition to PGMA, poly(methyl methacrylate) (PMMA) thin films were also deposited using iCVD but with triethylamine instead of TBPO as the initiator.⁴³

This chapter first reports the iCVD of linear PHEMA thin films using the initiator TBPO and the monomer 2-hydroxyethyl methacrylate (HEMA, Figure 2-1). The high degree of retention of hydroxyl groups in iCVD PHEMA and the deposition rate dependence on the partial pressure of HEMA in the chamber will be discussed. Then, the chapter will explore the addition of ethylene glycol diacrylate (EGDA, Figure 2-1) to the iCVD synthesis. The incorporation of EGDA into the thin films will be shown to increase systematically with the partial pressure of this divinyl monomer, resulting in cross-linked P(HEMA-*co*-EGDA) copolymers. The effects of EGDA incorporation on the thermal and the wetting properties will be discussed. The swelling properties of the films will also be presented, showing that the films function as hydrogels when soaked in water.

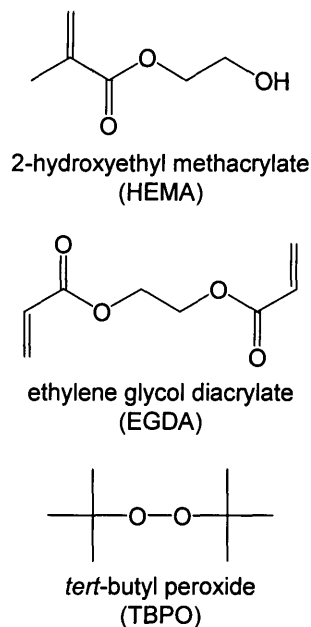


Figure 2–1. Precursor species being introduced into the vacuum chamber. HEMA is the monomer, EGDA is the cross-linking agent, and TBPO is the initiator.

2.2 EXPERIMENTAL METHODS

Films were deposited on 100-mm-diameter silicon (Si) substrates in a custom-built vacuum reactor (Sharon Vacuum). The reactor was cylindrical with a height of 3.3 cm and a radius of 12 cm. The inlet of precursor gases and the exhaust were at opposite ends of the reactor. The top of the reactor was covered by a removable quartz plate (~15 cm radius and 2.5 cm thick), allowing visual inspection, laser interferometry and placement of substrate. The reactor was equipped with a filament array, which provided thermal energy for selective decomposition of molecules, and a backside-cooled stage (35 °C) on which the substrate was placed. The clearance between the filaments and the stage was 29 mm. The Nichrome filaments (80% Ni/20% Cr, AWG 26, Omega Engineering) were resistively heated to 280 °C, as measured by a thermocouple (Type K, AWG 36,

Omega Engineering) directly attached to one of them. The reactor pressure was maintained at 350 mTorr with a throttling butterfly valve (Intellisys, Nor-Cal).

The monomer HEMA (99.0%+, Aldrich) and the cross-linking agent EGDA (90%, Aldrich) and the initiator TBPO (98%, Aldrich), were used without further purification. HEMA and EGDA liquids were vaporized in glass jars that were maintained at 70 ± 1 and 65 ± 1 °C, respectively. HEMA and EGDA vapors were metered into the reactor through mass-flow controllers (Model 1152C, MKS). TBPO was maintained at room temperature in a glass jar, and its vapor was also metered into the reactor through a mass flow controller (Model 1479A, MKS). All vapors were mixed together before entering the reactor through a side port. Depositions were monitored using an interferometry system equipped with a 633-nm HeNe laser source (JDS Uniphase). The cycle thickness was calculated by dividing the actual thickness, as measured using variable-angle spectroscopic ellipsometry (VASE), by the number of interferometric cycles. VASE was performed on a J. A. Woollam M-2000 spectroscopic ellipsometer with a xenon light source. Data were acquired at three angles (65°, 70°, and 75°) and 225 wavelengths, and the Cauchy-Urbach model was used to fit the data.

Two series of films were prepared. For the homopolymer experiments (linear PHEMA, denoted L1 to L5 in Table 2-1), no EGDA was introduced into the reactor. The flow rate of HEMA was varied between 3 and 5 sccm in increments of 0.5 sccm, whereas that of TBPO was kept constant at 1 sccm. A patch flow of nitrogen was also introduced into the reactor to keep the total flow rate at 7 sccm. This arrangement ensured the same residence time of 5 s for all experimental runs. For the cross-linking experiments (cross-linked PHEMA, denoted X1 through X5 in Table 2-1), both the flow rates of HEMA (4 sccm) and TBPO (1 sccm) were kept constant. A HEMA flow rate of 4 sccm was chosen because it was the midpoint of the linear series. The flow rate of EGDA was varied between 0 and 2 sccm in

increments of 0.5 sccm. A patch flow of nitrogen was also used to maintain the total flow rate at 7 sccm. All runs were carried out to produce films with thicknesses of ~1.4 μm .

Table 2-1. Details of experimental runs.

Sample	Flow Rate (sccm)			Partial Pressure (mTorr)		
	HEMA	EGDA	TBPO	N ₂	HEMA	EGDA
<i>Linear Series</i>						
L1	3.0	-	1.0	3.0	150	-
L2	3.5	-	1.0	2.5	175	-
L3	4.0	-	1.0	2.0	200	-
L4	4.5	-	1.0	1.5	225	-
L5	5.0	-	1.0	1.0	250	-
<i>Crosslinked Series</i>						
X1	4.0	0.0	1.0	2.0	200	0
X2	4.0	0.5	1.0	1.5	200	25
X3	4.0	1.0	1.0	1.0	200	50
X4	4.0	1.5	1.0	0.5	200	75
X5	4.0	2.0	1.0	0.0	200	100

Fourier-transform infrared (FTIR) measurements were performed on a Nicolet Nexus 870 ESP spectrometer in normal transmission mode using a DTGS KBr detector over the range of 400 to 4000 cm^{-1} at a 4- cm^{-1} resolution averaged over 64 scans. All spectra were baseline corrected and normalized to a thickness of 1 μm . The polymer films were degassed overnight in a vacuum oven maintained at 60 °C before FTIR measurements were taken. X-ray photoelectron spectroscopy (XPS) was done on a Kratos Axis Ultra spectrometer equipped with a monochromatized Al K α source. Contact-angle measurements were performed on a goniometer equipped with an automatic dispenser (Model 500, Ramé-Hart). Thermal properties were measured using the interferometry for thermal stability (ITS) apparatus described by Cruden *et al.*⁴⁴ The change in film thickness was monitored by noting the reflectance of a 633-nm HeNe laser beam off the substrate. All films used in the analyses had initial thicknesses of over 1.3 μm as

measured with VASE. The onset temperature of decomposition was taken as the temperature at which the laser signal started to fluctuate. The samples were kept under a nitrogen atmosphere throughout the annealing. They were heated to 150 °C from room temperature in 10 min. and kept at 150 °C for 30 min. The temperature was then raised to 240 °C in 30 min. and kept constant for another 30 min. Finally, the temperature was raised to 430 °C over the course of 60 min. The samples were then kept at this temperature for 90 min. before being cooled to room temperature. Prior to the end of the 90-min. period, the laser signal of each of the films had become steady indicating no further thickness change. This ramp-and-soak temperature profile was to facilitate equilibration of temperature within the apparatus. VASE was performed before and after annealing for evaluations of thickness losses.

As a comparison, a PHEMA standard (viscosity-average molecular weight ~ 300,000 g/mol) was obtained from Aldrich and was dissolved in N,N-dimethylformamide and cast onto a silicon substrate for FTIR and XPS analyses.

A simple liquid cell was obtained from J. A. Woollam for measurements of swelling properties. Each film-coated substrate was secured in the cell, and the cell was then placed on the stage of the M-2000 ellipsometer for measurements at a single angle of 75°, for which the cell was designed. Measurements were made before and after the cell was filled with water. The Cauchy-Urbach model was used to fit the data measured before filling, and the effective medium approximation (EMA) model, described elsewhere,⁴⁵ was used to fit the data measured after filling, with water as the ambient material. The EMA model was comprised of two materials—the polymer matrix and water. The material file (i.e. refractive index vs. wavelength) for the polymer matrix was generated using the data measured before filling. The material file for water was obtained from J. A. Woollam.

2.3 ICVD OF POLY(2-HYDROXYETHYL METHACRYLATE) HOMOPOLYMER_____

2.3.1 FOURIER-TRANSFORM INFRARED SPECTROSCOPY

Figure 2-2 shows the FTIR spectra of Sample L3 and the conventionally-polymerized PHEMA standard obtained from Aldrich. The FTIR spectra of the other four linear samples are similar to that of Sample L3. As seen from the figure, the spectrum of the iCVD film is essentially identical to that of the PHEMA standard. These spectra were thickness-normalized and baseline-corrected, and no other processing was performed. There are five main vibrational modes: O-H stretching ($3700\text{--}3050\text{ cm}^{-1}$), C-H stretching ($3050\text{--}2700\text{ cm}^{-1}$), C=O stretching ($1750\text{--}1690\text{ cm}^{-1}$), C-H bending ($1500\text{--}1350\text{ cm}^{-1}$), and C-O stretching ($1300\text{--}1200\text{ cm}^{-1}$). These assignments are based on the FTIR analyses of poly(methyl methacrylate)⁴⁶ and PHEMA⁴⁷ samples in the literature. The broad peak centered at $\sim 3450\text{ cm}^{-1}$ clearly signifies the retention of the hydroxyl group, and the retention of the carbonyl group is evident in the presence of the strong peak centered at 1727 cm^{-1} . These results indicate that the entire pendant group, $\text{-COOCH}_2\text{CH}_2\text{OH}$, is conserved in the iCVD process. The high resemblance in the C-H stretching and bending regions between the two spectra also precludes loss of the α -methyl group. All the peaks in the iCVD spectrum exemplify no broadening compared to the PHEMA standard spectrum. The lack of broadening further affirms the retention of functionalities in the iCVD process, as such an effect would indicate loss of homogeneity in bonding environments⁴⁸—a consequence of loss of functional groups.

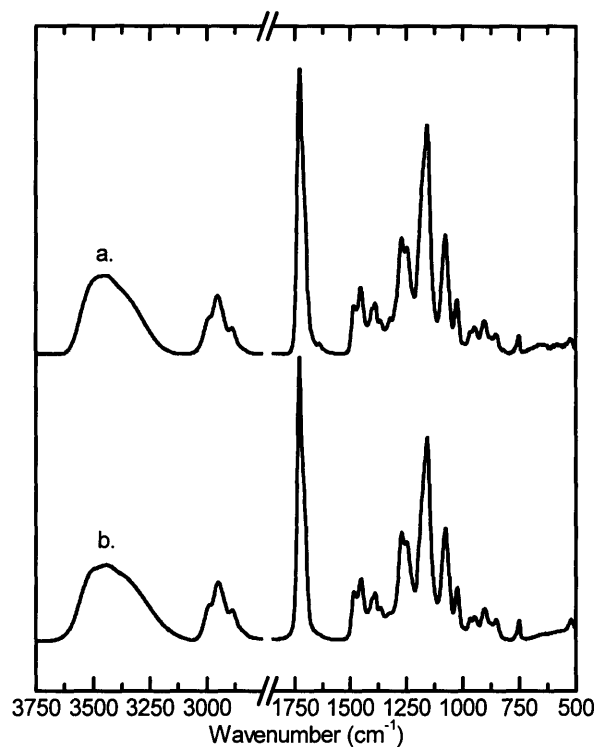


Figure 2-2. FTIR absorbance spectra of (a) PHEMA film synthesized from iCVD (Sample L3) and (b) spin-cast PHEMA standard obtained from Aldrich. The wide band centered at $\sim 3450\text{ cm}^{-1}$ indicates the retention of hydroxyl groups in the iCVD process. Baseline correction and thickness normalization were the only processing done on these spectra.

2.3.2 X-RAY PHOTOELECTRON SPECTROSCOPY

XPS survey scans of Sample L3 and the PHEMA standard revealed carbon-to-oxygen (C/O) ratios of 68.9:31.1 and 68.8:31.2, respectively. The discrepancy between the ratio of the PHEMA standard and the theoretical ratio, 66.7:33.3, can be attributed to the inaccuracies of the relative sensitivity factors (RSF) used to calculate the atomic percentages. The RSFs used are 0.780 and 0.278 for O 1s and C 1s core levels, respectively. It is known that RSFs vary from material to material, so it is more common to compare compositions of closely related samples than to use absolute compositions.⁴⁹ Indeed, the C/O ratios of the iCVD sample and the PHEMA standard are so close that one can conclude that they have the same atomic

compositions. The XPS high resolution scans show five carbon and three oxygen moieties, consistent with the structure of PHEMA (Figure 2-1). Table 2-1 shows excellent agreement of both the binding energies and peak area ratios of the iCVD sample with previously-reported results for conventionally-polymerized PHEMA.⁵⁰ The XPS results corroborate the FTIR results and support the hypothesis that iCVD produces PHEMA thin films that have the same linear structure as conventionally-polymerized PHEMA and have practically all of the functionalities retained. The linearity of the chains is further proven by that fact that iCVD PHEMA thin films are completely soluble in N,N-dimethylformamide, a common solvent used for gel permeation chromatography of PHEMA.

Table 2-2. High-Resolution XPS Scan Data of the iCVD PHEMA film (Sample L3). The literature values are from Ref. 50.

core level	peak	origin	iCVD film		PHEMA reference	
			binding energy (eV)	area (%)	binding energy (eV)	area (%)
C 1s	1	-C*H ₃ , -C-C*H ₂ -C-	285.00	34	285.00	34
	2	-C*(CH ₃)-CO-	285.66	16	285.73	17
	3	-CH ₂ -C*H ₂ -OH	286.61	17	286.53	17
	4	-O-C*H ₂ -CH ₂ -	286.94	16	286.89	17
	5	-C*=O	289.09	17	289.10	15
O 1s	1	-C=O*	532.32	33	532.32	33
	2	-O*H	533.11	34	533.09	33
	3	-CO-O*-CH ₂ -	533.80	33	533.86	33

2.3.3 DEPOSITION RATE

The maximum deposition rate achieved in this study was 110 nm/min (Sample L5). This rate is significantly higher than the rate of 13.4 nm/min reported for the PECVD of PHEMA.³⁴ Figure 2-3 shows the deposition rate of the linear iCVD films as a function of the partial pressure of HEMA in the vacuum chamber holding residence time and total pressure fixed. As can be seen, the deposition rate

increases nonlinearly with increasing partial pressure (i.e., gas-phase monomer concentration) and a nonlinear regression to a power law results in an exponent of 3.50 ± 0.30 . However, in the case of conventional solution-phase free-radical polymerization, the rate of propagation is linear in monomer concentration.⁵¹⁻⁵³ The observed nonlinear behavior has two likely origins, multilayer adsorption and primary radical termination. While one of these two effects may dominate, their effects can also be multiplicative.

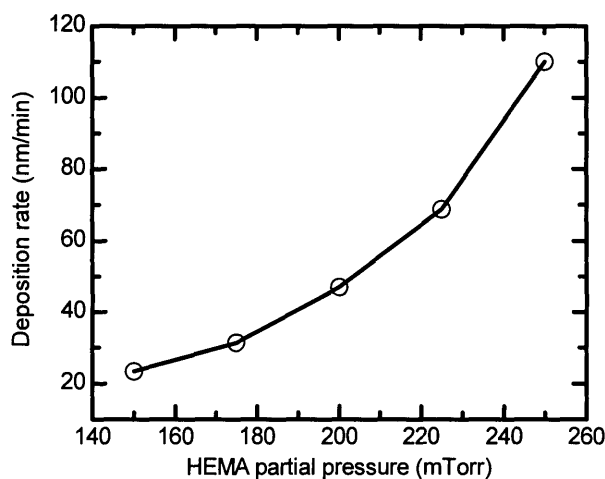


Figure 2-3. Deposition rate as a function of partial pressure of HEMA in the chamber. The nonlinearity has two likely origins: multilayer adsorption of HEMA on the surface and primary termination of chains.

In the case of surface polymerization, the surface concentration of monomer can be anticipated to depend nonlinearly on the gas phase concentration. The nonlinear relationship between surface and gas phase concentration is often seen in multilayered adsorption.⁵⁴ For a related monomer methyl methacrylate (MMA), Tsao and Ehrlich⁵⁵ studied the surface photopolymerization and employed a quartz-crystal microbalance to study the coverage of MMA on a substrate as a function of MMA partial pressure. In their study, the MMA adlayer thickness, or effectively the MMA concentration on the surface, was nonlinear in MMA partial pressure. Multilayer adsorption was observed at partial pressures exceeding 30% of

the saturation pressure of the monomer and adlayer thicknesses of more than 20 monolayers were observed at high partial pressures. In the current work, the highest partial pressure used in Figure 2–3 (250 mTorr) is 72% of the estimated saturation pressure of HEMA at 35 °C (345 mTorr). Additionally, the hydrogen bonding among HEMA molecules would be expected to promote the ease of multilayer adsorption.

It can also be argued that the surface concentration is linear to the monomer partial pressure but the rate is nonlinear to the surface concentration. This kind of nonlinearity may be due to primary termination. Primary termination differs from normal termination on that the growing polymer chains are not terminated by coupling or disproportionating with each other but are so by coupling with initiating radicals. This behavior can occur when the concentration of the growing chains are low compared to that of the initiating radicals or when the growing chains are not sufficiently mobile to engage in a termination event. When primary termination is the dominating termination mechanism, the rate of polymerization is no longer linear but to the square of the monomer concentration.⁵¹ The deviation from a power of 2 in this work could be due to experimental errors, but the immobility argument could very well be true considering that the chains are not as mobile on the surface as they would be in solution–phase polymerization.

The overall effect could also be a combination of the two nonlinearities described above. Further studies of surface concentration as a function of monomer partial pressure in the iCVD process will elucidate the nonlinearity between the growth rate and the partial pressure. Control of surface concentration not only allows control of growth rate but should also permit control of molecular weight. The molecular weight depends strongly on monomer concentration in solution–phase free–radical polymerization.^{51–53}

2.4 ICVD OF CROSS-LINKED POLY(2-HYDROXYETHYL METHACRYLATE)_____

2.4.1 FOURIER-TRANSFORM INFRARED SPECTROSCOPY

In order to synthesize cross-linked PHEMA films, EGDA was introduced together with HEMA into the vacuum chamber in a second series of experiments (X1 through X5 in Table 1), in which the EGDA partial pressure was varied while holding the residence time and the pressure constant. EGDA is a divinyl compound and is a common cross-linking agent used in solution-phase polymerization. Figure 2-4 shows the detailed FTIR analyses in the hydroxyl and the carbonyl stretching regions as the EGDA partial pressure is incremented. The intensities in the plots are normalized to a thickness of 1 μm . The O-H stretching intensity decreases and the C=O stretching intensity increases as the EGDA partial pressure increases. These trends are anticipated because EGDA does not contain any hydroxyl groups and has a higher density of carbonyl group per atom in the molecule.

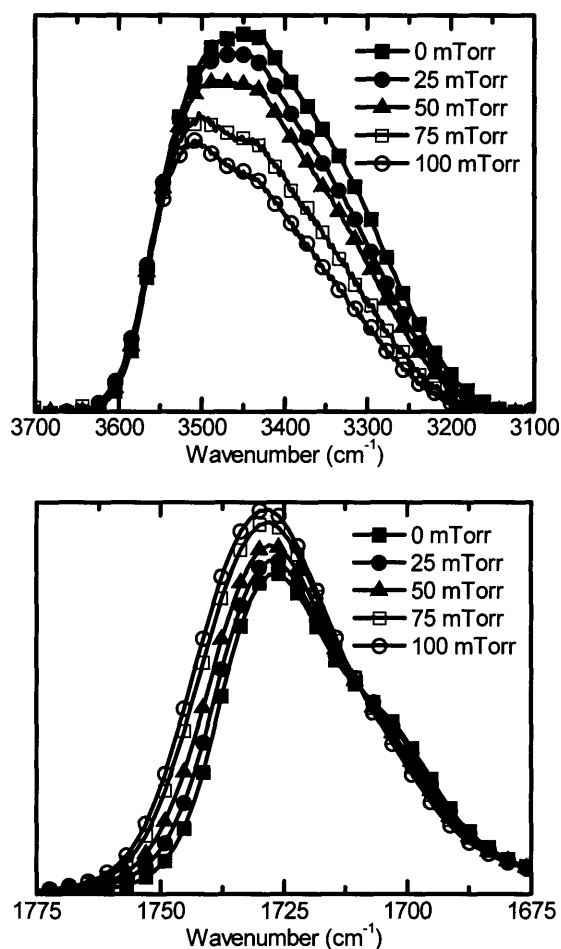


Figure 2-4. FTIR hydroxyl (top) and carbonyl stretching (bottom) absorbances normalized for film thickness as a function of the partial pressure of HEMA in the chamber. The hydroxyl intensity decreases and the carbonyl intensity increases with increasing EGDA partial pressure.

According to the Beer-Lambert equation,⁵⁶ the absorbance of a mode is proportional to the concentration of the moiety that is responsible for that particular mode, assuming that the bond oscillator strength is the same for each film. With this latter assumption, the areas under the peaks in Figure 2-4 are proportional to concentrations of O-H and C=O groups in the films. These concentrations in turn can be used to calculate the cross-link densities of these films. The underlying assumption in the calculations of this section is that the C=O

bond oscillator strengths of HEMA and EGDA units are identical. Stretching of a chemical bond, however, often exhibits different intensities depending on its bonding environment,^{56,57} so these FTIR results will also be compared to XPS data in the next section.

The calculation starts with the computation of the ratio (denoted r in Equation 2-1) of the peak area of the C=O stretching region to that of the O-H region in a linear PHEMA film that contains only HEMA units. Using this ratio of 0.59, the corresponding C=O intensity contributed by the HEMA units can be computed with the area under the O-H peak, A_{O-H} . The net intensity contributed by the EGDA units is then the total C=O intensity, $A_{C=O}$, less the contribution from the HEMA units, rA_{O-H} . Noting that each EGDA unit contains two C=O bonds, a ratio between the concentrations of EGDA and HEMA units can then be calculated (Equation 2-1) and serves as an indication of the degree of cross-linking.

$$\frac{[EGDA]}{[HEMA]} = \frac{(A_{C=O} - rA_{O-H})/2}{rA_{O-H}} \quad 2-1$$

Figure 2-6 shows the EGDA/HEMA ratio in the film as a function of the EGDA partial pressure. The incorporation of EGDA increases with increasing EGDA partial pressure. This result is anticipated, as the concentration of an adsorbed species on the surface increases with increasing partial pressure.

2.4.2 X-RAY PHOTOELECTRON SPECTROSCOPY

XPS high-resolution scan in the oxygen region was also used to determine the cross-link densities in the films. As seen from Figure 2-1, HEMA units have three different oxygen moieties, but EGDA units have only two. The binding energies of the photoelectrons of the C=O* oxygen (~532.3 eV) and the OC-O*

oxygen (~533.8 eV) should be the same in both the HEMA and EGDA units. The asterisk denotes the atom with which the binding energy is associated. However, only the HEMA units contain the O*–H oxygen (~533.1 eV). Figure 2–5 compares the XPS high resolution scans of the homopolymer (X1) and the most cross–linked (X5) films. In accordance with the FTIR results, the O*–H intensity (Peak 2) relative to the C=O* intensity (Peak 1) decreases with increasing EGDA partial pressure. The C=O* peak area is approximately the same as the OC–O* peak area (Peak 3) in all the films because these moieties are present in a 1:1 ratio in both HEMA and EGDA. It should be noted that the peak positions in Figure 2–5 are in close agreement with the literature values listed in Table 2–2. The contributions of HEMA and EGDA units to the C=O* intensity can be decoupled using the same logic as discussed in the FTIR section using Equation 2–2. Unlike Equation 2–1, Equation 2–2 does not require the use of a ratio because XPS measures directly the atomic contributions.

$$\frac{[EGDA]}{[HEMA]} = \frac{(A_{C=O^*} - A_{O^*-H})/2}{A_{O^*-H}} \quad 2-2$$

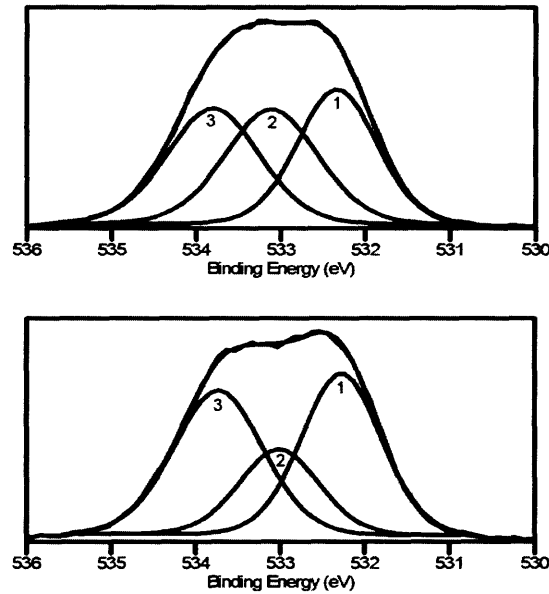


Figure 2-5. XPS high resolution scans of (top) the homopolymer film, Sample X1, and (bottom) the most cross-linked film, Sample X5. The intensity of Peak 2 that refers to the O*-H oxygen decreases with increasing degree of cross-linking.

Figure 2-6 shows the cross-link density as a function of EGDA partial pressure based on the XPS data. The XPS results agree very well with the FTIR results, affirming the validity of the calculated cross-link densities. It can also be inferred from the good agreement of the two sets of results that the C=O stretching in the HEMA units and that in the EGDA units have similar bond oscillator strengths, simplifying the calculation of the cross-link densities via the FTIR method.

Both the FTIR and the XPS results (Figure 2-6) show that the degree of cross-linking of an iCVD thin-film PHEMA hydrogel can be tuned between EGDA/HEMA ratios of 0.00 and ~0.46 by controlling the partial pressure of the cross-linking agent in the vacuum chamber. Plasma polymers are often intrinsically cross-linked without the use of a cross-linking agent. The degree of cross-linking can be controlled via pulsation or regulation of plasma power, but the deposition rate and

the degree of retention of functionalities are simultaneously altered.³⁴ iCVD provides excellent retention of functionalities and allows independent control of cross-link density. The dependence of deposition rate on the partial pressure of EGDA has not been investigated, but the introduction of a cross-linking agent does not need modification of the partial pressure of HEMA or the residence time of species in the chamber. The growth rate is expected to remain high as long as the partial pressure of HEMA remains high. Although not explored in depth, the growth rates of cross-linked PHEMA films, grown at a 200 mTorr HEMA partial pressure, were on par with the rate recorded for the linear PHEMA deposition at the same partial pressure (~45 nm/min as seen in Fig. 3).

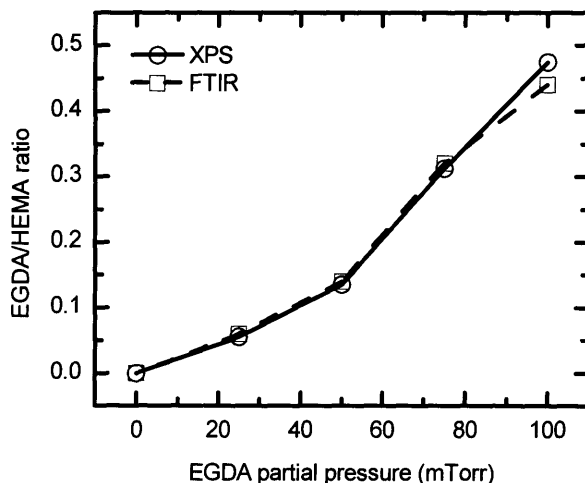


Figure 2-6. EGDA/HEMA ratio in iCVD films as a function of the partial pressure of EGDA in the chamber. More EGDA units are incorporated as the EGDA partial pressure increases.

2.4.3 THERMAL PROPERTIES

The effect of cross-linking on the thermal stability of the cross-linked PHEMA thin films is shown in Figure 2-7. The percent thickness removal decreases and the onset temperature of decomposition can be observed to increase with increasing cross-link density. The EGDA/HEMA ratios in this and subsequent

figures are mean values of the results derived from the FTIR and the XPS analyses. It is interesting to note the cleanliness of the decomposition even for the most cross-linked film. In fact, all the films had residue thicknesses of less than 0.01 μm (initial thicknesses $> 1.3 \mu\text{m}$). The non-cross-linked PHEMA film, grown at 0 mTorr EGDA partial pressure, had a 99.82% thickness loss. One previously reported percent degradation was 98% by weight, based on thermogravimetric analysis, for solution-polymerized PHEMA when the temperature was raised to 450 $^{\circ}\text{C}$.^{58,59} The difference between the results could be due to the bases of measurements (thickness vs. weight) and/or the difference in heating rates. One other possibility is that, in a thin-film setting, the degradation products are able to diffuse away quickly without being trapped inside the film and engaging in undesired chemical reactions. As seen in Figure 2-7, the cross-linked PHEMA films also degraded very cleanly.

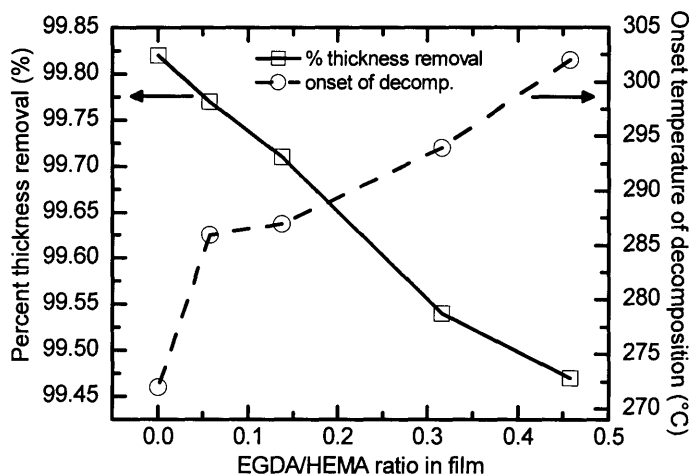


Figure 2-7. Percent thickness removal and onset temperature of decomposition as functions of EGDA/HEMA ratio in iCVD film.

The decomposition of cross-linked PHEMA has not been studied extensively. In a previous study⁶⁰ of cross-linked PMMA using ethylene glycol dimethacrylate,

the amount of residue was found not to be a strong function of cross-link density, in line with the results in Figure 2-7 (note the highly magnified y-axis), but the onset temperature of decomposition was found to decrease with increasing cross-link density, opposite to the trend in Figure 2-7. It is believed that the conflicting results are due to the difference in the nature of the cross-linking agents, one being a diacrylate and the other being a dimethacrylate. A study⁶¹ on the thermal decomposition of copolymers of HEMA and other acrylic and methacrylic monomers has shown that the thermal stability increases with increasing acrylic content but decreases with increasing methacrylic content. For instance, the thermal stability of HEMA-methyl acrylate (MA) increases with increasing MA content, whereas that of HEMA-MMA decreases with increasing MMA content. When the bond between two methacrylic repeat units is broken, one tertiary radical and one primary radical are formed. When, however, the bond between an acrylic unit and a methacrylic unit is broken, one secondary radical and one primary radical are formed. Tertiary radicals are more stable than secondary ones, so it is easier to break a HEMA-HEMA bond than a HEMA-EGDA bond. This logic is true even when the bond being broken is a head-to-head linkage. The interpretation here can explain the trend seen in Figure 2-7. As the acrylic content increases, the average strength of bonds within the polymer is higher and thus explains the increase in the onset temperature. The slight increase in the amount of residue with increasing cross-link density can be explained by the fact that polyacrylates decompose less cleanly than polymethacrylates.⁶² A different study⁶³ on the thermal degradation of copolymers of HEMA and *tert*-butyl acrylate also shows that the amount of residue increases with increasing acrylic content.

The thermal analyses of iCVD PHEMA films show that the films are of high thermal stabilities and are suitable for use in high-temperature applications. On the other hand, the films may be used as potential sacrificial materials because of

the minuscule amounts of residues remaining after decomposition. Cross-linking does not cause an appreciable increase in the amount of residue but should enhance the mechanical properties of the films. Sacrificial materials are commonly used in the fabrication of microelectromechanical systems (MEMS), in which there are stringent requirements for thermal stability and mechanical properties.⁶⁴

2.4.4 CONTACT-ANGLE MEASUREMENTS

PHEMA is hydrophilic because of its hydroxyl functionality. Contact-angle measurements were performed to test the hydrophilicity of the PHEMA thin films synthesized by iCVD. Sessile droplet (advancing and receding) contact angles were measured as a function of the water droplet volume. In each of the cases including non-cross-linked and cross-linked PHEMA films, the advancing angle reached a constant value as the water droplet volume increased, but the receding angle decreased gradually as the droplet volume decreased. The decrease is due to the fact that the contact area did not change even though the volume was decreasing. The three phase (air-water-polymer) contact line virtually did not recede. Figure 2-8 shows the measurements of two of the cross-linked films made at different EGDA partial pressures. In each of the measurements, the advancing angle is relatively constant as the droplet volume increases, but the receding angle decreases as the volume decreases. Also, the advancing angle is much larger than the receding angle. This effect is known as contact-angle hysteresis.⁶⁵⁻⁶⁹ Yasuda *et al.*⁶⁵ performed contact-angle measurements on gelatin and agar gels and observed the same advancing and receding trends. They attributed the effect to surface-configuration change and surface-state equilibration.

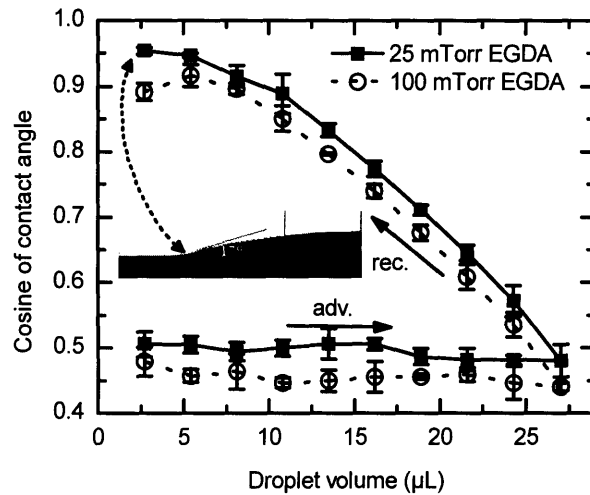


Figure 2-8. Advancing and receding contact angles as functions of the droplet volume. The film with more incorporation of EGDA has higher advancing and receding angles. The inset picture depicts the receding contact angle of 17° at the end of the advancing/receding cycle (ultimate receding angle) measured on Sample X2.

The surface state of a polymer equilibrates with the surrounding medium.^{65,69,70} When the medium is changed, the surface state of the polymer will begin to establish a new equilibrium with the new medium. When a polymer is exposed to a dry atmosphere, the surface configuration will progressively change, if allowed, to a more hydrophobic state. When the surrounding medium is changed from a dry atmosphere to a wet one, e.g. water, the surface configuration will become increasingly hydrophilic. It has been discussed⁷¹ that, when PHEMA is exposed to air, the hydrophobic methyl groups become directed toward air at the interface by chain rotation. When PHEMA is in contact with water, it reorients its hydrophilic groups toward water. Therefore, the contact angles measured depend very much on the medium to which the polymer has been exposed. This surface-configuration concept can explain the observed hysteresis for the iCVD PHEMA films. The advancing angles are high because the surface has been in equilibrium with air and thus appears hydrophobic. Once the surface has been soaked in water,

the PHEMA chains on the surface reconfigure themselves so that the surface becomes hydrophilic. The increase in hydrophilicity explains the decrease in the receding angle and why the three phase contact line does not recede. The contact angle of the reconfigured surface has become much lower than the advancing angle. When water is withdrawn from the surface, the three phase contact line needs not recede because the angle is still higher than what the contact angle should be. As a result, the water withdrawal causes mere flattening of the droplet until the true contact angle is reached. Since the contact area stays the same but the volume has decreased, the droplet is bound to flatten, leading to a decreased contact angle. On the other hand, the advancing angle does not change with droplet volume because the polymer-air interface beside the droplet has not yet been in contact with water and is hydrophobic. Figure 2-8 shows that the more cross-linked film has higher advancing and receding angles. The last receding angle measurement, hereby referred to as the ultimate receding angle, is representative of how hydrophilic the surface is after equilibration with water. Table 2-3 summarizes the advancing and the ultimate receding angles of films with different cross-link densities (Samples X1 to X5). These angles are results of the advancing/receding cycle, as represented by Figure 2-8. Both angles increase with increasing cross-link density. The increase in the EGDA content causes a decrease in hydrophilicity because the hydroxyl content is decreased. The ultimate receding angle of the non-cross-linked film, 17°, is in line with the value reported for the plasma PHEMA film.³⁴ It should be noted there was little if any time dependency on these contact-angle measurements. Measurements that were a month apart agreed well with each other. Unlike plasma films, which contain dangling bonds leading to change of contact angles over time,⁷² iCVD films do not exhibit such a change, which suggests that few if any dangling bonds exist and corroborates the free-radical mechanism involving the annihilation of radicals by termination. The inset

in Figure 2–8 depicts half of the droplet at the end of the advancing–receding cycle on Sample X2. A hydrophilic surface coating of PHEMA can indeed be synthesized using the iCVD process. This result supports the FTIR and XPS results that the hydroxyl functionality is retained in the iCVD process.

Table 2–3. Summary of advancing and ultimate receding angles of sessile contact angle measurements on iCVD films.

Sample	EGDA partial pressure (mTorr)	EGDA/HEMA in film	advancing angle (°)	ultimate receding angle (°)
X1	0	0.00	37	17
X2	25	0.06	49	17
X3	50	0.14	50	22
X4	75	0.32	54	28
X5	100	0.46	54	30

2.4.5 DEGREE OF SWELLING AND WATER CONTENT

Analyses of degree of swelling and water content of thin films using ellipsometry have been reported previously.^{45,66,73–75} A swollen hydrogel can be modeled as a composite material comprised of the polymer as the matrix and water as the filler. One method typically used for modeling composite materials is the effective medium approximation (EMA). The details of this method have been described elsewhere.⁴⁵ Figure 2–9 shows the thickness increase due to swelling and the refractive index of each of the swollen films (Samples X1–X5). The increase in the cross–link density limits the film’s ability to swell, as the polymer chains are held together more tightly as the cross–link density increases. The linear polymer (Sample X1, EGDA/HEMA = 0.0) has a thickness increase of 55%, while the most cross–linked one (Sample X5, EGDA/HEMA = 4.6) has only a 10% increase. The fact that cross–linking hinders the ability to hold water is reflected in the refractive index measurements (Figure 2–9), which show that the refractive

index increases with increasing cross-link density. Water has a lower refractive index ($n_{633} = 1.33$) than the polymer ($n_{633} = 1.49\text{--}1.51$), so an increase in water content results in a lower index.

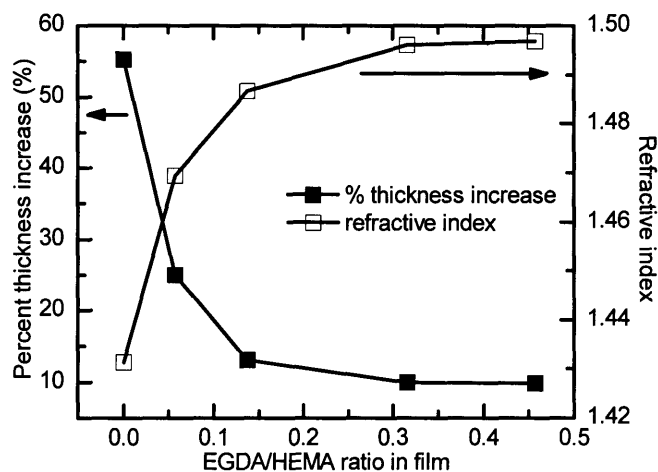


Figure 2-9. Changes in film thickness and refractive index of swollen film as functions of the EGDA/HEMA ratio in the film.

Figure 2-10 gives the water contents of the thin-film hydrogels based on EMA and on thickness increase. The values based on thickness increase were calculated assuming that the films swell only in the direction normal to the substrate, whereas those EMA values were generated by obtaining the best fit of the ellipsometry data. As can be seen, the two sets of data match closely, suggesting that the films do swell predominantly in the normal direction. As the films are not free-standing but adhered to the underlying Si substrates, it is reasonable that the films tend to swell preferentially in the normal direction. A compressive stress would have to be overcome for the films to swell laterally. As expected, the water content decreases with increasing cross-link density. The linear polymer (Sample X1) has about 35% (v/v) water, in line with results in the literature for PHEMA.^{8,70,76,77} The strong uptake of water further corroborates the spectroscopic

results and the contact-angle measurements that the hydrophilic pendant groups are retained in the iCVD process.

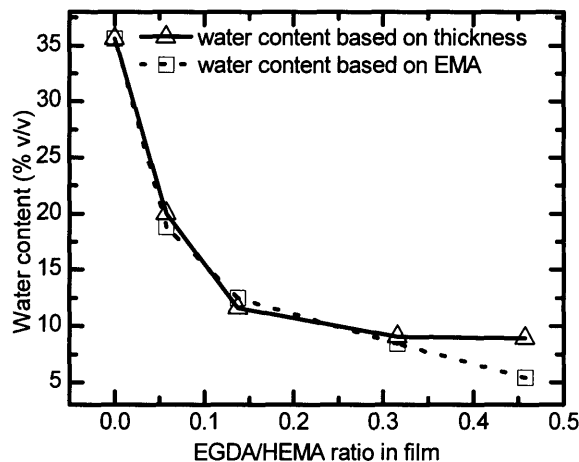


Figure 2-10. Water content of swollen film as a function of the EGDA/HEMA ratio in the film.

The results in this section show that the films produced using iCVD indeed function as hydrogels when soaked in water. The ability of iCVD to control the cross-link density and thus the degree of swelling through adjustment of the partial pressure of the cross-linking agent in the gas phase is clearly shown in Figure 2-9 and Figure 2-10.

2.5 CONCLUSIONS

This work demonstrates that iCVD can be used to deposit linear and cross-linked PHEMA thin films by feeding a mixture of the monomer HEMA, the cross-linker EGDA, and the initiator TBPO into a vacuum chamber equipped with a resistively-heated filament array and a substrate maintained at near room temperature (35 °C). iCVD is a one-step, dry technique and can be used to coat materials that would otherwise dissolve in solvents used in wet processes. Production of a 100-nm thick film requires a short deposition time of 55 s. As

shown in the analyses in this work, films with specific cross-link densities and hence thermal, wetting, and swelling properties can be synthesized in one single vacuum processing step which simultaneously achieves both polymerization of the monomers and coating of the substrate. Potential applications include coating of materials for sustained-release purposes. iCVD also allows control of cross-link density through control of the partial pressure of the cross-linker in the chamber. This ability not only allows customized films with different cross-link densities to be made with a quick modification of flow rates in the system but also enables the making of a single graded film with changing cross-link density as a function of film thickness.

The excellent structural retention of the iCVD process is clearly demonstrated by the FTIR and the XPS results. Compared to the PECVD work³⁴ that also gives good structural retention, iCVD has a much faster growth rate (110 vs. 13 nm/min) and at the same time allows control of cross-link density. In addition, the quality of iCVD films is expected to be higher because of the lack of UV irradiation and ion bombardment. The fact that the films are hydrophilic and swell in water further affirms the retention of hydroxyl groups.

The evaluation of the cross-link densities of iCVD films was demonstrated using FTIR and XPS, two commonly used characterization methods for thin films. Linear and cross-linked PHEMA iCVD films have excellent thermal stabilities, with onset temperatures of decomposition in the range of 270 to 302 °C. They also decompose cleanly during thermal annealing, leaving behind negligible residue when raised to 430 °C under a nitrogen atmosphere. These films may be used as self-decomposing sacrificial materials for fabricating microstructures or even air gaps.

This chapter lays the groundwork for making thin films for use as hydrogels, but further characterization is needed for complete evaluation of the materials.

Investigation of transport properties of materials through the films would certainly increase the understanding of the materials.

This work demonstrates that control of cross-linking is viable in the vapor-phase iCVD process as it is in solution-phase polymerization. Thin films of well-defined cross-link densities can be produced in one-step by carefully controlling the flow rates of species entering the chamber. This ability can be extended to producing thin films of other types of polymers. One possible application would be enhancing the mechanical properties of a linear polymer via cross-linking. Nevertheless, thin films of other networked hydrophilic polymers can also be made using iCVD. On the other hand, many of the hydrogel systems involve the use of comonomers, but there is no reason to deny iCVD's ability to produce a cross-linked copolymer, as the work in this chapter is fundamentally the copolymerization of HEMA and EGDA. With careful control of partial pressures of species in the chamber, films with well-defined comonomer ratios and well-defined cross-link densities can be made using iCVD. iCVD should have more success and be easier in producing very thin films of complex polymeric systems that include a number of monomers. Films with specific compositions can be tailored according to their applications. The concepts presented in this work are by no means limited to the area of hydrogels but can be and should be extended to other categories of copolymers and terpolymers with well-defined compositions and/or cross-link densities.

REFERENCES

- (1) Wichterle, O.; Lim, D. *Nature* 1960, 185, 117.
- (2) Folkman, J.; Moscona, A. *Nature* 1978, 273, 345.
- (3) Langer, R.; Folkman, J. *Nature* 1976, 263, 797.
- (4) Hsiue, G. H.; Guu, J. A.; Cheng, C. C. *Biomaterials* 2001, 22, 1763.
- (5) Ferreira, L.; Vidal, M. M.; Gil, M. H. *Int. J. Pharm.* 2000, 194, 169.
- (6) Blanco, M. D.; Trigo, R. M.; Garcia, O.; Teijon, J. M. *J. Biomater. Sci.-Polym. Ed.* 1997, 8, 709.
- (7) Blanco, M. D.; Garcia, O.; Gomez, C.; Sastre, R. L.; Teijon, J. M. *J. Pharm. Pharmacol.* 2000, 52, 1319.
- (8) Trigo, R. M.; Blanco, M. D.; Teijon, J. M.; Sastre, R. *Biomaterials* 1994, 15, 1181.
- (9) Brazel, C. S.; Peppas, N. A. *STP Pharma Sci.* 1999, 9, 473.
- (10) Garcia, O.; Blanco, M. D.; Gomez, C.; Teijon, J. M. *Polym. Bull.* 1997, 38, 55.
- (11) Garcia, O.; Trigo, R. M.; Blanco, M. D.; Teijon, J. M. *Biomaterials* 1994, 15, 689.
- (12) Lehr, C. M.; Bouwstra, J. A.; Vanhal, D. A.; Verhoef, J. C.; Junginger, H. E. *Eur. J. Pharm. Biopharm.* 1992, 38, 55.
- (13) Harkes, G.; Feijen, J.; Dankert, J. *Biomaterials* 1991, 12, 853.
- (14) Guan, J. J.; Gao, G. Y.; Feng, L. X.; Sheng, J. C. *J. Biomater. Sci.-Polym. Ed.* 2000, 11, 523.
- (15) Lopez, G. P.; Ratner, B. D.; Rapoza, R. J.; Horbett, T. A. *Macromolecules* 1993, 26, 3247.
- (16) Morra, M.; Cassinelli, C. *J. Biomed. Mater. Res.* 1995, 29, 39.
- (17) Denizli, A.; Say, R.; Patir, S.; Arica, M. Y. *React. Funct. Polym.* 2000, 43, 17.
- (18) Ibrahim, E. H.; Denizli, A.; Bektas, S.; Genc, O.; Piskin, E. *J. Chromatogr. B* 1998, 720, 217.
- (19) Arica, M. Y.; Senel, S.; Alaeddinoglu, N. G.; Patir, S.; Denizli, A. *J. Appl. Polym. Sci.* 2000, 75, 1685.
- (20) Osada, Y.; Iriyama, Y. *Thin Solid Films* 1984, 118, 197.
- (21) Vasilopoulou, M.; Boyatzis, S.; Raptis, I.; Dimotikalli, D.; Argitis, P. *J. Mater. Chem.* 2004, 14, 3312.
- (22) Zaikov, G. E.; Aseeva, R. M. 1993, 74, 21.
- (23) Chandra, R.; Saini, R. *J. Macromol. Sci.-Rev. Macromol. Chem. Phys.* 1990, C30, 155.
- (24) Zulfiqar, S.; Akhtar, N.; Zulfiqar, M.; McNeill, I. C. *Polym. Degrad. Stabil.* 1989, 23, 299.
- (25) Zulfiqar, S.; Piracha, A.; Masud, K. *Polym. Degrad. Stabil.* 1996, 52, 89.

- (26) Zulfiqar, S.; Zulfiqar, M.; Nawaz, M.; McNeill, I. C.; Gorman, J. G. *Polym. Degrad. Stabil.* 1990, 30, 195.
- (27) Lee, J. W.; Kim, E. H.; Jhon, M. S. *Bull. Korean Chem. Soc.* 1983, 4, 162.
- (28) Perera, D. I.; Shanks, R. A. *Polym. Int.* 1995, 37, 133.
- (29) Zubaidi; Hirotsu, T. *J. Appl. Polym. Sci.* 1996, 61, 1579.
- (30) Feng, M.; Morales, A. B.; Beugeling, T.; Bantjes, A.; vanderWerf, K.; Gosselink, G.; deGroot, B.; Greve, J. *J. Colloid Interface Sci.* 1996, 177, 364.
- (31) Chilkoti, A.; Lopez, G. P.; Ratner, B. D.; Hearn, M. J.; Briggs, D. *Macromolecules* 1993, 26, 4825.
- (32) Murthy, S. K.; Gleason, K. K. *Macromolecules* 2002, 35, 1967.
- (33) Pierson, H. O. *Handbook of Chemical Vapor Deposition*, 2nd ed.; Noyes Publications: Norwich, NY, 1999.
- (34) Tarducci, C.; Schofield, W. C. E.; Badyal, J. P. S. *Chem. Mat.* 2002, 14, 2541.
- (35) Limb, S. J.; Lau, K. K. S.; Edell, D. J.; Gleason, E. F.; Gleason, K. K. *Plasmas Polym.* 1999, 4, 21.
- (36) Mao, Y.; Gleason, K. K. *Langmuir* 2004, 20, 2484.
- (37) Pryce Lewis, H. G.; Caulfield, J. A.; Gleason, K. K. *Langmuir* 2001, 17, 7652.
- (38) Murthy, S. K.; Olsen, B. D.; Gleason, K. K. *Langmuir* 2002, 18, 6424.
- (39) Lau, K. K. S.; Gleason, K. K. *J. Fluor. Chem.* 2000, 104, 119.
- (40) Loo, L. S.; Gleason, K. K. *Electrochem. Solid State Lett.* 2001, 4, G81.
- (41) Pryce Lewis, H. G.; Casserly, T. B.; Gleason, K. K. *J. Electrochem. Soc.* 2001, 148, F212.
- (42) Limb, S. J.; Labelle, C. B.; Gleason, K. K.; Edell, D. J.; Gleason, E. F. *Appl. Phys. Lett.* 1996, 68, 2810.
- (43) Chan, K.; Gleason, K. K. *Chem. Vapor Deposition*, submitted.
- (44) Cruden, B.; Chu, K.; Gleason, K.; Sawin, H. *J. Electrochem. Soc.* 1999, 146, 4590.
- (45) Tang, Y.; Lu, J. R.; Lewis, A. L.; Vick, T. A.; Stratford, P. W. *Macromolecules* 2001, 34, 8768.
- (46) Nagai, H. *J. Appl. Polym. Sci.* 1963, 7, 1697.
- (47) Perova, T. S.; Vij, J. K.; Xu, H. *Colloid Polym. Sci.* 1997, 275, 323.
- (48) Cox, J. N. In *Encyclopedia of Materials Characterization: Surfaces, Interfaces, Thin Films*; Brundle, C. R., Evans, C. A., Wilson, S., Eds.; Butterworth-Heinemann: Stoneham, MA, 1992; p 422.
- (49) Brundle, C. R. In *Encyclopedia of Materials Characterization: Surfaces, Interfaces, Thin Films*; Brundle, C. R., Evans, C. A., Wilson, S., Eds.; Butterworth-Heinemann: Stoneham, MA, 1992; p 287.

- (50) Beamson, G.; Briggs, D. *High Resolution XPS of Organic Polymers: the Scienta ESCA300 Database*; Wiley: Chichester, West Sussex, England, 1992.
- (51) Odian, G. G. *Principles of Polymerization*, 3rd ed.; Wiley: New York, 1991.
- (52) Rodriguez, F. *Principles of Polymer Systems*, 4th ed.; Taylor & Francis: Washington, DC, 1996.
- (53) Kumar, A. S.; Gupta, R. K. *Fundamentals of Polymers*; McGraw-Hill: New York, 1998.
- (54) Masel, R. I. *Principles of Adsorption and Reaction on Solid Surfaces*; Wiley: New York, 1996.
- (55) Tsao, J. Y.; Ehrlich, D. J. *Appl. Phys. Lett.* **1983**, *42*, 997.
- (56) Lin-Vien, D.; Colthup, N. B.; Fateley, W. G.; Grasselli, J. G. *The Handbook of Infrared and Raman Characteristic Frequencies of Organic Molecules*; Academic Press: San Diego, CA, 1991.
- (57) Roeges, N. P. G. *A Guide to the Complete Interpretation of Infrared Spectra of Organic Structures*; Wiley: Chichester, West Sussex, England, 1994.
- (58) Demirelli, K.; Coskun, M.; Kaya, E. *Polym. Degrad. Stabil.* **2001**, *72*, 75.
- (59) Demirelli, K.; Coskun, M. F.; Kaya, E.; Coskun, M. *Polym. Degrad. Stabil.* **2002**, *78*, 333.
- (60) Levchik, G. F.; Si, K.; Levchik, S. V.; Camino, G.; Wilkie, C. A. *Polym. Degrad. Stabil.* **1999**, *65*, 395.
- (61) Varma, I. K.; Patnaik, S. *J. Polym. Sci. Pol. Chem.* **1979**, *17*, 3279.
- (62) Ali, A. H.; Srinivasan, K. S. V. *J. Macromol. Sci.-Pure Appl. Chem.* **1997**, *A34*, 235.
- (63) Martinez, G.; Sanchez-Chaves, M.; Rocha, C. M.; Ellis, G. *Polym. Degrad. Stabil.* **2002**, *76*, 205.
- (64) Senturia, S. D. *Microsystem Design*; Kluwer Academic Publishers: Boston, MA, 2001.
- (65) Yasuda, T.; Okuno, T.; Yasuda, H. *Langmuir* **1994**, *10*, 2435.
- (66) Hennig, A.; Eichhorn, K. J.; Staudinger, U.; Sahre, K.; Rogalli, M.; Stamm, M.; Neumann, A. W.; Grundke, K. *Langmuir* **2004**, *20*, 6685.
- (67) Yasuda, H.; Charlson, E. J.; Charlson, E. M.; Yasuda, T.; Miyama, M.; Okuno, T. *Langmuir* **1991**, *7*, 2394.
- (68) Extrand, C. W.; Kumagai, Y. *J. Colloid Interface Sci.* **1997**, *191*, 378.
- (69) Morra, M.; Occhiello, E.; Garbassi, F. *J. Colloid Interface Sci.* **1992**, *149*, 84.
- (70) Holly, F. J.; Refojo, M. F. *J. Biomed. Mater. Res.* **1975**, *9*, 315.
- (71) Tonge, S.; Jones, L.; Goodall, S.; Tighe, B. *Curr. Eye Res.* **2001**, *23*, 51.
- (72) Gengenbach, T. R.; Griesser, H. J. *Surf. Interface Anal.* **1998**, *26*, 498.
- (73) Zudans, I.; Heineman, W. R.; Seliskar, C. J. *Chem. Mat.* **2004**, *16*, 3339.
- (74) Tanchak, O. M.; Barrett, C. J. *Chem. Mat.* **2004**, *16*, 2734.

- (75) Toomey, R.; Freidank, D.; Ruhe, J. *Macromolecules* **2004**, *37*, 882.
- (76) Hermitte, L.; Thomas, F.; Bougaran, R.; Martelet, C. *J. Colloid Interface Sci.* **2004**, *272*, 82.
- (77) Davis, T. P.; Huglin, M. B. *Angew. Makromol. Chem.* **1991**, *189*, 195.



CHAPTER THREE

AIR-GAP FABRICATION USING A SACRIFICIAL
POLYMERIC THIN FILM SYNTHESIZED VIA INITIATED
CHEMICAL VAPOR DEPOSITION

ABSTRACT

Thin film of a polymeric sacrificial material based on poly(cyclohexyl methacrylate) (PCHMA) was synthesized using initiated chemical vapor deposition (iCVD). iCVD is able to make cross-linked PCHMA *in situ* on the surface of a substrate in one step without using any solvents. Although cross-linked, the material was found to decompose cleanly, leaving behind a maximum of 0.3% of residue by thickness upon completion of annealing. Cross-linking renders the polymer stable in practically all solvents, so the photoresist used for patterning can be removed by dissolution instead of ashing. The high etch rate (0.35 $\mu\text{m}/\text{min}$) in oxygen reactive-ion etching in addition to the stability in solvents eliminates the need of a hard mask during etching. This use of no hard mask represents an improvement over previously-reported spin-on sacrificial materials. Infrared spectroscopy and solubility tests confirm the identity of the iCVD polymer and its stability in solvents. The onset of thermal decomposition is 270 $^{\circ}\text{C}$, meaning that the polymer can survive other high-temperature processing steps. Fabrication using conventional lithographic, etching, and deposition techniques resulted in void structures having feature sizes of a minimum of 1.5 μm , as visualized using environmental scanning electron microscopy. With better lithographic technologies, void structures of smaller feature sizes can be fabricated. This work represents a novel approach, combining the rationale behind cross-linking and the technique required for synthesis, of air-gap fabrication using a sacrificial polymer.

3.1 INTRODUCTION

Sacrificial materials are used frequently in the micromachining of microelectromechanical systems^{1,2} (MEMS) and recently in the fabrication of void-containing microstructures for low-dielectric-constant (low-k) and low-refractive-index (low-n) applications. Void, or air in the context of this work, has the lowest possible dielectric constant of 1.0 and the lowest possible refractive index of 1.0, which is the rationale behind its potential use in integrated circuits (IC) and optical devices. Incorporation of air as a low-k dielectric would significantly reduce the resistance-capacitance (RC) delay, the power consumption, and the cross-talk noise between metal lines in ICs.³⁻⁷ Using air as low-n layers in optical devices would enable high-performance reflectors and mirrors to be made with fewer bilayers due to the increased index contrast.⁸⁻¹³ In the field of MEMS, sacrificial materials are widely used in the making of traditional systems such as accelerometers, actuators, beams, and cantilevers.^{1,2} Recently, the increase in research in microfluidics^{7,14-17} and antiresonant reflecting optical waveguides^{18,19} (ARROW) has resulted in expanded use of sacrificial materials to make air channels.

Figure 3-1 illustrates a scheme of using a sacrificial material to make a simple void structure. In order to achieve the end product, a sacrificial layer has to support the deposition of the top layer, or act as a placeholder, and then be removed later to leave behind empty space between the top cover layer and the substrate. Conventional methods of removal include selective dissolution, wet etching, and dry etching of the sacrificial materials. These techniques require the use of processing steps involving solutions or etchants, and consequently etch holes are often integrated in the cover layer to facilitate the removal process. Recently heat-decomposing sacrificial materials have been proposed as an alternative to conventional ones.^{3,6,7,14,15,17,20-27} This type of materials needs no

etchant or solvent but instead decomposes at elevated temperatures to form small molecules which diffuse through the cover layer. The immediate advantage lies with the dryness of the removal process that does not require etch holes in the cover layer. Closed-cavity void structures can be made without the need of sealing any openings, and the removal process is compatible with a wide range of overcoat materials. The lack of a wet step also prevents collapse of structures induced by surface tension between the layers during evaporation of solution.^{8,12,28}

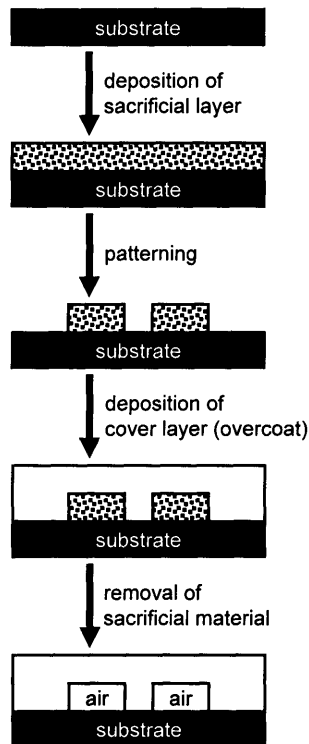


Figure 3-1. Scheme of using a sacrificial material to make a simple void structure. In the final step, the sacrificial material decomposes to form small molecules capable of diffusing through the top cover layer.

Heat-depolymerizable polymeric sacrificial materials have been studied by a number of researchers because of their ease of deposition, clean decomposition, and small decomposition products. Spin-on sacrificial polymers such as

polycarbonates^{6,14,15,24,29} and polynorbornenes^{7,17,20,22,25,29} have proven to be successful in fabricating void structures. Chemical vapor deposition (CVD) has also been used to deposit sacrificial polymers such as polyoxymethylene²⁶ (POM) and poly(methyl methacrylate)³⁰ (PMMA). Polymeric materials are advantageous because they often offer good mechanical properties at room temperature and are able to act as placeholders during microfabrication.

Polymer CVD is a dry technique for depositing polymers and is complementary to spin-on deposition (SOD). It is capable of producing films of nanoscale thicknesses with macroscale uniformity on complex geometries due to the dry nature of the process. It synthesizes polymers *in situ* on surfaces without using solvents, so polymers can be deposited on substrates that would otherwise dissolve in solvents used for SOD. It also eliminates non-uniform wetting and surface-tension effects that are typically associated with wet processes. Plasma-enhanced CVD (PECVD) is a widely-used CVD technique capable of depositing many different polymers.³¹⁻³³ The electric discharge during PECVD, however, often causes undesired bond breakage leading to bonding inhomogeneity in the resulting polymers. Homogeneity in chemical bonding is crucial for sacrificial polymers because the deposition mechanisms for polymer decomposition are highly dependent on the chemical structure and a slight imperfection in structural integrity is capable of stopping the decomposition and leads to char formation. For instance, PMMA's decomposition is by unzipping of methyl methacrylate (MMA) units from the chain.³⁰ If there is an imperfection along the chain, e.g. a single oxygen atom included along the carbon backbone, the decomposition would stall at the point of imperfection and be unable to proceed further. To this end, Gleason and coworkers³⁴⁻³⁸ have devised initiated CVD (iCVD) to produce polymeric thin films with few if any imperfections. iCVD is a thermal process that makes use of an initiator whose decomposition inside the CVD chamber is the only bond-breaking

reaction. The initiator breaks down into radicals that initiate free-radical polymerization, much like conventional bulk- and solution-phase processes but in an all-dry manner on the surface of the substrate. In particular, iCVD poly(2-hydroxyethyl methacrylate)³⁵ (PHEMA) is spectroscopically indistinguishable from traditional PHEMA. As a result of the bonding homogeneity, both linear and cross-linked iCVD PHEMA decompose cleanly (less than 0.6% residue by thickness). Cross-linked iCVD PHEMA is made through the use of ethylene glycol diacrylate (EGDA) as a cross-linker. Although cross-linked, the entire polymer is still of acrylate nature, leading to clean decomposition. iCVD PHEMA-based thin films, however, swell heavily in water and are therefore unsuitable for use in microfabrication, which involves many aqueous-based solvents. This recent study motivates the iCVD work in this chapter, which employs cyclohexyl methacrylate (CHMA) as the monomer, ethylene glycol dimethacrylate (EGDMA) as the cross-linker, and *tert*-butyl peroxide (TBPO) as the initiator (Figure 3-2). Poly(CHMA) (PCHMA) is hydrophobic, and EGDMA is used instead of EGDA because polymethacrylates are known to decompose more cleanly than polyacrylates. Cross-linking offers added benefits such as enhanced stability in solvents, improved mechanical properties, and higher glass-transition temperatures. Not only do these benefits enhance the placeholder functionality of the polymer as a sacrificial material, they also simplify the pattern-transfer step during microfabrication compared to spin-on polymers, as will be seen in this chapter. iCVD's ability to synthesize as-deposited, cross-linked sacrificial polymers is crucial to the making of cross-linked PCHMA thin films as sacrificial layers.

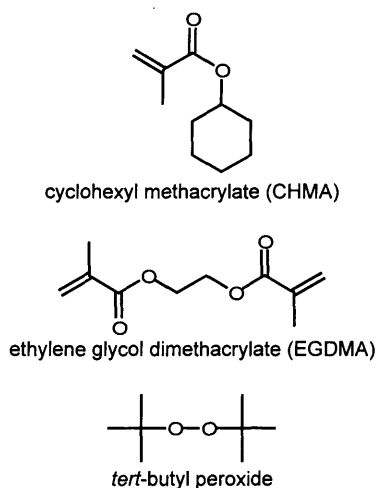


Figure 3–2. Species used in the iCVD synthesis of sacrificial polymer.

This chapter describes the structural and thermal properties of the iCVD P(CHMA-*co*-EGDMA) polymer and demonstrates its compatibility with conventional lithographic, etching, and deposition techniques used in clean rooms.

3.2 EXPERIMENTAL METHODS

Polymer iCVD. Polymer films were deposited on 100-mm-diameter silicon (Si) substrates in a custom-built vacuum reactor (Sharon Vacuum). The reactor was cylindrical with a height of 3.3 cm and a radius of 12 cm. The inlet of precursor gases and the exhaust were at opposite ends of the reactor. The top of the reactor was covered by a removable quartz plate (~15 cm radius and 2.5 cm thick), allowing visual inspection, laser interferometry, and placement of substrate. The reactor was equipped with a filament array, which provided thermal energy for selective decomposition of molecules, and a backside-cooled stage (45 °C) on which the substrate was placed. The clearance between the filaments and the stage was 29 mm. The Nichrome filaments (80% Ni/20% Cr, AWG 26, Omega Engineering) were resistively heated to 330 °C, as measured by a thermocouple (Type K, AWG 36,

Omega Engineering) directly attached to one of them. The reactor pressure was maintained at 430 mTorr with a throttling butterfly valve (Intellisys, Nor-Cal).

The monomer CHMA (97%, Alfa Aesar) and the cross-linking agent EGDMA (98%, Alfa Aesar) and the initiator TBPO (98%, Aldrich), were used without further purification. CHMA and EGDMA liquids were vaporized in glass jars that were maintained at 73.5 and 75.0 °C, respectively. CHMA and EGDMA vapors were metered into the reactor through mass-flow controllers (Model 1152C, MKS). TBPO was maintained at room temperature in a glass jar, and its vapor was also metered into the reactor through a mass flow controller (Model 1479A, MKS). All vapors were mixed together before entering the reactor through a side port, and the flow rates of CHMA, EGDMA, and TBPO were 7.0 sccm, 0.5 sccm, and 1 sccm, respectively. The flow rates and the reactor pressure were allowed time to stabilize before the filaments were turned on to start the deposition. Depositions were monitored using an interferometry system equipped with a 633-nm HeNe laser source (JDS Uniphase). The cycle thickness was calculated by dividing the actual thickness, as measured using variable-angle spectroscopic ellipsometry (VASE), by the number of interferometric cycles.

Thickness measurement. Thicknesses were measured using variable-angle spectroscopic ellipsometry (VASE). VASE was performed on a J. A. Woollam M-2000 spectroscopic ellipsometer with a xenon light source. Data were acquired at three angles (65°, 70°, and 75°) and 225 wavelengths, and the Cauchy-Urbach model was used to fit the data.

Fourier-transform infrared spectroscopy. Fourier-transform infrared (FTIR) measurements were performed on a Nicolet Nexus 870 ESP spectrometer in normal transmission mode using a DTGS KBr detector over the range of 400 to 4000 cm^{-1} at a 4- cm^{-1} resolution averaged over 64 scans. All spectra were baseline-corrected.

Analyses of thermal properties. Thermal properties were measured using the interferometry for thermal stability (ITS) apparatus described by Cruden *et al.* The change in film thickness was monitored by noting the reflectance of a 633-nm HeNe laser beam off the substrate. All films used in the analyses had initial thicknesses of over 1.3 μm as measured with VASE. The onset temperature of decomposition was taken as the temperature at which the laser signal started to fluctuate. The samples were kept under a nitrogen atmosphere throughout the annealing. They were heated to 150 °C from room temperature in 10 min. and kept at 150 °C for 30 min. The temperature was then raised to 240 °C in 30 min. and kept constant for another 30 min. Finally, the temperature was raised to 430 °C over the course of 60 min. The samples were then kept at this temperature for 90 min. before being cooled to room temperature. Prior to the end of the 90-min. period, the laser signal of each of the films had become steady indicating no further thickness change. This ramp-and-soak temperature profile was to facilitate equilibration of temperature within the apparatus. VASE was performed before and after annealing for evaluations of thickness losses.

Photolithography. Hexamethyldisilazane (HMDS, Arch Chemicals) was cast onto the polymer-coated substrate at 4000 rpm for 40 s to promote photoresist (PR) adhesion. A standard positive PR (OCG 825 20CS, Arch Chemicals) was then spun onto the substrate at 3000 rpm for 40 s. After resist coating, the substrate was baked in a convection oven at 90 °C for 15 min. The baked substrate was then exposed under a broadband UV lamp for 3 s in hard contact with a mask. The PR was then developed in a tetramethylammonium hydroxide solution (OCG 934, Arch Chemicals) for approximately 2 min. After development, the substrate was baked in a convection oven at 130 °C for 15 min.

Reactive-ion etching and plasma-enhanced CVD. Oxygen (O_2) reactive-ion etching (RIE) was used to etch the iCVD polymer film. It was performed using a

Plasma–Therm 700 Series deposition/etching tool. O₂ was metered into the RIE chamber at 30 sccm. The plasma power and the pressure were maintained at 250 W and 40 mTorr, respectively. The substrate temperature was not controlled actively for O₂ RIE. Silicon dioxide (SiO₂) was deposited via PECVD using the same tool but in the deposition chamber. Silane (5% in helium) and nitrous oxide were metered into the chamber at 195 and 600 sccm, respectively. The substrate temperature, the plasma power, and the pressure were maintained at 250 °C, 25 W, and 500 mTorr, respectively. In all of these PECVD and RIE processes, the flow rates and the pressure were allowed time to stabilize before the plasma was turned on.

iCVD polymer decomposition. Samples were annealed in the iCVD chamber installed with a hot plate (Watlow Electric). A thermocouple (Type K, AWG 36, Omega Engineering) was attached to the hot plate for temperature sensing. A ramp–soak temperature controller (Model CN3251, Omega Engineering) connected to a solid–state relay was used to control the temperature of the hot plate during annealing. The temperature profile was programmed to ramp linearly from room temperature to 500 °C over 4 hr. This long annealing time was chosen to ensure no pressure buildup within would occur within cavities and certainly does not represent the minimum time required for proper release of decomposition products. During annealing, the pressure of the chamber was maintained at atmospheric pressure with a continuous purge of nitrogen.

Silicon–dioxide–based fabrication of single–level air–gap structure. Figure 3–3 shows the process flow of the fabrication scheme used in this work to make a prototype single–level air–gap. It started with the iCVD of the copolymer film on a silicon substrate (~0.5 μm, Step 1), which was then transferred to a spin coater for the coating of HMDS and PR (Step 2). After photolithography (Step 3), strips of PR remained on top of the polymer for pattern transfer using O₂ RIE (Step 4). The PR

was then stripped away by soaking the substrate in acetone (Step 5). At this point, the substrate was left with strips of iCVD copolymer on top. The substrate was then transferred to the deposition tool for a blanket PECVD of SiO₂ (Step 6). In this step, the entire substrate was blanketed with SiO₂, filling the spaces between copolymer strips as well as covering the top of them. In the final step, thermal annealing (Step 7) was performed to decompose the copolymer.

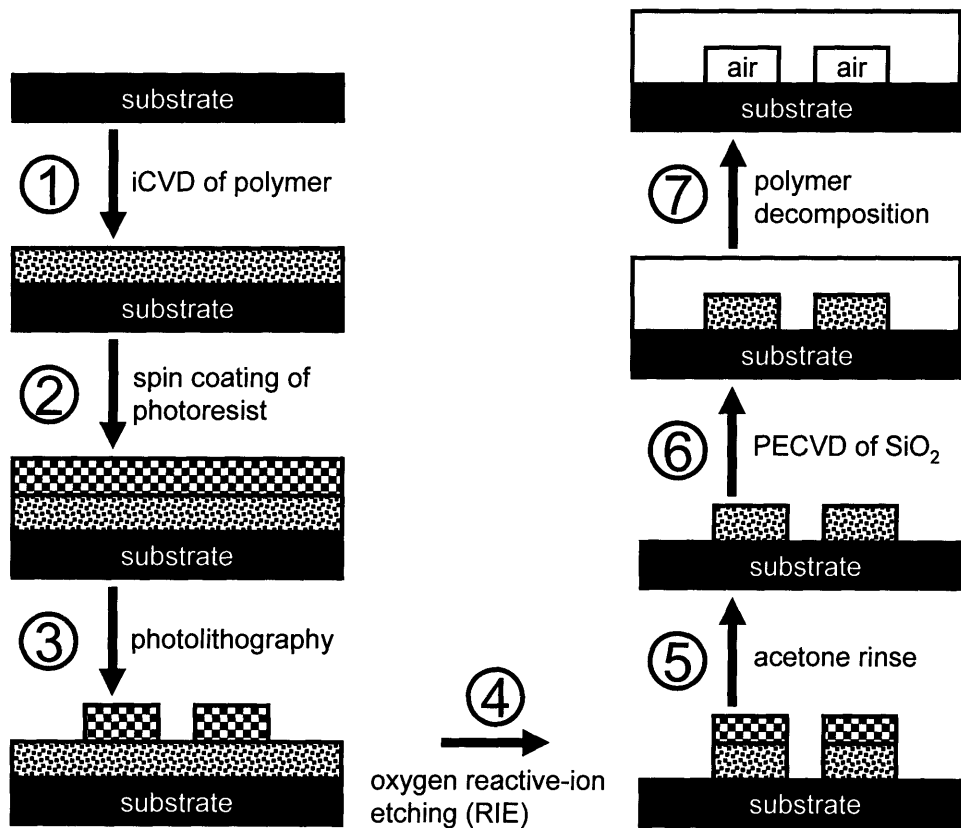


Figure 3–3. Fabrication scheme used to make a single-level air-gap prototype. The topography after PECVD is not explicitly represented.

Scanning electron microscopy. The void structures were observed under a FEI/Philips XL30 environmental scanning electron microscope (Philips, The Netherlands). The samples were cleaved with a diamond scribe prior to observation, and the cross-section was coated with approximately 100 Å of gold

using evaporative deposition. Samples were mounted on stages for cross-sectional view under the microscope for imaging.

3.3 iCVD POLYMER FILM PROPERTIES

Chemical structure. The chemical structure of a polymer is crucial to its applications, and in this work the methacrylate nature of P(CHMA-*co*-EGDMA) is important for its clean decomposition. Figure 3-4 shows the FTIR spectrum of the iCVD film of P(CHMA-*co*-EGDMA). The spectrum contains peaks that are characteristic of methacrylates: C-H stretching (3100-2800 cm^{-1}), C=O (centered at 1724 cm^{-1}), C-H bending (1500-1350 cm^{-1}), and C-O stretching (1300-1200 cm^{-1}). These assignments are based on the FTIR analysis of PMMA³⁹ and on the FTIR reference by Lin-Vien *et al.*⁴⁰ Compared to the FTIR spectrum of PMMA,³⁹ the spectrum in Figure 3-4 shows a much higher intensity of C-H stretching relative to that of C=O stretching, which is expected because CHMA has many more C-H bonds than MMA does. This high C-H intensity indicates the incorporation of CHMA in the copolymer because the C-H to C=O ratio is even lower for EGDMA (CHMA has 16 C-H bonds per C=O bond; MMA has 8; EGDMA has 7). This high incorporation of the pendant cyclohexyl rings indicates that iCVD is a nondestructive process and is able to retain the functionality. The methacrylate nature of the monomers must be retained in order to attain a clean decomposition, which is why iCVD is preferred over PECVD for this particular application. The peaks associated with EGDMA are embedded within the CHMA peaks and are not distinguishable.

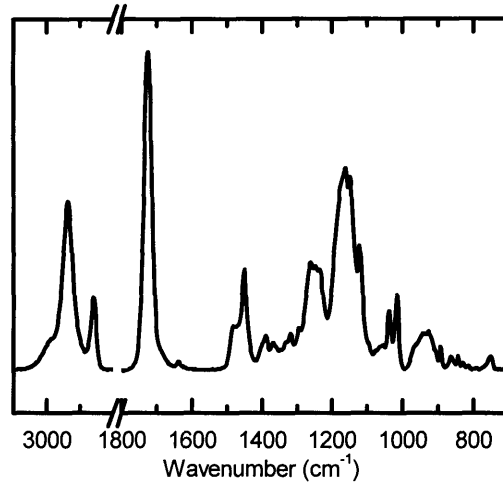


Figure 3-4. Absorbance infrared spectrum of iCVD P(CHMA-co-EGDMA).

Stability in solvents. It is important that the sacrificial polymer film is stable against solvents commonly used in microfabrication. Cross-linking is a prominent way of making the polymer insoluble in solvents. iCVD offers in situ cross-linking of polymer in one step with the use of a cross-linker, which is the primary reason why it was chosen to be the method of choice in this work. The iCVD copolymer film is insoluble in acetone, unlike the homopolymer of CHMA. Acetone is used in the stripping of the photoresist in this work, and the sacrificial film must be stable against acetone for successful patterning. This insolubility proves that the copolymer film is cross-linked and EGDMA is incorporated into the film, which was difficult to realize from the FTIR spectrum in Figure 3-4. Although PECVD also synthesizes as-deposited, cross-linked polymers, it is a more destructive method and is often unable to have high functionality retention. For instance, the PECVD of PMMA has resulted in loss of structural homogeneity due to undesired bond breaking,⁴¹⁻⁴⁷ while the iCVD PMMA has shown good structural resemblance to conventional PMMA.³⁴ Not only does the iCVD copolymer not dissolve in acetone, it also does not delaminate from the Si substrate when soaked in acetone. Adherence to substrate is as important as insolubility. Cross-linked polymers tend to swell in

solvents that dissolve the corresponding homopolymers. Sometimes the degree of swelling is so high that the interfacial stress between the swollen film and the substrate causes delamination. In addition to acetone, the iCVD polymer film is also stable against water and alcohols. Aqueous-based solutions are used in photoresist development, and alcohols are commonly used for cleaning and rinsing.

Thermal properties. Both the cleanliness of decomposition and the thermal stability are important characteristics of a sacrificial polymer. While it is required to decompose cleanly leaving behind negligible residue, it also has to be stable up to a certain temperature to prevent premature deposition. This requirement is necessary because other microfabrication steps may be operated at high temperatures. In the work in this chapter, the depositions of silicon dioxide and silicon nitride were run at a substrate temperature of 250 °C, so the polymer in use must be stable up to this temperature. ITS results indicate that the onset of thermal decomposition of the iCVD copolymer is at approximately 270 °C. The thickness remaining on the Si substrate as measured by VASE after decomposition in the ITS apparatus was consistently less than 40 Å. Compared to the initial film thickness of over 14,000 Å, the final thickness corresponds to a thickness decrease of 99.7%. The iCVD copolymer thus satisfies both the criteria of cleanliness of decomposition and thermal stability. The results here also support the hypothesis that cross-linking does not hinder decomposition. P(CHMA-co-EGDMA), although cross-linked, is still composed of methacrylates. The unzipping of methacrylate monomer units from polymer chains are expected to proceed regardless of whether the unit is monofunctional or bifunctional. Figure 3-5 details this unzipping mechanism involving a cross-linking agent. As can be seen, the two chains are linked together in the middle by EGDMA. Unzipping starts when main-chain scission has occurred at a certain point along the chain (represented by the radical at the end of the chain). The depropagation, or depolymerization, releases CHMA

units from the chains. Within individual chain, the backbone is composed of entirely methacrylate units, so unzipping can proceed although the polymer is cross-linked. As the chains unzip, the cross-linker EGDMA is eventually released, even though one end of the molecule may be released prior to the other. While the composition of the iCVD copolymer in this work is arbitrary, it is believed that the relative amounts of CHMA and EGDMA do not cast a significant effect on the cleanliness of decomposition. Since both monomers are methacrylates, the main-chain C-C bonding within the copolymer is homogeneous. As thermal decomposition of methacrylates involves main-chain scission, the thermal properties of interest are anticipated to be largely independent of the composition. In fact, it has been observed that cross-linking with EGDMA does not affect the amount of residue remaining after decomposition.⁴⁸ In some cases,^{48,49} cross-linking with EGDMA actually decreases thermal stability and results in a lower onset temperature of decomposition.

The results here show that iCVD is able to create a cross-linked polymer with well-defined chemical structure that does not dissolve in solvents but at the same time is able to decompose cleanly.

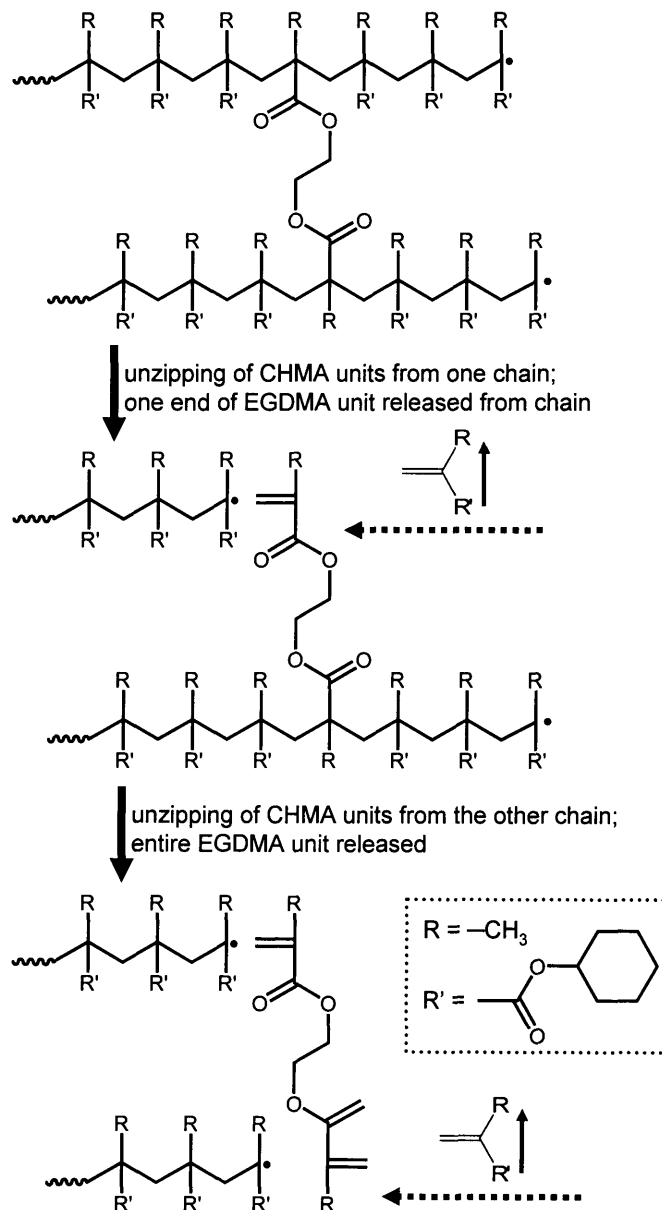


Figure 3–5. Details of the unzipping mechanism involving the cross-linker EGDMA. Main-chain scission results in depropagation by release of CHMA units. The cross-linker EGDMA is eventually released when the chains with which it is associated have both unzipped through the point of cross-linking.

3.4 SINGLE-LEVEL AIR-GAP FABRICATION

A number of properties of iCVD P(CHMA-co-EGDMA) contribute to its success in the fabrication process: (1) it has good adhesion to both the substrate and the PR; (2) it has a high etch rate (0.35 $\mu\text{m}/\text{min}$), so the pattern transfer does not require a separate layer of hard mask; (3) it does not dissolve or delaminate when soaked in acetone for PR stripping; (4) it has a sufficiently high onset temperature of decomposition (270 $^{\circ}\text{C}$) to survive the PECVD of SiO_2 ; and (5) most importantly it decomposes cleanly leaving behind negligible residue. During annealing, the methacrylate copolymer reverts back to its comonomers through unzipping from scissioned chained ends. The comonomers exit either via diffusion through the top SiO_2 layer or through the ends of the open channels.

FTIR analyses in Figure 3-6 show the removal of the iCVD copolymer upon thermal annealing. Figure 3-6b is the absorbance spectrum taken via infrared transmission through the bilayer of PECVD SiO_2 and the iCVD copolymer. As anticipated, it shows characteristic peaks of both the copolymer (Figure 3-6a) and PECVD SiO_2 (Figure 3-6c). In particular, the bilayer is showing absorption of C-H and C=O stretching, a signature of the iCVD polymer, and both symmetric and asymmetric Si-O-Si stretching, key infrared bands of SiO_2 . After thermal annealing, the infrared spectrum (Figure 3-6d) contains only the bands of SiO_2 but not those of the iCVD copolymer, indicating that thermal decomposition has occurred. The fact that the C-H and C=O stretching bands have completely disappeared corroborates the clean deposition result from the ITS study.

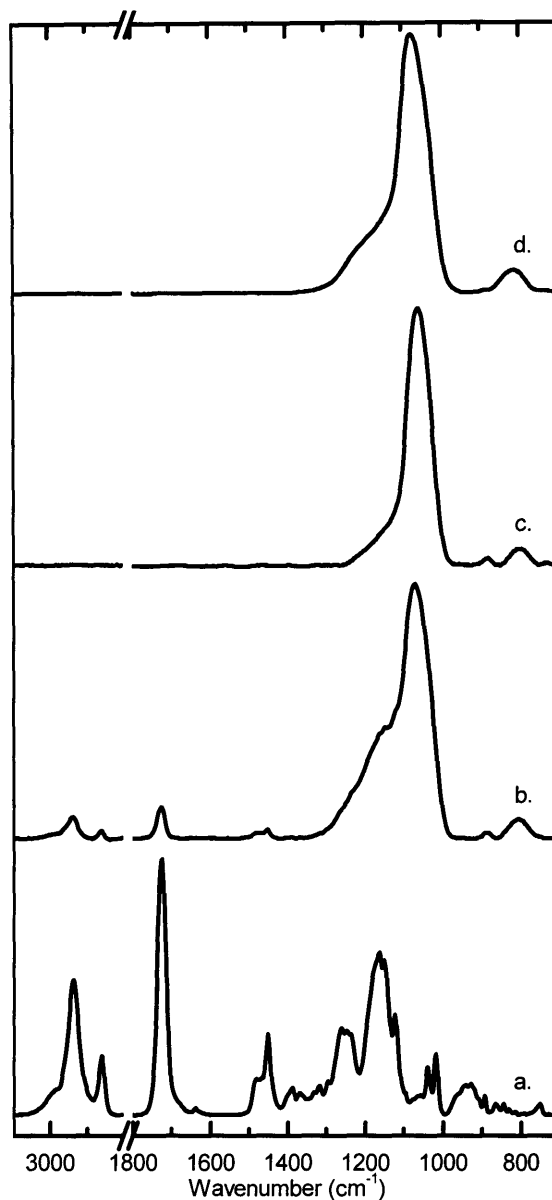


Figure 3-6. FTIR spectra of (a) iCVD cross-linked PCHMA, (b) air-gap structure before annealing comprised of PECVD SiO₂ on top of iCVD cross-linked PCHMA, (c) PECVD SiO₂, and (d) air-gap structure after annealing. The absence of the C–H stretching bands (3050–2800 cm⁻¹) and the C=O stretching band (centered at 1726 cm⁻¹) in (d) indicates removal of cross-linked PCHMA during annealing.

Environmental scanning electron microscopy was also used to visualize the air-gap formation. Figure 3-7 shows the single-level air-gap microstructure made using the fabrication scheme outlined in the experimental section of this chapter.

Both of the pictures in the figure show an approximately 0.5- μm -thick cavity sandwiched between the top SiO_2 layer and the underlying Si substrate. There is no apparent contrast between SiO_2 and Si in the pictures because the cross-sections were coated with gold. Both air gaps were made using the same photomask on the same piece of substrate. The widths of the air gaps, 1.5 and 5 μm , correspond well to the widths of the lines on the mask, although there is undercut due to oxygen-plasma etching. In addition, there are no visible defects in the SiO_2 layer above the cavity, meaning that the annealing of the polymer to form monomers did not cause damages. This result shows that the sacrificial polymer is compatible with SiO_2 as an overcoat. The slight sagging of the 5- μm -wide air-gap structure is likely due to the intrinsic compressive stress within PECVD SiO_2 . With better photolithographic tools, narrower air gaps may be fabricated because the widths depend solely on lithographic imaging. On the other hand, the heights of the structures depend on the thicknesses of the iCVD copolymer layers, which can be controlled via timed depositions.

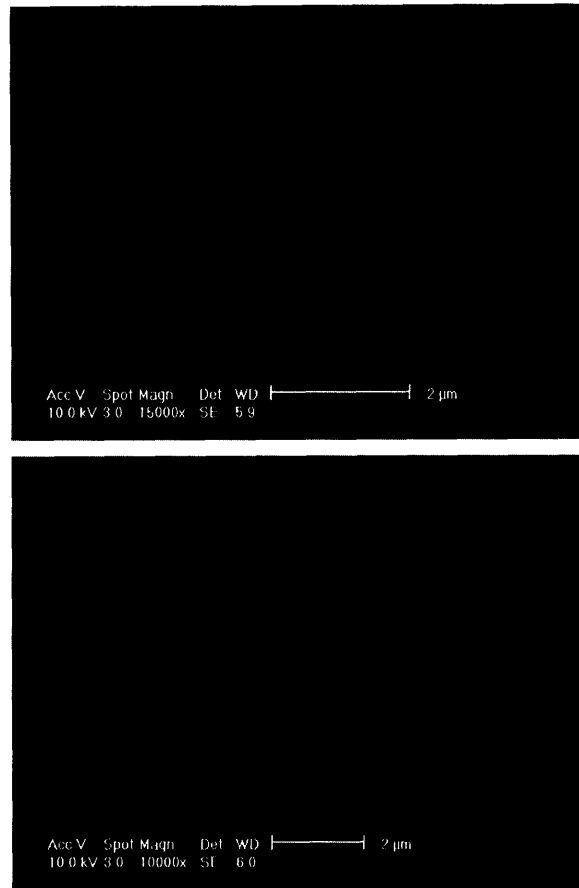


Figure 3–7. Cross–sectional scanning electron micrograph depicting the single–level air–gap structure.

3.5 CONCLUSIONS

This work shows that iCVD P(CHMA-*co*-EGDMA) is a viable sacrificial material for fabricating void-containing microstructures. The decomposition of the polymer under a nitrogen atmosphere is clean, leaving behind less than 0.3% of residue by thickness, yet the onset temperature of decomposition is high at 270 °C, allowing it to survive other high-temperature microfabrication steps. The clean deposition supports the hypothesis that this manner of cross-linking does not hinder decomposition and cause char formation. Although cross-linked, the polymer is composed of entirely methacrylates. The unzipping of monomers from

polymer chains during decomposition is able to proceed even though EGDMA is bifunctional. Due to cross-linking, the polymer is insoluble in practically any solvents and does not delaminate from the substrate when soaked in acetone, which is used to remove photoresists. This insolubility in addition to the use of no hard mask simplifies the overall fabrication process. The iCVD polymer also exhibits good adhesion to Si substrates and the photoresist, making fabrication of the single-level air-gap structure possible. Infrared spectra and ESEM pictures clearly show the removal of the polymer.

The polymer possesses desirable properties of a sacrificial material, but the key to its thin films is iCVD. iCVD is able to produce polymers with no loss of functionality and with full methacrylic content. The ability to produce a cross-linked network within a thin film without secondary processing and without solvents is the key inspiration in this work. The need for no hard mask represents an improvement over previously-reported spin-on sacrificial polymers.^{6,7,17,29} Unlike directly-patternable sacrificial polymers,^{14,15,24,25} the polymer presented here does require the use of a photoresist, but the feature sizes of void structures made from these polymers are much larger than the one reported here or the patterning requires the use of an electron beam. With a state-of-the-art photoresist, very small features may be fabricated using the iCVD polymer. This use of a photoresist eliminates the need for fine tuning both the thermal and the lithographic properties, as needed for directly-patternable sacrificial polymers. In addition, the feasibility of engineering polymers on the surface potentially allows tuning of mechanical and thermal properties by adding other monomer(s) to the system.

REFERENCES

- (1) Madou, M. J. *Fundamentals of Microfabrication: the Science of Miniaturization*, 2nd ed.; CRC Press: Boca Raton, FL, 2002.
- (2) Senturia, S. D. *Microsystem Design*; Kluwer Academic Publishers: Boston, MA, 2003.
- (3) Anand, M. B.; Yamada, M.; Shibata, H. *IEEE Trans. Electron Devices* 1997, 44, 1965.
- (4) Kohl, P. A.; Zhao, Q.; Patel, K.; Schmidt, D.; Bidstrup-Allen, S. A.; Shick, R.; Jayaraman, S. *Electrochem. Solid State Lett.* 1998, 1, 49.
- (5) Kohl, P. A.; Bhusari, D. M.; Wedlake, M.; Case, C.; Klemens, F. P.; Miner, J.; Lee, B. C.; Gutmann, R. J.; Shick, R. *IEEE Electron Device Lett.* 2000, 21, 557.
- (6) Reed, H. A.; White, C. E.; Rao, V.; Allen, S. A. B.; Henderson, C. L.; Kohl, P. A. *J. Micromech. Microeng.* 2001, 11, 733.
- (7) Bhusari, D.; Reed, H. A.; Wedlake, M.; Padovani, A. M.; Allen, S. A. B.; Kohl, P. A. *J. Microelectromech. Syst.* 2001, 10, 400.
- (8) Ho, S. T.; McCall, S. L.; Slusher, R. E.; Pfeiffer, L. N.; West, K. W.; Levi, A. F. J.; Blonder, G. E.; Jewell, J. L. *Appl. Phys. Lett.* 1990, 57, 1387.
- (9) Tsai, J. Y.; Lu, T. C.; Wang, S. C. *Solid-State Electron.* 2003, 47, 1825.
- (10) Irmer, S.; Alex, K.; Daleiden, J.; Kommallein, I.; Oliveira, M.; Romer, F.; Tarraf, A.; Hillmer, H. *J. Micromech. Microeng.* 2005, 15, 867.
- (11) Spisser, A.; Ledantec, R.; Seassal, C.; Leclercq, J. L.; Benyattou, T.; Rondi, D.; Blondeau, R.; Guillot, G.; Viktorovitch, P. *IEEE Photonics Technol. Lett.* 1998, 10, 1259.
- (12) Streubel, K.; Rapp, S.; Andre, J.; Chitica, N. *Mater. Sci. Eng. B-Solid State Mater. Adv. Technol.* 1997, 44, 364.
- (13) Leclercq, J. L.; Garrigues, M.; Letartre, X.; Seassal, C.; Viktorovitch, P. *J. Micromech. Microeng.* 2000, 10, 287.
- (14) Harnett, C. K.; Coates, G. W.; Craighead, H. G. *J. Vac. Sci. Technol. B* 2001, 19, 2842.
- (15) Metz, S.; Jiguet, S.; Bertsch, A.; Renaud, P. *Lab Chip* 2004, 4, 114.
- (16) Peeni, B. A.; Conkey, D. B.; Barber, J. P.; Kelly, R. T.; Lee, M. L.; Woolley, A. T.; Hawkins, A. R. *Lab Chip* 2005, 5, 501.
- (17) Li, W. L.; Tegenfeldt, J. O.; Chen, L.; Austin, R. H.; Chou, S. Y.; Kohl, P. A.; Krotine, J.; Sturm, J. C. *Nanotechnology* 2003, 14, 578.
- (18) Yin, D.; Schmidt, H.; Barber, J. P.; Hawkins, A. R. *Opt. Express* 2004, 12, 2710.
- (19) Barber, J. P.; Conkey, D. B.; Lee, J. R.; Hubbard, N. B.; Howell, L. L.; Yin, D. L.; Schmidt, H.; Hawkins, A. R. *IEEE Photonics Technol. Lett.* 2005, 17, 363.

- (20) Wu, X. Q.; Reed, H. A.; Rhodes, L. F.; Elce, E.; Ravikiran, R.; Shick, R. A.; Henderson, C. L.; Allen, S. A. B.; Kohl, P. A. *J. Electrochem. Soc.* 2002, 149, G555.
- (21) Padovani, A. M.; Rhodes, L.; Riester, L.; Lohman, G.; Tsuie, B.; Conner, J.; Allen, S. A. B.; Kohl, P. A. *Electrochem. Solid State Lett.* 2001, 4, F25.
- (22) Wu, X. Q.; Reed, H. A.; Rhodes, L. F.; Elce, E.; Ravikiran, R.; Shick, R. A.; Henderson, C. L.; Allen, S. A. B.; Kohl, P. A. *J. Appl. Polym. Sci.* 2003, 88, 1186.
- (23) Kohl, A. T.; Mimna, R.; Shick, R.; Rhodes, L.; Wang, Z. L.; Kohl, P. A. *Electrochem. Solid State Lett.* 1999, 2, 77.
- (24) Jayachandran, J. P.; Reed, H. A.; Zhen, H. S.; Rhodes, L. F.; Henderson, C. L.; Allen, S. A. B.; Kohl, P. A. *J. Microelectromech. Syst.* 2003, 12, 147.
- (25) Wu, X. Q.; Reed, H. A.; Wang, Y.; Rhodes, L. F.; Elce, E.; Ravikiran, R.; Shick, R. A.; Henderson, C. L.; Allen, S. A. B.; Kohl, P. A. *J. Electrochem. Soc.* 2003, 150, H205.
- (26) Loo, L. S.; Gleason, K. K. *Electrochem. Solid State Lett.* 2001, 4, G81.
- (27) Suh, H. J.; Bharathi, P.; Beebe, D. J.; Moore, J. S. *J. Microelectromech. Syst.* 2000, 9, 198.
- (28) Kobayashi, D.; Kim, C. J.; Fujita, H. *Jpn. J. Appl. Phys. Part 2 – Lett.* 1993, 32, L1642.
- (29) Joseph, P. J.; Kelleher, H. A.; Allen, S. A. B.; Kohl, P. A. *J. Micromech. Microeng.* 2005, 15, 35.
- (30) Casserly, T. B.; Gleason, K. K. *Chem. Vapor Deposition* 2005, submitted.
- (31) Morosoff, N. In *Plasma Deposition, Treatment, and Etching of Polymers*; d'Agostino, R., Ed. Academic Press: Boston, MA, 1990; p 1.
- (32) Yasuda, H. *Plasma Polymerization*; Academic: Orlando, FL, 1985.
- (33) Inagaki, N. *Plasma Surface Modification and Plasma Polymerization*; Technomic: Lancaster, PA, 1996.
- (34) Chan, K.; Gleason, K. K. *Chem. Vapor Deposition*, 2005, submitted.
- (35) Chan, K.; Gleason, K. K. *Langmuir* 2005, accepted.
- (36) Murthy, S. K.; Olsen, B. D.; Gleason, K. K. *Langmuir* 2002, 18, 6424.
- (37) Mao, Y.; Gleason, K. K. *Langmuir* 2004, 20, 2484.
- (38) Pryce Lewis, H. G.; Caulfield, J. A.; Gleason, K. K. *Langmuir* 2001, 17, 7652.
- (39) Nagai, H. *J. Appl. Polym. Sci.* 1963, 7, 1697.
- (40) Lin-Vien, D.; Colthup, N. B.; Fateley, W. G.; Grasselli, J. G. *The Handbook of Infrared and Raman Characteristic Frequencies of Organic Molecules*; Academic Press: San Diego, CA, 1991.
- (41) Morita, S.; Tamano, J.; Hattori, S.; Ieda, M. *J. Appl. Phys.* 1980, 51, 3938.
- (42) Yamada, M.; Tamano, J.; Yoneda, K.; Morita, S.; Hattori, S. *Jpn. J. Appl. Phys. Part 1 – Regul. Pap. Short Notes Rev. Pap.* 1982, 21, 768.

- (43) Li, G. F.; Tobin, J. A.; Denton, D. D. *Appl. Phys. Lett.* **1993**, *62*, 1582.
- (44) Pan, Y. V.; Barrios, E. Z.; Denton, D. D. *J. Polym. Sci. Pol. Chem.* **1998**, *36*, 587.
- (45) Pan, Y. V.; Barrios, E. Z.; Denton, D. D. *Appl. Phys. Lett.* **1996**, *68*, 3386.
- (46) Zhang, C.; Wyatt, J.; Weinkauff, D. H. *Polymer* **2004**, *45*, 7665.
- (47) Jeon, H. S.; Wyatt, J.; Harper-Nixon, D.; Weinkauff, D. H. *J. Polym. Sci., Part B: Polym. Phys.* **2004**, *42*, 2522.
- (48) Levchik, G. F.; Si, K.; Levchik, S. V.; Camino, G.; Wilkie, C. A. *Polym. Degrad. Stabil.* **1999**, *65*, 395.
- (49) Varma, I. K.; Patnaik, S. *J. Polym. Sci. Pol. Chem.* **1979**, *17*, 3279.

CHAPTER FOUR

A MECHANISTIC STUDY OF INITIATED CHEMICAL VAPOR DEPOSITION: ANALYSES OF DEPOSITION RATE AND MOLECULAR WEIGHT

ABSTRACT

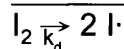
The work in this chapter studies the effects of changing equilibrium monomer surface concentration on the deposition rates and the number-average molecular weights, M_n , of polymers deposited from glycidyl methacrylate and cyclohexyl methacrylate using initiated chemical vapor deposition (iCVD) with *tert*-butyl peroxide as the initiator. Both the surface temperature and the monomer partial pressure were varied to effect different surface concentrations, measured using a quartz-crystal microbalance. In both cases, the deposition rate and M_n were found to be linear in equilibrium monomer surface concentration. This strong dependence concludes that chain propagation occurs predominantly on the surface and suggests that the surface concentration is at equilibrium during iCVD, which in turn infers that the adsorption of monomer is not the rate-limiting step in the polymerization process.

4.1 INTRODUCTION

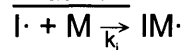
Initiated chemical vapor deposition (iCVD) is a novel technique of depositing polymeric thin films. It has been used to deposit a wide variety of polymers such as poly(methyl methacrylate),¹ poly(2-hydroxyethyl methacrylate) and its copolymers,² poly(glycidyl methacrylate) (PGMA),³ poly(tetrafluoroethylene),⁴ and fluorocarbon-organosilicon copolymer.⁵ iCVD is a subset of hot-filament chemical vapor deposition (HFCVD) in which selective thermal decomposition of species is achieved using resistively-heated filaments. The substrate to be coated is backside-cooled to promote adsorption of species. iCVD differs from HFCVD on one main count—an initiator in addition to the monomer is fed into the chamber. For example, *tert*-butyl peroxide (TBPO) has been used in the iCVD of PGMA.³ Much like conventional free-radical polymerization, iCVD proceeds via four elementary reaction steps shown in Figure 4-1. Monomer and initiator are fed into an iCVD chamber as vapors. Radical generation is the process of breaking down the initiator molecule into radicals. These radicals in turn initiate the polymerization by attacking the vinyl bonds of the monomer molecules. Propagation proceeds via successive additions of monomer molecules to the growing radical chains. Termination refers to the annihilation of radicals by coupling or disproportionation. In conventional free-radical polymerization, all these reaction steps happen in the same phase with all their kinetics controlled by a single temperature. In the case of iCVD, there has not been a consensus of where propagation and termination occur predominantly, although radical generation is believed to occur in the gas phase.¹⁻⁵ Propagation and termination can occur in the gas phase, on the surface, or both. The goal of this work is to provide data on the surface absorption of the vinyl monomers and to determine the relationship of this adsorption to the overall deposition kinetics and number-average molecular weights of the deposited polymeric films. It is

important to realize that this work does not intend to make generalization of all iCVD systems. The exact locations of reactions depend strongly on reaction conditions inside the chamber. The study here serves as a groundwork for increased understanding of iCVD as a method for depositing polymeric thin films.

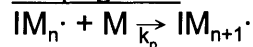
Radical generation (gas phase/filament)



Initiation



Propagation



Termination

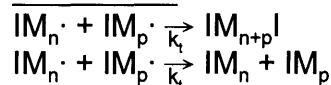


Figure 4-1. Free-radical polymerization scheme. I_2 = initiator; $I\cdot$ = initiating radical; M = monomer; $IM_x\cdot$ = growing radical chain (where x is any integer).

Two methacrylic monomers and TBPO have been used in this study and are shown in Figure 4-2. Glycidyl methacrylate (GMA) and cyclohexyl methacrylate (CHMA) were chosen because of their iCVD success and their solubility in tetrahydrofuran (THF) for gel-permeation chromatography. The surface concentration was determined using a quartz-crystal microbalance (QCM), whereas the deposition rate and the molecular weight were determined from the iCVD experiments. The surface concentration cannot be determined during iCVD because a polymer film would be deposited on the crystal and make static surface concentration measurement impossible. The surface concentrations measured using the QCM are equilibrium values, but the actual surface concentration during iCVD may or may not be at equilibrium. It must be therefore emphasized that the

analysis here is to correlate equilibrium surface concentration to deposition rate and molecular weight. If there is a strong correlation, propagation likely happens predominantly on the surface. The surface concentration can be altered via two parameters: the surface temperature and the partial pressure. In this chapter, a section is devoted to the effects of each of these parameters.

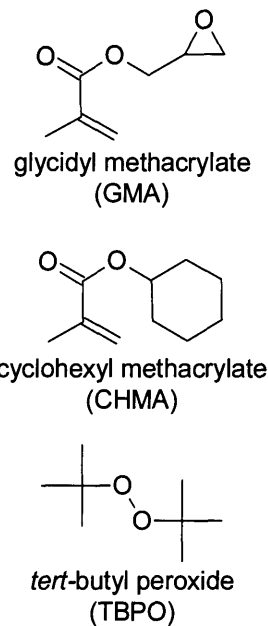


Figure 4-2. Monomers and initiator used in this work.

4.2 EXPERIMENTAL METHODS

4.2.1 ICVD EXPERIMENTS

Films were deposited on 100-mm-diameter silicon (Si) substrates in a custom-built vacuum chamber. The inside of the chamber was cylindrical with a height of 3.3 cm and a radius of 12 cm. The inlet of precursor gases and the exhaust were at opposite ends of the chamber. The top of the chamber was covered by a removable quartz plate (~15 cm radius and 2.5 cm thick), allowing

placement of substrate, visual inspection, and laser interferometry. The chamber was equipped with a filament array, which provided thermal energy for selective decomposition of molecules. The clearance between the filaments and the stage was 29 mm. The Nichrome filaments (80% Ni/20% Cr, AWG 26, Omega Engineering) were resistively heated to 330 °C, as measured by a thermocouple (Type K, AWG 36, Omega Engineering) directly attached to one of them. The chamber had a backside-cooled stage on which the substrate was placed and maintained at a constant temperature adjustable between 25 and 45 °C. The chamber pressure was maintained at 500 mTorr with a throttling butterfly valve (Intellisys, Nor-Cal).

The monomers GMA (97.0%+, Aldrich) and CHMA (97.0%, Aldrich) and the initiator TBPO (98%, Aldrich) were used without further purification. GMA liquid was vaporized in a glass jar maintained at 50 ± 1 °C, and this vapor was metered into the chamber through a mass-flow controller (Model 1152C, MKS). The CHMA liquid was treated the same way except that the jar was kept at a higher temperature of 60 ± 1 °C. TBPO was maintained at room temperature in a glass jar, and its vapor was metered into the chamber through a different mass-flow controller (Model 1479A, MKS). At any time only one monomer was used together with TBPO. Monomer and TBPO vapors were mixed together before entering the chamber through a side port. Depositions were monitored using an interferometry system equipped with a 633-nm HeNe laser source (JDS Uniphase). The cycle thickness was calculated by dividing the actual thickness, as measured using variable-angle spectroscopic ellipsometry (VASE), by the number of cycles. VASE was performed on a J. A. Woollam M-2000 spectroscopic ellipsometer with a xenon light source. Data were acquired at three angles (65°, 70°, and 75°) and 225 wavelengths, and the Cauchy-Urbach model was used to fit the data.

Table 4-1 details the four sets of iCVD runs in this work. They are divided into two main categories: temperature and pressure series. In the temperature

series, samples were made with the substrate temperature varied between 25 and 45 °C and other parameters fixed. Samples TG and TC are two sets of such samples. In the pressure series, samples were made with varying monomer partial pressure and other parameters fixed. Samples PG and PC are two sets of such samples. It should be noted that in the pressure series the total flow rate was kept constant with a patch flow of nitrogen (N₂) while the monomer flow rate was varied. This setup was to maintain the same residence time for all runs. The total flow rate (6 sccm), the filament temperature (330 °C), and the chamber pressure (500 mTorr) were the same for all 23 samples in Table 1. For each of the iCVD runs, the flow rates and the chamber pressure were allowed time to stabilize before voltage was supplied to the filament. All samples were grown to an approximate thickness of 1.3 μm.

Table 4-1. Details of iCVD experiments.

iCVD Sample	Monomer	Sub. Temp. (°C)	Flow Rate (sccm)			Partial Pressure (mTorr)
			Monomer	TBPO	N ₂	Monomer
TG1	GMA	25	3.0	1.0	2.0	250
TG2	GMA	30	3.0	1.0	2.0	250
TG3	GMA	35	3.0	1.0	2.0	250
TG4	GMA	40	3.0	1.0	2.0	250
TG5	GMA	45	3.0	1.0	2.0	250
TC1	CHMA	25	2.0	1.0	3.0	167
TC2	CHMA	30	2.0	1.0	3.0	167
TC3	CHMA	35	2.0	1.0	3.0	167
TC4	CHMA	40	2.0	1.0	3.0	167
TC5	CHMA	45	2.0	1.0	3.0	167
PG1	GMA	35	3.5	1.0	1.5	292
PG2	GMA	35	3.0	1.0	2.0	250
PG3	GMA	35	2.5	1.0	2.5	208
PG4	GMA	35	2.0	1.0	3.0	167
PG5	GMA	35	1.5	1.0	3.5	125
PC1	CHMA	35	2.5	1.0	2.5	208
PC2	CHMA	35	2.0	1.0	3.0	167
PC3	CHMA	35	1.5	1.0	3.5	125

Films were dissolved in tetrahydrofuran (THF) for GPC measurements. The GPC system was comprised of a Waters 1515 isocratic high-performance liquid chromatography (HPLC) pump, a Waters 2414 refractive index detector, and two Styragel® HR 4 7.8 × 300 mm columns. Poly(methyl methacrylate) (PMMA) standards (Polymer Laboratories, Amherst, MA) dissolved in THF were used for calibration at 35 °C.

4.2.2 QUARTZ-CRYSTAL MICROBALANCE MEASUREMENTS

A quartz-crystal microbalance (QCM, Model VSO-100) with a 14-mm-diameter gold-coated quartz sensor crystal (Model 500-117) was obtained from

Sycon Instruments (Syracuse, NY). It was placed inside the iCVD chamber described in Section 2.1 and was actively cooled or heated with temperature-controlled water. The QCM output its signal to a board monitor (Model STM-1, Sycon) through industry-standard coaxial cables via a filter (Model OSC-100A, Sycon). The board monitor was connected to a Windows-based computer through its RS-232 interface with USB interface conversion. Software supplied by Sycon installed on the computer monitored the thickness of material on the sensor crystal.

The QCM was used to obtain surface monomer concentration data. The software was configured to output the thickness of material. Thicknesses in angstroms were converted to normalized monomer surface concentrations, [M], in arbitrary units using Equation 4-1. This normalization is a conversion from the thickness to a quantity representative of the number of molecules on the surface. The reference thickness is taken to be the lowest thickness obtained in this work for GMA (reference molecular weight = 142.15 g/mol).

$$[M] = \frac{d}{FW} \bigg/ \frac{d_r}{FW_r} \quad 4-1$$

where

[M] = monomer surface concentration (in a.u.)

d = thickness (in Å)

FW = formula weight of monomer (in g/mol)

d_r = reference thickness (5.41 Å)

FW_r = reference formula weight (142.15 g/mol)

Eighteen different QCM measurements were done to mimic the iCVD conditions listed in Table 1. The only differences between the corresponding QCM conditions were that TBPO was replaced with nitrogen and the filaments were off. For instance, the corresponding QCM measurement for iCVD Sample TG1 in Table 4-1 was performed with a QCM temperature of 25 °C, a GMA flow rate of 3.0 sccm,

a nitrogen flow rate of 3.0 sccm, and total pressure of 500 mTorr. The flow rates and the total pressure were allowed time to stabilize before the QCM was turned on. When the thickness measured by the QCM stabilized at a constant value, data logging was started and the nitrogen flow rate was increased to 6.0 sccm. Immediately after the flow of nitrogen was increased, the monomer flow was stopped, so that the only species flowing through the chamber was nitrogen. This procedure purged the reactor with nitrogen while maintaining the total pressure at 500 mTorr. The monomer molecules that were previously adsorbed onto the QCM desorbed from the surface because the monomer partial pressure decreased to zero due to purging, causing the measured thickness to decrease. When the thickness stabilized and stopped fluctuating, data logging was halted. The difference between the final and the initial thicknesses corresponds to the amount of monomer that was desorbed from the sensor crystal and represents the equilibrium monomer surface concentration under the conditions before the nitrogen flow was increased and the monomer flow was stopped. The thickness differentials were converted to surface concentrations using Equation 4-1.

4.3 RESULTS AND DISCUSSION

4.3.1 EFFECTS OF SURFACE TEMPERATURE ON DEPOSITION RATE AND MOLECULAR WEIGHT

Figure 4-3 shows the QCM data of equilibrium surface concentration as a function of surface temperature. Everything but the crystal temperature was fixed in these measurements. The crystal temperature was varied between 25 and 45 °C in 5-°C increments. The partial pressures of GMA and CHMA were fixed at 208 and 167 mTorr, respectively. These pressures were chosen to avoid condensation at 25

°C and to match those of iCVD experiments (Series TG and TC in Table 4-1). As seen from Figure 4-3, the equilibrium surface concentration increases with decreasing surface temperature in a nonlinear manner.

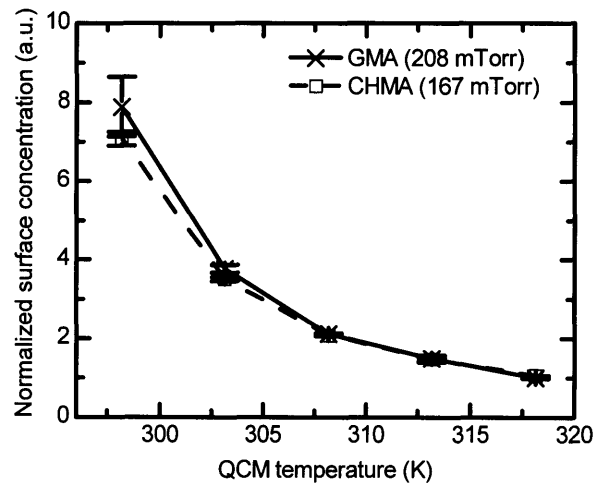


Figure 4-3. Equilibrium monomer surface concentration as a function of surface temperature as measured by the quartz-crystal microbalance (QCM). The partial pressure of GMA was fixed at 208 mTorr for the experiment, while that of CHMA was set at 167 mTorr.

iCVD experiments were run with the same conditions used for the QCM measurements. The design was to keep the partial pressure of the monomer in the gas phase constant while varying the substrate temperature but holding all other reactor settings constant. In the gas phase, initiator molecules are broken down into initiating radicals, and it is assumed that the change in substrate temperature does not affect the gas temperature. Therefore, the kinetics of radical generation and the gas-phase concentration of the initiating radicals stayed constant in both the TG and the TC series. This assumption is justified because of two reasons. First, the measured filament temperature has never been observed to decrease when lower substrate temperatures are used. Second the heat transfer between the gas phase and the surface at the conditions during iCVD at a vacuum pressure of

500 mTorr was estimated to be poor using the forced convection equation developed for flow parallel to planar surfaces.^{6,7}

Figures 4-4 and 4-5 show the deposition rate and the molecular weight, respectively, as functions of substrate temperature. Both quantities increase with decreasing substrate temperature. Not only do these quantities follow the same trends as the equilibrium surface concentration, they also provide the same nonlinear response as observed in Figure 4-3. This can be seen explicitly by plotting deposition rate and number-average molecular weight, M_n , directly against the equilibrium surface concentration. These graphs can be made because both the deposition and the QCM experiments were designed to have matching conditions—the partial pressure of the monomer, the total pressure, and the total flow rate were identical. The common variable was the surface temperature. Figures 4-6 and 4-7 which plot the deposition rate and M_n , respectively, against equilibrium surface concentration, both show a linear relationship. Each data point is the average of three measurements, and the R^2 values of the linear fits are all higher than 0.97. This strong dependence on substrate temperature/surface concentration is consistent with chain propagation occurring predominantly on the surface because the substrate temperature should have little effect on the molecular weight had the propagation occurred in the gas phase. If propagation occurred in the gas phase, a decrease in substrate temperature would facilitate the adsorption of shorter chains in the gas phase, thereby decreasing instead of increasing the molecular weight. From a different point of view, a higher substrate temperature would filter out the shorter chains, resulting in a higher average molecular weight. The opposite, however, is observed in this work. Additionally, bimolecular gas-phase reactions at hundreds of mTorr are unfavorable (concentrations are in the range of tens of μM based on ideal gas law), and the volatility of species containing more than one monomer unit is very low (a growing chain with two monomer units has a molecular

weight of over 350 g/mol). Altogether these facts strongly support the hypothesis that propagation occurs predominantly on the surface, and the increase in deposition rate and molecular weight can be attributed to the increase in surface concentration of monomer as surface temperature decreases. Additionally, the observation that the deposition rate and M_n align well with the equilibrium surface concentration as measured by the QCM signifies that the surface monomer concentration is likely at equilibrium with its gas-phase concentration during actual deposition. Such an equilibrium indicates that iCVD is not monomer-adsorption limited and the process is subject to some other limitation, which could be the arrival of initiating radicals or propagation. A rate-limiting step is often encountered in heterogeneous reaction systems.⁸

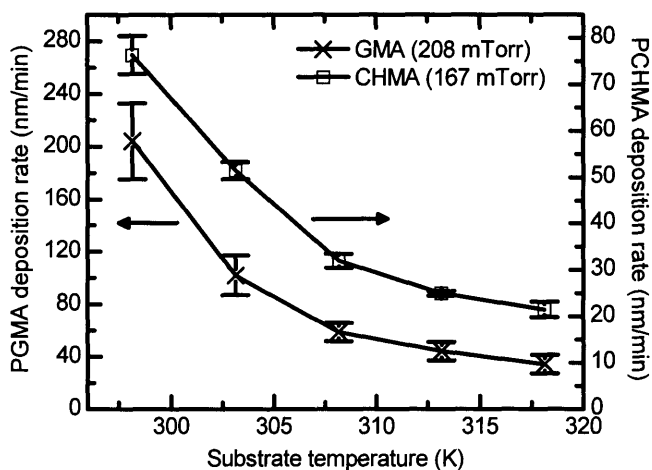


Figure 4-4. Deposition rate as a function of substrate temperature. The partial pressure of GMA was fixed at 208 mTorr, while that of CHMA was maintained at 167 mTorr.

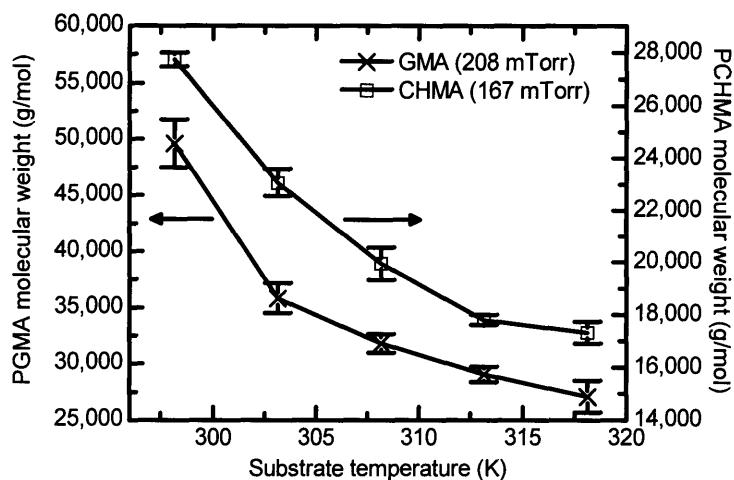


Figure 4-5. Number-average molecular weight as a function of substrate temperature. The partial pressures of GMA and CHMA were set at 208 and 167 mTorr, respectively.

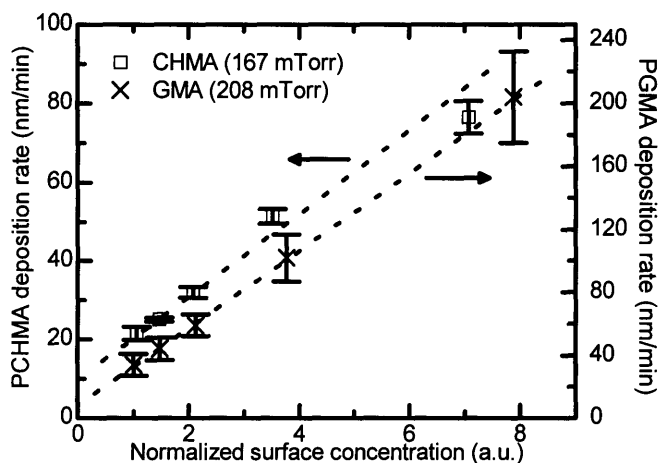


Figure 4-6. Plot of deposition rate data from iCVD experiments against equilibrium surface concentration data from QCM measurements. For each of the monomers, the iCVD and the QCM data were collected at the same monomer partial pressure.

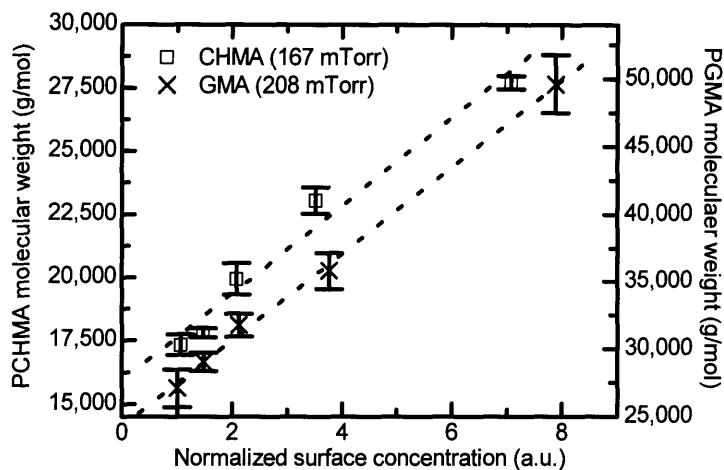


Figure 4-7. Plot of number-average molecular weight from GPC measurements on dissolved iCVD polymer films against equilibrium surface concentration data from QCM measurements. The iCVD and the QCM experiments had matching monomer partial pressures.

4.3.2 MODELING iCVD POLYMERIZATION

The linearity in Figures 4-6 and 4-7 can be rationalized by understanding the kinetics of polymerization. The discussion here will start with a review of the traditional polymerization model and then its extension to the iCVD system. For traditional free-radical polymerization, the kinetic chain length, ν (Equation 4-2), is expressed as a function of the propagation rate constant (k_p), the termination rate constant (k_t), the initiator decomposition rate constant (k_d), the initiator efficiency (f), the monomer concentration ($[M]$), and the initiator concentration ($[I]$).⁹⁻¹¹ The kinetic chain length is a representation of the molecular weight. In the case of hypothetical gas-phase propagation, all the parameters in Equation 4-2 would stay constant despite the change in substrate temperature. As a result, the molecular weight would be unchanged in the gas phase as the substrate temperature decreases, whereas that on the surface would decrease due to the filtering effect as described earlier. Therefore, the increase in molecular weight with decreasing substrate temperature cannot be explained by gas-phase propagation.

$$v = \frac{k_p [M]}{2(fk_d k_t [I])^{0.5}}$$

4-2

To justify that propagation happens on the surface, one needs to develop an expression similar to Equation 4-2, which, however, cannot be used for iCVD because radical generation and propagation do not occur in the same phase and must be treated separately. TBPO decomposes in the gas phase to form *tert*-butoxy radicals, and these radicals travel to the surface to initiate polymerization. It is assumed in the treatment here that this decomposition is the only reaction occurring in the gas phase. The gas phase effectively is a flow reactor for radical generation and is expected to contain a constant concentration of radicals at steady state. As in traditional free-radical treatment, steady-state analysis is performed on the concentration of radicals on the surface, meaning that there is no net accumulation. The objective here is to obtain expressions for the rate of polymerization and the kinetic chain length. The arrival of radicals onto the surface depends on the mass transfer from the gas phase to the substrate. It is expected that adsorption equilibrium is nonexistent for the initiating radicals. Once they collide with the surface, they are expected to react instantaneously, and there should not be an appreciable concentration of radicals on the surface to equilibrate with the gas phase. The consumption of radicals on the surface is by initiation. One can therefore write the balance of radicals as in Equation 4-3. The concentration of I· near the surface is anticipated to be very small, leading to the simplification of the equation.

$$\frac{d[I\cdot]}{dt} = \frac{k_c}{RT_\infty} \left(p_{I,\infty} - p_{I,0} \frac{T_\infty}{T_0} \right) - k_i [I\cdot][M] = \frac{k_c p_{I,\infty}}{RT_\infty} - k_i [I\cdot][M] = 0 \quad 4-3$$

where

$p_{I,\infty}$ = partial pressure of radicals in gas phase far away from surface

$p_{I,0}$ = partial pressure of radicals in gas phase in close proximity to surface

T_∞ = temperature of gas far away from surface

T_0 = surface temperature

k_c = mass-transfer coefficient based on concentration

k_i = initiation rate constant

R = universal gas constant

$[I\cdot]$ = surface concentration of initiation radicals

$[M]$ = surface concentration of monomer

The other kind of radicals on the surface is $IM_x\cdot$, where x is any integer. This notation refers to any growing chain. The assumption used in traditional free-radical treatment¹⁷⁻¹⁹ is also used here, stating that all untermiated, growing chains have equal reactivity, regardless of its length or size. The generation of $IM_x\cdot$ is from initiation, whereas its consumption is by termination. Propagation does not generate nor consume $IM_x\cdot$. The balance of $IM_x\cdot$ can therefore be written in the following form.

$$\frac{d[IM_x\cdot]}{dt} = k_i [I\cdot][M] - 2k_t [IM_x\cdot]^2 = 0 \quad 4-4$$

where

k_i = initiation rate constant

k_t = termination rate constant

$[I\cdot]$ = surface concentration of initiating radicals

$[M]$ = surface concentration of monomer

$[IM_x\cdot]$ = surface concentration of untermiated, growing radicals

The rate of polymerization, R_p , is practically the rate of propagation and can be expressed in the following form, by solving $[IM_x \cdot]$ in terms of other quantities with the help of Equations 4-3 and 4-4.

$$R_p = k_p [IM_x \cdot] [M] = \left(\frac{k_p^2 k_c p_{I, \infty}}{2k_t RT_\infty} \right)^{0.5} [M] \quad 4-5$$

The kinetic chain length is the average number of monomer molecules consumed per terminating event and can be expressed as follows.

$$\nu = \frac{R_p}{R_t} = \frac{k_p [M] [IM \cdot]}{2k_t [IM \cdot]^2} = \frac{k_p [M]}{2k_t [IM \cdot]} = \left(\frac{k_p^2 RT_\infty}{2k_t k_c p_{I, \infty}} \right)^{0.5} [M] \quad 4-6$$

Now one can analyze the effects of decreasing substrate temperature using Equations 4-5 and 4-6. These equations state that both R_p and ν are proportional to $[M]$. The increase in molecular weight with decreasing substrate temperature can be explained using Equation 4-6. The surface concentration of monomer increases with decreasing surface temperature due to increased adsorption, leading to a higher $[M]$. Although the kinetic parameters decrease with decreasing temperature, their change may not be as pronounced as that in concentration, which contributes to the linearity in Figures 4-6 and 4-7.

Since the surface concentration is linear in partial pressure, one can replace surface concentration, $[M]$, in Equations 4-5 and 4-6 with the product of the equilibrium constant, K_M , and the partial pressure, $p_{M, \infty}$, since the adsorption is at equilibrium. Now the increase in rate and molecular weight can be interpreted as a result of the increase in the equilibrium constant, K_M , as the substrate becomes

cooler. As seen from Figure 4-3, K_M , which is the ratio between equilibrium surface concentration and partial pressure, increases with decreasing surface temperature.

$$R_p = \left(\frac{k_p^2 k_c P_{I,\infty}}{2k_t RT_\infty} \right)^{0.5} [M] = \left(\frac{k_p^2 k_c P_{I,\infty}}{2k_t RT_\infty} \right)^{0.5} K_M P_{M,\infty} \quad 4-7$$

$$v = \left(\frac{k_p^2 RT_\infty}{2k_t k_c P_{I,\infty}} \right)^{0.5} [M] = \left(\frac{k_p^2 RT_\infty}{2k_t k_c P_{I,\infty}} \right)^{0.5} K_M P_{M,\infty} \quad 4-8$$

4.3.3 EFFECTS OF MONOMER PARTIAL PRESSURE ON DEPOSITION RATE AND MOLECULAR WEIGHT

The discussion here is extended to changing surface concentration through manipulation of the partial pressure. Figure 4-8 shows that the equilibrium surface concentrations of both monomers, as measured by the QCM, increase linearly with increasing monomer partial pressure. At any given monomer partial pressure, the surface concentration of CHMA is higher than that of GMA, consistent with the fact that CHMA is heavier than GMA.

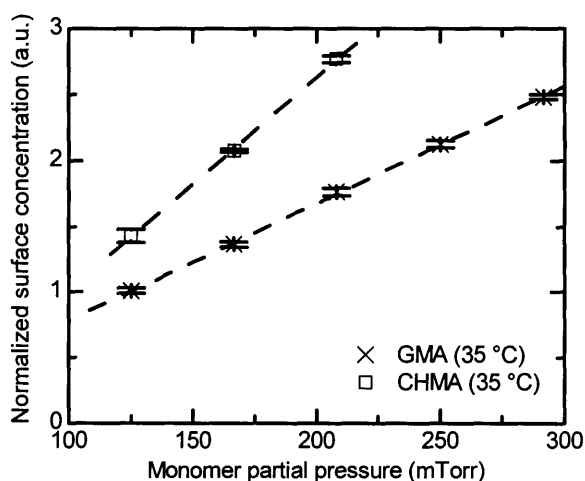


Figure 4-8. Normalized surface concentration as a function of monomer partial pressure. Both sets of measurements were performed at a crystal temperature of 35 °C.

For the iCVD runs in Series TG and TC (Table 1), the temperature was altered to manipulate surface concentration. Here in Series PG and PC, the partial pressure was varied to effect different surface concentrations. The design was to keep the surface temperature constant while varying the monomer partial pressure but keeping all other parameters constant. As with the temperature series, the deposition rate and the number-average molecular weight data are plotted against the equilibrium surface concentration data, shown in Figures 4-9 and 4-10. For each of the monomers, the deposition rate and the number-average molecular weight are linear in surface concentration, consistent with the Equations 4-5 and 4-6 and providing additional evidence that propagation occurs predominantly on the surface.

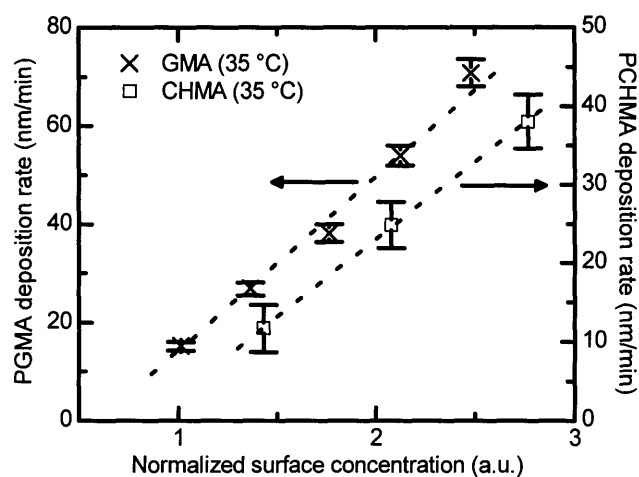


Figure 4-9. Deposition rate from iCVD experiments as a function of normalized surface concentration from QCM measurements.

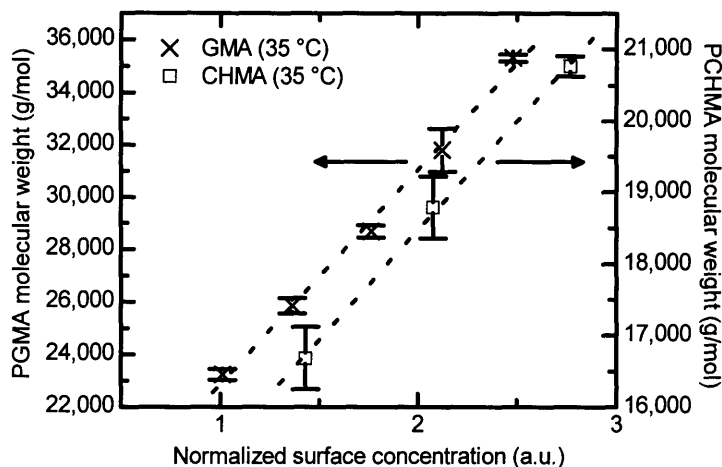


Figure 4-10. Number-average molecular weight as a function of monomer partial pressure.

One can see that at any given surface concentration, the iCVD of PGMA has a higher deposition rate and a high molecular weight. The slopes of the fitted lines of the GMA series in Figures 4-9 and 4-10 are 37.2 nm/min-a.u. and 8120 g/mol-a.u., respectively, compared to 19.7 nm/min-a.u. and 3051 g/mol-a.u. for CHMA. The difference in deposition rates is wider than the difference stemming from the deviation in molecular weights (i.e. per unit thickness there are more GMA than CHMA units). The consistently higher slopes for GMA likely stem from the difference(s) in kinetic parameter(s) in Equations 4-5 and 4-6. In these equations, k_c , $p_{l,\infty}$, and T_∞ are expected to be the same for both monomers because both the substrate and the filament temperatures are constant. As a result the rate and molecular-weight differences should be linked to either k_p or k_t , or both. The dominate difference is likely in k_t as the k_p for both GMA and CHMA are similar according to the literature based on PLP-SEC (pulsed laser polymerization-size exclusion chromatography) experiments.¹² After correcting for the difference in molecular weights, the ratio of the slopes between GMA and CHMA in Figure 4-9 is 2.6, whereas the ratio in Figure 4-10 is 2.7. Using the average of these numbers, it can be calculated that the k_t of CHMA is approximately seven times higher than that

of GMA. This higher k_t of CHMA leads to lower deposition rates and molecular weights.

4.4 CONCLUSIONS

This work shows that chain propagation occurs predominantly on the surface of the substrate for the iCVD of PGMA and PCHMA. The fact that the molecular weight increases with decreasing substrate temperature is a strong support of the hypothesis of a surface mechanism for the propagation step of the polymerization. The linearity between the deposition rate and the molecular weight data from iCVD experiments and the equilibrium surface concentration data from QCM measurements shows that the kinetics of polymerization depends strongly on the equilibrium surface concentration. This dependence infers that the surface concentration is at equilibrium during iCVD and that the rate-limiting step is not the adsorption of monomer. The inherently slow deposition and low molecular weight of iCVD PCHMA is likely due to faster termination kinetics.

REFERENCES

- (1) Chan, K.; Gleason, K. K. *Chem. Vapor Deposition* 2005, submitted.
- (2) Chan, K.; Gleason, K. K. *Langmuir* 2005, accepted.
- (3) Mao, Y.; Gleason, K. K. *Langmuir* 2004, 20, 2484.
- (4) Pryce Lewis, H. G.; Caulfield, J. A.; Gleason, K. K. *Langmuir* 2001, 17, 7652.
- (5) Murthy, S. K.; Olsen, B. D.; Gleason, K. K. *Langmuir* 2002, 18, 6424.
- (6) Welty, J. R.; Wicks, C. E.; Wilson, R. E. *Fundamentals of Momentum, Heat, and Mass Transfer*, 3rd ed.; Wiley: New York, 1984.
- (7) Geankoplis, C. J. *Transport Processes and Unit Operations*, 3rd ed.; Prentice Hall: Englewood Cliffs, NJ, 1993.
- (8) Fogler, H. S. *Elements of Chemical Reaction Engineering*, 3rd ed.; Prentice Hall: Upper Saddle River, NJ, 1999.
- (9) Rodriguez, F. *Principles of Polymer Systems*, 4th ed.; Taylor & Francis: Washington, DC, 1996.
- (10) Kumar, A. S.; Gupta, R. K. *Fundamentals of Polymers*; McGraw-Hill: New York, 1998.
- (11) Odian, G. G. *Principles of Polymerization*, 3rd ed.; Wiley: New York, 1991.
- (12) Beuermann, S.; Buback, M.; Davis, T. P.; Garcia, N.; Gilbert, R. G.; Hutchinson, R. A.; Kajiwarra, A.; Kamachi, M.; Lacik, I.; Russell, G. T. *Macromol. Chem. Phys.* 2003, 204, 1338.

CHAPTER FIVE

PHOTO-INITIATED CHEMICAL VAPOR DEPOSITION OF POLYMERIC THIN FILMS USING A VOLATILE PHOTOINITIATOR

ABSTRACT

Photo-initiated chemical vapor deposition (piCVD) is an evolutionary CVD technique for depositing polymeric thin films in one step without using any solvents. The technique requires no pre- or post-treatment and uses a volatile photoinitiator to initiate free-radical polymerization of gaseous monomers under UV irradiation. Glycidyl methacrylate (GMA) was used as a test monomer for its ability to undergo free-radical polymerization, and 2,2'-azobis(2-methylpropane) (ABMP) was used as the photoinitiator, as it is known to produce radicals when excited by photons. GMA and ABMP vapors were fed into a vacuum chamber in which film growth was observed on a substrate exposed to UV irradiation. The resulting poly(glycidyl methacrylate) (PGMA) thin films were comprised of linear chains and had high structural resemblance to conventionally-polymerized PGMA as shown by the high solubility in tetrahydrofuran and the infrared and X-ray photoelectron spectroscopy measurements. The introduction of ABMP into the vacuum chamber significantly increased growth rates. The maximum growth rate achieved was ~140 nm/min and represents a seven-fold enhancement over the case without ABMP. The molecular weight was found to increase with increasing monomer-to-initiator (M/I) feed ratio, and the polydispersity indices (PDI) of the samples were between 1.8 and 2.2, lower than the values obtained in conventional batch polymerization but in agreement with the theoretical expressions developed for low-conversion solution-phase polymerization, which are applicable to continuous processes such as piCVD. Molecular-weight distributions can be narrowed by filtering out wavelengths shorter than 300 nm, which induce branching and/or cross-linking. The strong dependence of the molecular weight on the M/I ratio, the rate enhancement due to the use of a radical photoinitiator, the good agreement between the experimental and the theoretical PDIs provide

evidence of a free-radical mechanism in piCVD. The clear films obtained in this work had number-average molecular weights between 12,500 and 97,000 g/mol. The similarities in growth conditions, growth rates, and molecular weights between the initiated CVD, a previously-reported thermal process able to synthesize a wide range of polymers, and the piCVD of PGMA suggest that piCVD can also be used to produce those polymers and potentially others whose monomers undergo free-radical mechanisms. This paper serves as an introduction to the technique by demonstrating piCVD's ability in synthesizing high-molecular-weight PGMA thin films with narrow molecular-weight distributions from vapors of GMA and ABMP in a single, dry step under UV irradiation.

5.1 INTRODUCTION

The goal of this work is to demonstrate an evolutionary chemical vapor deposition (CVD) technique for producing polymeric thin films from monomers that polymerize via free-radical mechanisms. The technique, hereby referred to as photo-initiated CVD (piCVD), is a one-step, all-dry process that uses photolysis of a gaseous photoinitiator in the presence of a gaseous monomer to produce linear polymeric thin films with high structural retention. Examples of such monomers include, but are not limited to, styrene derivatives, acrylic derivatives, methacrylic derivatives, itaconic derivatives, fumaric derivatives, vinyl halides, vinyl esters, vinyl ethers, and vinyl heteroaromatics.

CVD is an all-dry, one-step process that is able to produce films of nanoscale thicknesses with macroscale uniformity and can be applied to complex geometries.¹ It can be used to coat nanoscale features, as there are no surface tension and non-uniform wetting effects typically associated with wet processes. It also provides environmental benefits by mitigating the use of solvents.

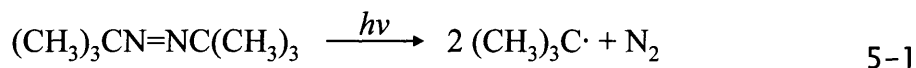
CVD methods are widely used for depositing polymeric thin films. For instance, plasma-enhanced CVD (PECVD) is a well-studied, established method for depositing such materials.²⁻⁵ Novel methods such as hot-filament CVD (HFCVD) and initiated CVD (iCVD) have also been used.⁶⁻¹² In particular, iCVD uses selective thermal degradation of an initiator to create radicals for initiating polymerizations. This selective process provides excellent control of chemistry and allows polymer films of well-defined chemical structures to be made. For example, iCVD has been used to deposit poly(methyl methacrylate) (PMMA),¹² poly(2-hydroxyethyl methacrylate) and its copolymers,¹² poly(glycidyl methacrylate) (PGMA),¹³ poly(tetrafluoroethylene),⁹ and fluorocarbon-organosilicon copolymer thin films.¹⁰ Spectroscopic studies of these iCVD films have shown excellent structural

resemblance to conventionally-polymerized counterparts and affirm iCVD's ability to produce linear polymers with a high degree of structural retention. Linear polymers retain solubility and allow subsequent selective chemistry as cross-linked sites would not react in the same manner as their linear counterparts. Structural retention is also crucial, as the properties and the corresponding applications of polymers are often defined by the functional groups pendant to their backbones. For example, PGMA's epoxide groups are important for its functions, as they can be converted to other functionalities through ring-opening reactions. Its ability to self-cross-link requires the presence of the epoxide groups. The uses of PGMA thin films for surface modification,¹⁴ as high-performance membranes,¹⁵ and for lithographic imaging^{13,16,17} have been demonstrated and require structural integrity. In order for PGMA thin films to function as electron-beam (e-beam) resists,^{13,16} the epoxide groups must be retained. E-beam irradiation causes a ring-opening reaction among the epoxide groups, resulting in cross-linked PGMA. The solubility difference between exposed and unexposed areas provides the contrast for development.

Both iCVD and piCVD employ initiator species sufficiently volatile to enter the vacuum chamber as vapors. The primary objective in this work is to use UV irradiation to selectively produce radicals for initiation, just as thermal energy has been used to selectively pyrolyze *tert*-butyl peroxide¹¹ (TBPO) and perfluorooctanesulfonyl fluoride⁹ in iCVD. Other works have demonstrated the use of UV irradiation to initiate polymerization of monomer vapors.¹⁸⁻²¹ These previous reports, however, do not involve the use of a separate initiator, so the initiation depends on the fragmentation of the monomers themselves. The breakdown of monomers, which are more stable than initiators, requires short-wavelength irradiation and sometimes laser irradiation. High-energy irradiation damages the film, creating dangling bonds²² that can cause cross-linking and/or branching. In

particular, heavy cross-linking has been reported for the laser-induced photopolymerization of methyl acrylate.²⁰ The separate introduction of a photoinitiator allows the use of low-energy irradiation and potential acceleration of deposition and control of molecular weight, as seen in iCVD.⁹⁻¹¹ Yasutake *et al.*²³ pre-deposited the nonvolatile initiator azobisisobutyronitrile for the photopolymerization of MMA under a mercury(xenon) lamp and shown molecular-weight control. The pre-deposition, however, requires the use of a solvent (acetone) and renders the entire technique a multi-step process.

The benefits of introducing an initiator motivate the current investigation of an all-dry photo-initiated CVD process that uses a gaseous photoinitiator and a gaseous monomer. Azo compounds are known to undergo photolysis under near-UV irradiation.²⁴ The photoinitiator chosen for the piCVD work reported here is 2,2'-azobis(2-methylpropane) (ABMP). The most probable transition wavelength (λ_{max}) of ABMP is 366 nm,²⁵ and its estimated vapor pressure is 4.9 Torr at 25 °C. Under UV irradiation, ABMP undergoes photolytic scission to form *tert*-butyl radicals and nitrogen,²⁶ shown in Equation 5-1. TBPO can be used as a photoinitiator also, but the photolysis is efficient only at shorter wavelengths.^{27,28} Use of short wavelengths can be damaging to both the monomer and the polymer.



There are several anticipated advantages of pursuing the photochemical instead of the thermal pathway as used in iCVD. First, the chamber design can be greatly simplified as the filament array is no longer needed. Second, heat transfer from the filament array is also eliminated, allowing tight control of substrate temperature. Substrate temperature has been shown to affect strongly the surface

concentration of monomer species.¹⁹ Third, the technique can easily be scaled up for large substrates or even three-dimensional objects, as uniform deposition can be achieved with uniform light intensity on the surface. piCVD may also be used to coat the inside of hollow objects that are transparent to UV, provided that the precursor gases are able to reach the area of interest.

Glycidyl methacrylate (GMA) has been chosen as the test monomer in this study because of its successful polymerization in the iCVD process.¹¹ Another reason is that its characteristic epoxide functional groups are straightforward to detect spectroscopically and represent a benchmark for structural integrity. As will be seen, this work demonstrates that piCVD is able to produce PGMA thin films from a mixture of gaseous GMA and gaseous ABMP under UV irradiation. The resulting films have excellent structural retention and have low polydispersity indices (PDI). The deposition rate can be controlled by changing the lamp power, and the molecular weight can be controlled by tuning the monomer-to-initiator (M/I) ratio. These results position piCVD as a complementary method to existing CVD techniques for depositing polymeric thin films. In addition to PGMA, piCVD has also been used to deposit poly(cyclohexyl methacrylate) and polyvinylpyrrolidone from cyclohexyl methacrylate and 1-vinyl-2-pyrrolidone, respectively. The analyses in this work are focused on the deposition of PGMA because a direct comparison to iCVD PGMA can be made and most experimental work was performed using GMA as the monomer.

5.2 EXPERIMENTAL METHODS

Films were deposited on 100-mm-diameter silicon (Si) substrates in a custom-built vacuum chamber (Figure 5-1, Sharon Vacuum). The inside of the

chamber was cylindrical with a height of 3.3 cm and a radius of 12 cm. The inlet of precursor gases and the exhaust were at opposite ends of the chamber. The top of the chamber was covered by a removable quartz plate (~15 cm radius and 2.5 cm thick), allowing placement of substrate, visual inspection, laser interferometry, and entrance of UV light. The chamber was equipped with a backside-cooled stage (25 °C) on which the substrate was placed. The chamber pressure was maintained at 500 mTorr with a throttling butterfly valve (Intellisys, Nor-Cal).

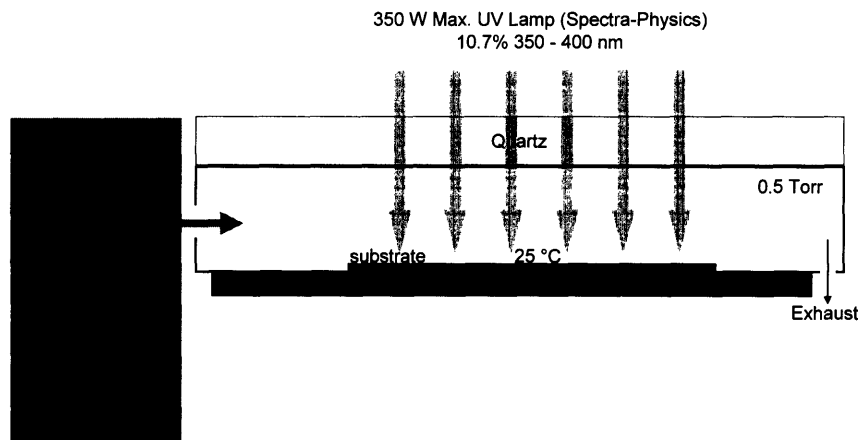


Figure 5-1. Schematic of the vacuum chamber (not to scale).

All components in the UV light source were purchased from Spectra-Physics unless otherwise noted. The mercury (Hg) lamp (Model 6286, 350 W max.) was placed inside an arc lamp housing (Model 66902), which was positioned upside-down and affixed to the ceiling of a fume hood. A beam turner (Model 66245) equipped with a full reflector (Model 66215) was attached to the housing to direct the UV light vertically down through the quartz plate onto the substrate, which was approximately 46.5 cm away from the reflector. The condenser lens of the housing was adjusted to focus the light onto the substrate. This adjustment resulted in light intensities of 134.6 ± 6.7 , 110.5 ± 5.5 , and 84.0 ± 4.2 mW/cm² when the lamp power was set to 350, 300, and 250 W, respectively. These intensities were

measured using a photodiode placed on the top of the center of the substrate with the quartz plate in place (340-nm calibration, filter in, Model PD300-UV-SH, Ophir Optronics, Wilmington, MA). In all experimental runs, the UV lamp was turned on when the precursor flow rates and the chamber pressure had stabilized. For experiments in which a long-pass filter was used, a filter holder (Model 71260) equipped with a 324-nm cut-on glass filter (Model 59458) was affixed between the housing and the beam turner. According to specifications from Spectra-Physics, the external transmittance of the filter below 300 nm is zero, whereas that at 366 nm is approximately 0.9.

The monomer GMA (97.0%+, Aldrich) and the initiator ABMP (97%, Aldrich), were used without further purification. GMA liquid was vaporized in a glass jar maintained at 65 ± 1 °C, and this vapor was metered into the chamber through a mass-flow controller (Model 1152C, MKS). ABMP was maintained at room temperature in a glass jar, and its vapor was also metered into the chamber through a mass-flow controller (Model 1479A, MKS). Both vapors were mixed together before entering the chamber through a side port. Depositions were monitored using an interferometry system equipped with a 633-nm HeNe laser source (JDS Uniphase). The cycle thickness was calculated by dividing the actual thickness, as measured using variable-angle spectroscopic ellipsometry (VASE), by the number of cycles. VASE was performed on a J. A. Woollam M-2000 spectroscopic ellipsometer with a xenon light source. Data were acquired at three angles (65°, 70°, and 75°) and 225 wavelengths, and the Cauchy-Urbach model was used to fit the data.

Table 5-1 details the two sets of experimental runs in this work. In the first set of experiments with a fixed lamp power of 350 W, the flow rate of GMA was fixed at 3.0 sccm, whereas that of ABMP was varied between 0.0 to 3.0 sccm in increments of 0.5 sccm. In order to keep the residence time (7 s) constant, a patch

flow of nitrogen was introduced to keep the total flow rate at 6.0 sccm in these runs. In the other set of experiments, the flow rates of GMA and ABMP were both fixed at 3.0 sccm, whereas the lamp power was varied between 250 and 350 W in increments of 50 W. This arrangement allowed investigation of the dependence of the deposition rate and film properties on the M/I ratio and the lamp power. A control experiment with the initiator but no UV light was also performed (P0). For the flow-rate series, two extra runs were performed with the long-pass filter in place. They were done to elucidate the effects of eliminating wavelengths shorter than 300 nm on deposition rate, molecular weight, and PDI.

Table 5-1. Details of experimental runs.

Sample	Lamp Power (W)	Flow Rate (sccm)			Partial Pressure (mTorr)		Flow-Rate Ratio
		GMA	ABMP	N ₂	GMA	ABMP	GMA/ABMP
<i>Flow-Rate Series</i>							
F1	350	3.0	0.0	3.0	250	0	N/A
F2	350	3.0	0.5	2.5	250	42	6
F3	350	3.0	1.0	2.0	250	83	3
F4	350	3.0	1.5	1.5	250	125	2
F5	350	3.0	2.0	1.0	250	167	1.5
F6	350	3.0	2.5	0.5	250	208	1.2
F7	350	3.0	3.0	0.0	250	250	1
<i>Power Series</i>							
P1	250	3.0	3.0	-	250	250	1
P2	300	3.0	3.0	-	250	250	1
P3	350	3.0	3.0	-	250	250	1

Fourier-transform infrared (FTIR) measurements were performed on a Nicolet Nexus 870 ESP spectrometer in normal transmission mode using a DTGS KBr detector over the range of 400 to 4000 cm⁻¹ at a 4-cm⁻¹ resolution averaged over 64 scans. All spectra were baseline corrected. The polymer films were degassed overnight in a vacuum oven maintained at 60 °C before FTIR measurements were taken. X-ray photoelectron spectroscopy (XPS) was done on a Kratos Axis Ultra spectrometer equipped with a monochromatized Al K α source. A PGMA standard

(Polymer Source, Montreal, Québec, Canada) was dissolved in acetone and cast onto a silicon wafer for FTIR measurements. An iCVD film was synthesized for comparison using a previously-described procedure.¹¹

Films were dissolved in tetrahydrofuran (THF) for gel permeation chromatography (GPC) measurements. The GPC system was comprised of a Waters 1515 isocratic high-performance liquid chromatography (HPLC) pump, a Waters 2414 refractive index detector, and two Styragel® HR 4 7.8 × 300 mm columns. Poly(methyl methacrylate) (PMMA) standards (Polymer Laboratories, Amherst, MA) dissolved in THF were used for calibration at 35 °C.

5.3 RESULTS AND DISCUSSION

5.3.1 FOURIER–TRANSFORM INFRARED SPECTROSCOPY

Figure 5–2 shows the FTIR spectra of Sample F7 (piCVD film), the iCVD PGMA film, and the PGMA standard obtained from Polymer Source. The spectra of all the other piCVD samples in Table 5–1 are similar to that of Sample F7. All films in Figure 5–2 show alkyl C–H stretching (3000–2840 cm⁻¹), ester C=O stretching (1750–1725 cm⁻¹), alkyl C–H bending (1470–1340 cm⁻¹), and ester C–O stretching (1300–1200 cm⁻¹), typical for polymethacrylates. These assignments are based on FTIR analyses of PMMA²⁹ and other organic molecules³⁰ in the literature. There is much evidence in the piCVD spectrum that shows the retention of the entire pendant group, –COOCH₂CH(–O–)CH₂. First, the retention of the carbonyl groups is evident in the presence of the strong peak centered at ~1730 cm⁻¹. Also, the peaks at 907, 848, and 760 cm⁻¹, assigned to the characteristic absorption bands of the epoxide groups,^{14,31,32} are present in the piCVD spectrum. The high-frequency C–H stretching at above ~3040 cm⁻¹ (shoulder in Figure 5–2),

assigned to the antisymmetric oxirane C–H stretching,³⁰ further confirms the presence of the epoxy rings. These results show not only the retention of the pendant groups but also the intactness of the epoxy groups. It can therefore be inferred that the UV irradiation, intended solely for the fragmentation of ABMP, does not cause ring opening or loss of pendant group to a significant degree. The high resemblance in the C–H stretching and bending regions between the piCVD spectrum and the standard spectrum also precludes loss of the α -methyl groups. All the peaks in the piCVD spectrum exemplify no broadening compared to the standard spectrum. The lack of broadening further affirms the retention of functionalities in the piCVD process, as such an effect would indicate loss of homogeneity in bonding environments³³—a consequence of loss of functional groups. Peak broadening has been reported previously for plasma-deposited PGMA films at low power.¹¹ The slightly wider C–O–C band ($\sim 1125\text{ cm}^{-1}$) in the spectrum of the PGMA standard may be due to retained solvent, a common problem for solution-cast polymers.

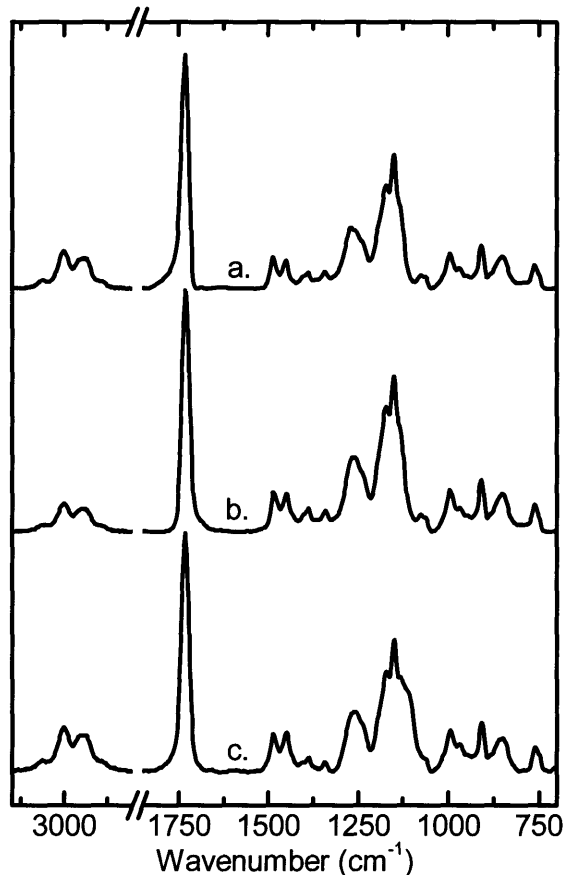


Figure 5-2. FTIR spectra of (a) piCVD PGMA film, (b) iCVD PGMA film, and (c) spin-cast PGMA obtained from Polymer Source. The absorption peaks at 907, 848, and 760 cm^{-1} are assigned to the characteristic absorption bands of the epoxide group.^{14,31,32}

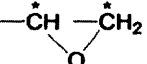
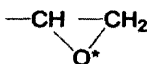
5.3.2 X-RAY PHOTOELECTRON SPECTROSCOPY

The C 1s and O 1s high-resolution XPS scans of Sample F7 show five carbon and three oxygen moieties, consistent with the molecular structure of PGMA. The binding energies and the peak area percentages of the moieties are listed in Table 5-2. As can be seen, there is good agreement between the piCVD values and the literature values for solution-polymerized PGMA,³⁴ indicating retention of functional groups. These results corroborate the FTIR results and support the hypothesis that piCVD (1) produces the same linear polymeric structure as solution

polymerization and (2) retains virtually all of the pendant epoxide functional groups.

The FTIR and the XPS results show that PGMA thin films can be synthesized by feeding a gaseous mixture of the monomer GMA and the initiator ABMP into a vacuum chamber equipped with a UV light source.

Table 5-2. High-resolution XPS scan data of the piCVD PGMA film.

core level	peak	origin	piCVD film		PGMA reference ³⁴	
			binding energy (eV)	area (%)	binding energy (eV)	area (%)
C 1s	1	-C*H ₃ , -C-C*H ₂ -C-	285.00	29	285.00	29
	2	-C*(CH ₃)-CO-	285.71	14	285.67	15
	3	-O-C*H ₂ -	286.64	14	286.71	15
	4		287.02	29	287.02	29
	5	-C*=O	289.11	14	289.15	13
O 1s	1	-C=O*	532.32	33	532.32	33
	2		533.17	33	533.13	34
	3	-CO-O*-CH ₂ -	533.86	33	533.79	34

5.3.3 MOLECULAR-WEIGHT CONTROL

The ability to control the molecular weight of a polymer in solution-phase polymerization by adjusting the concentrations of the monomer and the initiator is well known.³⁵⁻³⁷ The molecular weight is known to increase with increasing M/I ratio. A similar analysis was performed for piCVD to test if the same type of control could be implemented. One primary advantage of piCVD is that the resulting polymer is soluble and can be analyzed using conventional solution techniques. In the case of iCVD, high solubility is a result of the selective thermal decomposition of the initiator. The absence of bond-breaking chemistry for the monomer or the polymer avoids undesired cross-linking, which would otherwise lead to poor

solubility. In this work, piCVD PGMA thin films deposited using ABMP as the initiator were completely soluble in THF and were analyzed with GPC, suggesting that linear chains were synthesized predominantly. The dependence of the molecular weight on the M/I ratio was studied and is shown in Figure 5-3. Both the number-average (M_n) and the weight-average (M_w) molecular weights increase with increasing M/I ratio and follow a near linear relationship. The number-average molecular weight ranges between 12,500 (Sample F6) and 97,000 (Sample F2) g/mol, compared to 15,000–35,000 g/mol reported in the iCVD work.¹¹ Direct comparison between the two CVD techniques is not possible because the actual number of radicals generated are not known in either case. Nonetheless, the molecular weights in the two cases are on the same order of magnitude. Figure 5-3 demonstrates that the molecular weight can be controlled systematically by changing the M/I ratio. This result supports the proposed free-radical mechanism by clearly demonstrating the effect on the molecular weight of varying the M/I ratio. The PDIs of the films in Figure 5-3 (Sample F2 to F6) range between 1.9–2.1 with the exception of that of Sample F2 (3.1). The high PDI of Sample F2 is likely due to branching and/or cross-linking (discussed in a subsequent section), as the growth rate was relatively low because of the small amount (0.5 sccm) of initiator. Excluding sample F2, the entire sample set in this work has PDIs in the range between 1.8 and 2.2, which are low compared to 2.0–5.0 for conventional high-conversion free-radical polymerization.³⁵ The two sets of results, however, cannot be compared directly because piCVD is a continuous process, whereas conventional free-radical polymerization is usually a batch process. The polymer molecular weight depends on the ratio $[\text{monomer}]/[\text{initiator}]^{0.5}$ in solution-phase polymerization.³⁵⁻³⁷ In a batch setting, these concentrations are not constant, so the molecular weight changes with the conversion, which leads to polydispersed polymers. piCVD, in contrast, has continuous supplies of the monomer and the

photoinitiator. Assuming steady-state operation, all partial pressures and surface concentrations in the chamber are constant, so the ratio $[\text{monomer}]/[\text{initiator}]^{0.5}$ is constant. This constancy is also seen in low-conversion batch polymerizations, in which a majority of the monomer and the initiator have not reacted. Theoretical expressions have been developed to calculate PDIs for low-conversion polymerizations.^{35,38} For a system in which disproportionation, or chain transfer, or a combination of both is the dominant termination mechanism, the PDI ranges between 1.0 and 2.0 and leans toward 2.0 for high polymers. When coupling is the dominant mechanism, the PDI ranges between 1.0 and 1.5 and leans toward 1.5 for high polymers. All these termination mechanisms are possible in piCVD (see Figure 5-5). The growing chains on the surface can participate in disproportionation and coupling reactions and can also transfer to the monomer and the initiator. Primary termination (coupling of a chain with the primary radical, $I\cdot$) can also occur and be viewed as a transfer reaction to the initiator. Since long chains are made in the piCVD process, the PDI should lie somewhere between 1.5 and 2.0 based on the theoretical expressions. The range of 1.8–2.2 is close to the theoretical range. It must be noted that this range takes into account branching or cross-linking arising from side-group scission (discussed in a subsequent section), which increases the PDI. The initial transient period, during which constancy has not been realized, may also widen the distribution. The analysis here shows that piCVD is able to produce high-molecular-weight PGMA thin films with low PDIs. The results agree well with the theoretical model, providing evidence that the polymerization mechanism is free-radical.

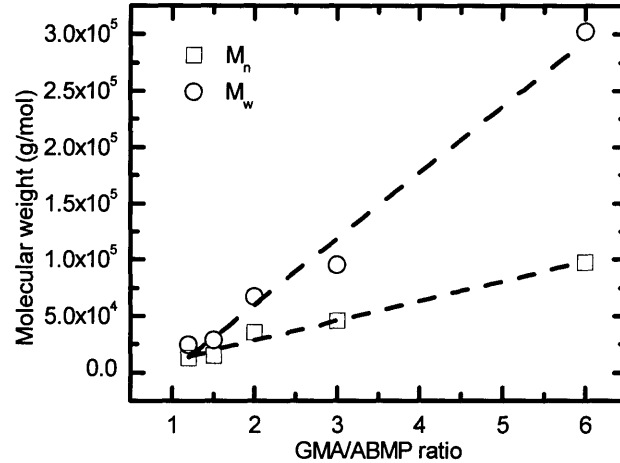


Figure 5-3. Number-average (M_n) and weight-average (M_w) molecular weights as functions of the monomer-to-initiator ratio. Both increase with increasing M/I ratio.

5.3.4 RATE ENHANCEMENT DUE TO INITIATOR

Comparison between Samples F1 and F7 clearly demonstrates the importance of the initiator ABMP for substantially enhancing polymer film growth rates. The depositions of Samples F1 and F7 employed identical flow rates of GMA and identical overall flow rates. The growth rate of Sample F7 using ABMP was ~140 nm/min. When nitrogen replaced ABMP (Sample F1), film deposition occurred at a much lower rate of ~20 nm/min. There was not a systematic increase of deposition rate from Sample F2 to Sample F7 as the flow rate of ABMP was increased incrementally from 0.5 to 3 sccm. The lack of a clear trend may be a result of competition for surface sites between GMA and ABMP. At high ABMP partial pressure, radical generation increases, but more surface sites are occupied by ABMP, decreasing the surface concentration of GMA. Additional work is required to elucidate the trade-off between the two effects. The rate enhancement due to the use of a radical photoinitiator provides evidence that the polymerization undergoes a free-radical mechanism. In the absence of ABMP, radicals are most likely generated for initiation of polymerization from the fragmentation of GMA,

similar to the mechanism previously reported²⁰ for the photopolymerization of methyl acrylate (MA) where MA self-initiates when irradiated with UV light. Under exposure, MA, by two-photon absorption,²⁰ is excited to a high-energy state and then fragments into a vinyl radical and a methoxycarbonyl radical, which further dissociates into a methyl radical and carbon dioxide. The vinyl and the methyl radicals are capable of initiating the polymerization of MA. A similar fragmentation may occur for GMA, as both monomers belong to the acrylic/methacrylic family. It is reasonable to assume that GMA fragments in a similar fashion, and the expected products are the 2-propylenyl radical, the $\cdot\text{CH}_2\text{-CH}(\text{-O-})\text{CH}_2$ radical, and carbon dioxide. These radicals, likewise, can initiate the polymerization of GMA. The slower deposition without ABMP can be attributed to the difference in absorption characteristics of the chromophores. The Hg arc lamp in use has the strongest intensity at 366 nm, which is the λ_{max} (the most probable transition wavelength) of ABMP.²⁵ Although the exact λ_{max} of GMA is not known, it is anticipated that it absorbs at a shorter wavelength, as the λ_{max} 's of methyl methacrylate, ethyl methacrylate, and butyl methacrylate range between 211 and 216 nm.³⁹ The intensity of the lamp below 250 nm is only 2.4% of the total emission power, compared to 10.7% between 350 and 400 nm, as specified by Spectra-Physics.

A noteworthy fact is that the film made without ABMP (Sample F1) is insoluble in THF while in contrast all the other samples (Samples F2–F7) made with ABMP are soluble in THF. The insolubility of Sample F1 is likely a result of a high degree of cross-linking. Although possible, cross-linking due to ring-opening of the epoxide group is not likely the reason because the strong characteristic absorption peaks of the epoxide groups are still present in the FTIR spectrum of Sample F1. Alternatively, cross-linking can occur when a chain is initiated and terminated by 2-propylenyl radicals and/or when side-group scission occurs. When a chain is unsaturated at both ends, it is effectively a difunctional

macromonomer. A number of these macromonomers on the surface would cause cross-linking. It is, however, believed that side-group scission of chains is more likely the reason behind the insolubility. First, since the deposition is initiation-limited, the molecular weight of the film is expected to be high. Long chains with unsaturated ends would not cause cross-linking significant enough to cause complete insolubility. In addition, this consideration does not take into account the initiating and terminating action of the other radical arising from GMA fragmentation. Side-group scission, on the other hand, occurs when the chains are exposed to UV. Poly(methyl methacrylate) is known to degrade under UV exposure.⁴⁰ Its photodegradation occurs by (1) random homolytic scission of the polymer backbone, (2) photolysis of the ester side group, and (3) photolysis of the methyl side group. PGMA can undergo the same photolysis, turning the chains into macroradicals. The macroradicals in turn can initiate polymerization. A number of these side-group scission events on the chains on the surface would cause significant cross-linking and/or branching. It can be argued that the film made with ABMP is also cross-linked because the growing film is also irradiated. However, since the growth rate is much faster with ABMP, the average time of exposure of a chain to UV is significantly shorter. It cannot be ruled out that there is some degree of branching or cross-linking, but the solubility in THF proves that there is, if any, insignificant cross-linking. The results here show that the addition of ABMP enhances the growth rate and, by doing so, reduces cross-linking/branching. Nevertheless, cross-linking and/or branching may potentially be reduced by filtering out wavelengths that are not needed for the photolysis of ABMP. To demonstrate this filtering, a long-pass filter was used to filter out wavelengths shorter than 300 nm while keeping the strong 366-nm emission (Samples F1' and F2'). Comparison between Samples F2 and F2' shows that the latter has a lower M_n (14% decrease), a lower M_w (36% decrease), and a lower PDI

(2.3 compared to 3.1). The reduction in branching is clearly demonstrated by the reduced molecular weights and PDI, and the reduced radical generation from GMA is exemplified by the slower deposition of Sample F1' (0 nm/min, no deposition) compared to that of Sample F1 (~20 nm/min). This result agrees well with the assertion that photolysis of GMA requires high-energy photons. On the other hand, the fact that Sample F1' did not grow a film but Sample F2' did proves the function of ABMP as an initiator under UV irradiation. Wavelength filtering can be implemented when the degree of branching and/or cross-linking needs to be low.

5.3.5 COMPARISON BETWEEN piCVD AND iCVD

The acceleration of deposition is seen for previous iCVD works⁹⁻¹¹ also, but the breakdown of the initiator is a thermal process. The selection of an initiator for piCVD is dictated by absorption characteristics, whereas that for iCVD is concerned with the activation energies for dissociation. Figure 5-4 shows that the deposition rate increases linearly with increasing lamp power (Samples P1, P2, and P3 in Table 5-1). This increase can be attributed to the increase in number of photons, leading to increased fragmentation of ABMP. This linearity also corresponds well to the light intensity measurements described in the experimental section, which show a linear increase in light intensity with power. The straight line in Figure 5-4 does not intercept (0,0) because there is a minimum required power for the lamp to ignite.⁴¹ In contrast to iCVD, whose deposition rate shows an Arrhenius-type behavior with respect to filament temperature, the deposition rate of piCVD depends on the number of photons emitted from the lamp. When no UV light was used (Sample P0), there was no deposition, showing that photons are required for radical generation.

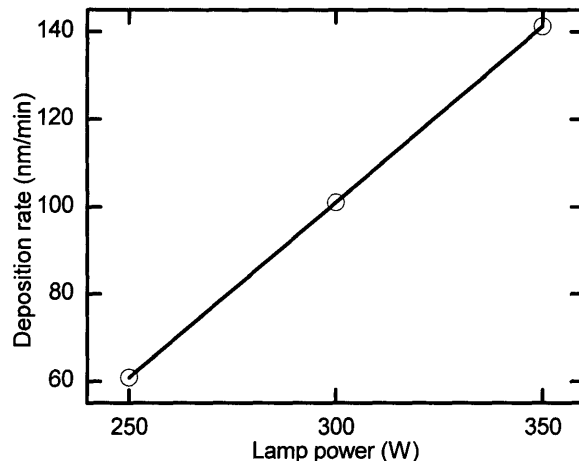


Figure 5-4. Deposition rate as a function of the lamp power. The increase in rate can be attributed to the increase in the concentration of initiating radicals with increasing lamp power.

When 3 sccm of ABMP is used (Sample F7), the deposition rate approaches 140 $\mu\text{m}/\text{min}$, on the same order of magnitude achieved with iCVD.¹¹ In iCVD, TBPO was used as the initiator and was pyrolyzed into *tert*-butoxy radicals by the heated filaments. This work employs ABMP, which undergoes photolytic scission to form *tert*-butyl radicals and nitrogen (Equation 5-1).²⁶ Apart from the difference in the initiation mechanisms and the types of radicals being generated, it is reasonable to regard that the propagation and the termination mechanisms are similar, if not identical. First, the two processes use the same chamber pressure (500 mTorr), same substrate temperature (25 °C), and similar flow rates of initiator and monomer (2.5 to 3.0 sccm). Second, the molecular weights are on the same order of magnitude (Section 3.3). It appears that neither the method of radical generation nor the nature of the radical affects chain propagation to a significant degree. This observation is in line with the propagation kinetics of radical-chain polymerization, which states that the rate of propagation, k_p , depends on the identity of the monomer and is independent of the length of the propagating radical.^{31,35,37} The increase in deposition rate with the use of a radical initiator and the similarities

between piCVD and iCVD provide evidence that the piCVD of PGMA undergoes a free-radical mechanism. Figure 5–5 illustrates the proposed mechanism for piCVD. The fragmentation of the initiator, however, may occur at different locations within the reactor chamber for the iCVD and piCVD methods. In the case of iCVD,¹¹ the filament wires are suspended 2.2 cm above the substrate and the substrate is actively cooled, it is anticipated that TBPO either breaks down around the filament wires in the gas phase or on the surface of the wires. In the case of piCVD, it is hitherto not certain whether the breakdown of ABMP occurs in the gas phase, on the surface of the substrate, or both.

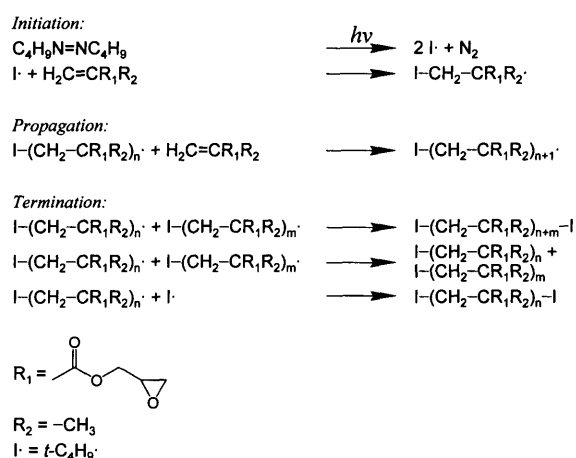


Figure 5–5. Postulated free-radical polymerization mechanism in the piCVD process using 2,2'-azobis(2-methylpropane) as the photoinitiator.

In the previous iCVD PGMA work,¹¹ the molecular weight was shown to decrease with increasing filament temperature. The number of initiating radicals increases as the temperature increases, which contributes to a decreased M/I ratio leading to shorter chains. One can expect that increasing the UV intensity would also increase the number of radicals. Figure 5–6 shows that both the molecular weight and the PDI increase with increasing lamp power. The increase in molecular weight may seem anti-intuitive because more radicals are expected to generate

from ABMP when the lamp power is increased. The increase in radicals would in turn cause a decrease in molecular weight because of the decreased M/I ratio. Yet, the molecular weight increases instead of decreases. The increase in molecular weight can be attributed to a small degree of cross-linking or branching, which can also explain the increase in PDI. As discussed previously, side-group scission occurs and can be anticipated to increase with increasing lamp power. A higher lamp power causes more side-group scission, leading to more branching and/or cross-linking. This effect is not sufficiently strong to cause solubility problems since the growth rate is still high due to the use of 3 sccm of ABMP.

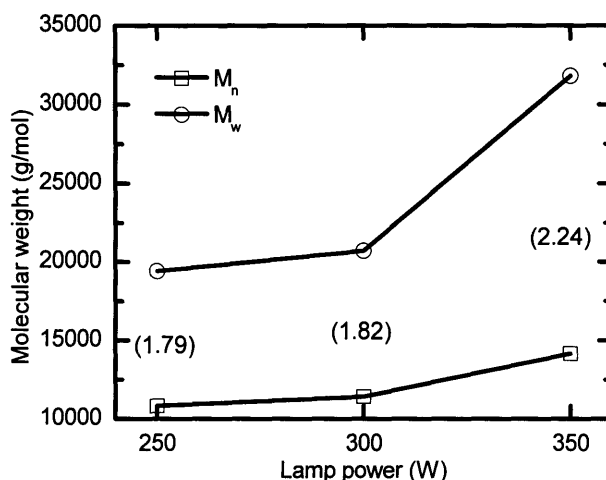


Figure 5–6. Number-average and weight-average molecular weights as functions of the lamp power. The numbers in parentheses are the respective polydispersity indices (PDI) of the piCVD PGMA films made at different lamp powers.

5.4 CONCLUSIONS

This work demonstrates that polymeric thin films can be deposited by feeding a gaseous mixture of monomer and the photoinitiator ABMP into a vacuum chamber equipped with an external UV light source with intensity at 366 nm. The

substrate can easily be maintained at room temperature since energy flux is on the order of 100 mW/cm².

FTIR and XPS measurements show high retention of the pendant epoxide groups, and the high solubility of the samples show that they are comprised mainly of linear chains. The maximum growth rate achieved in this work is ~140 nm/min, so the growth of a 1- μ m film would take about 7 min. These results demonstrate that piCVD is a viable process for depositing polymer thin films with well-defined chemical structures at appreciable growth rates. The clear films made in this work have number-average molecular weights ranging from 12,500 to 97,000 g/mol, controllable through adjustment of the M/I ratio. A majority of the samples have PDIs in the range of 1.8–2.2, consistent with the theoretical expressions derived for low-conversion free-radical polymerizations. This PDI result and the significant rate enhancement due to the use of a free-radical photoinitiator provide evidence that GMA polymerizes to form PGMA in the chamber through a free-radical mechanism. When a low degree of branching and/or cross-linking is desired, wavelength filtering can be implemented to eliminate short wavelengths. The use of photons instead of heat for initiation differentiates piCVD from iCVD. Yet, the similarities in growth conditions, growth rates, and mechanisms between piCVD and iCVD suggest that polymers that can be made using iCVD can also be made using piCVD. A wide variety of functional polymers have already been deposited using iCVD. They include both hydrophilic, hydrophobic, and biopassivating polymers. Nonetheless, this technique can be extended to other monomers that are known to undergo free-radical polymerization. The use of UV light to initiate film growth allows potential simplification of chamber design, as the light source can be placed outside of the chamber, whereas the heating element in iCVD must be placed within the chamber. Such versatility also allows potential coating of the inside of structures on the condition that the structures are UV-transparent and the

gaseous mixture of the monomer and the photoinitiator is able to reach the area of interest.

REFERENCES

- (1) Pierson, H. O. *Handbook of Chemical Vapor Deposition*, 2nd ed.; Noyes Publications: Norwich, NY, 1999.
- (2) Morosoff, N. In *Plasma Deposition, Treatment, and Etching of Polymers*; d'Agostino, R., Ed. Academic Press: Boston, MA, 1990; p 1.
- (3) Inagaki, N. *Plasma Surface Modification and Plasma Polymerization*; Technomic: Lancaster, PA, 1996.
- (4) Hollahan, J. R.; Bell, A. T. *Techniques and Applications of Plasma Chemistry*; Wiley: New York, 1974.
- (5) Yasuda, H. *Plasma Polymerization*; Academic: Orlando, FL, 1985.
- (6) Lau, K. K. S.; Gleason, K. K. *J. Fluor. Chem.* 2000, 104, 119.
- (7) Loo, L. S.; Gleason, K. K. *Electrochem. Solid State Lett.* 2001, 4, G81.
- (8) Pryce Lewis, H. G.; Casserly, T. B.; Gleason, K. K. *J. Electrochem. Soc.* 2001, 148, F212.
- (9) Pryce Lewis, H. G.; Caulfield, J. A.; Gleason, K. K. *Langmuir* 2001, 17, 7652.
- (10) Murthy, S. K.; Olsen, B. D.; Gleason, K. K. *Langmuir* 2002, 18, 6424.
- (11) Mao, Y.; Gleason, K. K. *Langmuir* 2004, 20, 2484.
- (12) Chan, K.; Gleason, K. K. *Chem. Vapor Deposition*, submitted.
- (13) Mao, Y.; Felix, N. M.; Nguyen, P. T.; Ober, C. K.; Gleason, K. K. *J. Vac. Sci. Technol. B* 2004, 22, 2473.
- (14) Yang, G. H.; Kang, E. T.; Neoh, K. G. *J. Polym. Sci. Pol. Chem.* 2000, 38, 3498.
- (15) Lee, W.; Oshikiri, T.; Saito, K.; Sugita, K.; Sugo, T. *Chem. Mat.* 1996, 8, 2618.
- (16) Thompson, L. F.; Willson, C. G.; Bowden, M. J. *Introduction to Microlithography*, 2nd ed.; American Chemical Society: Washington, DC, 1994.
- (17) Shirai, M.; Sumino, T.; Tsunooka, M. In *Polymeric Materials for Microelectronic Applications: Science and Technology*; Ito, H., Tagawa, S., Horie, K., Eds.; American Chemical Society: Washington, DC, 1994; p 185.
- (18) Melville, H. W. *Proc. R. Soc. London, Ser. A* 1937, 163, 511.
- (19) Tsao, J. Y.; Ehrlich, D. J. *Appl. Phys. Lett.* 1983, 42, 997.
- (20) Morita, H.; Sadakiyo, T. *J. Photochem. Photobiol. A-Chem.* 1995, 87, 163.
- (21) Hsieh, M. D.; Zellers, E. T. *Sens. Actuator B-Chem.* 2002, 82, 287.
- (22) Limb, S. J.; Labelle, C. B.; Gleason, K. K.; Edell, D. J.; Gleason, E. F. *Appl. Phys. Lett.* 1996, 68, 2810.

- (23) Yasutake, M.; Andou, Y.; Hiki, S.; Nishida, H.; Endo, T. *Macromol. Chem. Phys.* 2004, 205, 492.
- (24) Patai, S., *The Chemistry of the Hydrazo, Azo and Azoxy Groups: Part 2*. Wiley: New York, 1975.
- (25) Schmittel, M.; Ruechardt, C. *J. Am. Chem. Soc.* 1987, 109, 2750.
- (26) Thomas, S. S.; Calvert, J. G. *J. Am. Chem. Soc.* 1962, 84, 4207.
- (27) Dorfman, L. M.; Salsburg, Z. W. *J. Am. Chem. Soc.* 1951, 73, 255.
- (28) McMillan, G. R. *J. Am. Chem. Soc.* 1962, 84, 2514.
- (29) Nagai, H. *J. Appl. Polym. Sci.* 1963, 7, 1697.
- (30) Lin-Vien, D.; Colthup, N. B.; Fateley, W. G.; Grasselli, J. G. *The Handbook of Infrared and Raman Characteristic Frequencies of Organic Molecules*; Academic Press: San Diego, CA, 1991.
- (31) Kumar, R. N.; Woo, C. K.; Abusamah, A. *J. Appl. Polym. Sci.* 1999, 73, 1569.
- (32) Davidson, K.; El-Attawy, S.; El-Gamal, M.; Khattab, M. A.; El-Demerdach, A. M. *High Perform. Polym.* 2002, 14, 3.
- (33) Cox, J. N. In *Encyclopedia of Materials Characterization: Surfaces, Interfaces, Thin Films*; Brundle, C. R., Evans, C. A., Wilson, S., Eds.; Butterworth-Heinemann: Stoneham, MA, 1992; pp 416.
- (34) Beamson, G.; Briggs, D. *High Resolution XPS of Organic Polymers: the Scienta ESCA300 Database*; Wiley: Chichester, West Sussex, England, 1992.
- (35) Odian, G. G. *Principles of Polymerization*, 4th ed.; Wiley: Hoboken, NJ, 2004.
- (36) Kumar, A. S.; Gupta, R. K. *Fundamentals of Polymers*; McGraw-Hill: New York, 1998.
- (37) Rodriguez, F. *Principles of Polymer Systems*, 4th ed.; Taylor & Francis: Washington, DC, 1996.
- (38) Barner-Kowollik, C.; Vana, P.; Davis, T. P. In *Handbook of Radical Polymerization*; Matyjaszewski, K., Davis, T. P., Eds.; Wiley: Hoboken, NJ, 2002; p 226.
- (39) Ungnade, H. E.; Ortega, I. *J. Am. Chem. Soc.* 1951, 73, 1564.
- (40) Rabek, J. F. *Polymer Photodegradation: Mechanisms and Experimental Methods*; Chapman & Hall: London, England, 1995.
- (41) Phillips, R. *Sources and Applications of Ultraviolet Radiation*; Academic Press: London, England, 1983.



CHAPTER SIX

INITIATED CHEMICAL VAPOR DEPOSITION OF POLY(METHYL METHACRYLATE) THIN FILMS

ABSTRACT

Initiated CVD (iCVD), a dry method, is able to produce poly(methyl methacrylate) (PMMA) thin films by utilizing a reactive gaseous mixture of the monomer methyl methacrylate and the initiator triethylamine. The deposition rate is 20 times faster with the use of the initiator. Fourier-transform infrared spectroscopy and X-ray photoelectron spectroscopy (XPS) show high structural resemblance between iCVD PMMA and conventional PMMA, and the degree of functionality retention increases with decreasing residence time in the vacuum chamber. XPS detection of nitrogen incorporation is consistent with the incorporation of the initiator into the polymer chains. Nuclear magnetic resonance spectroscopy on completely dissolved films shows that the tacticity of iCVD PMMA resembles that of conventional radically-polymerized PMMA. Altogether these observations support the hypothesis that, for iCVD PMMA, the polymerization is by a free-radical mechanism.

6.1 INTRODUCTION

Poly(methyl methacrylate) (PMMA) thin films are of great interest because of their wide variety of uses in coatings,^{1,2} membranes,¹⁻⁴ relative-humidity sensing,⁵ solid-state dye layers,⁶ gas and organic vapor sensing,^{4,7,8} dielectric sacrificial layers,^{1,2,9} electron-beam lithography,¹⁰⁻¹³ and photonic applications.^{6,14,15}

There are many advantages of using a dry process such as chemical vapor deposition (CVD) to produce polymer thin films. CVD avoids environmental concerns arising from solvent usage and allows films of nanoscale thicknesses with macroscale uniformity to be produced on substrates with complex geometries.¹⁶ Also, CVD can be used to coat nanoscale features, as there are no surface tension and non-uniform wetting effects typically associated with wet processes. Unlike spin-on deposition (SOD) or curing, CVD is a one-step, vacuum process, in which there are no solvents or volatiles involved. CVD can be used to deposit films of even insoluble materials. SOD, a physical process, is able to produce thin films from polymer solutions with full retention of functionalities such as pendant groups on polymer chains. Since the functions of a polymer are often defined by the nature of its functional group(s), it is important that CVD is also able to produce the same polymer with a high degree of functionality retention to make the process complementary to SOD. In this work, initiated CVD (iCVD) is explored as a method for achieving vapor-phase deposition of PMMA, from its monomer methyl methacrylate (MMA), with a high degree of retention of its pendant groups.

Recently, Mao and Gleason¹⁷ demonstrated the use of *tert*-butyl peroxide (TBPO) as an initiator for rapid polymer film vapor deposition from a related methacrylate monomer glycidyl methacrylate (GMA) in a vacuum chamber. In their iCVD work, low filament temperatures (180–250 °C) were sufficient because of the weakness of the peroxy bond in TBPO. iCVD, a subset of hot-filament chemical

vapor deposition (HFCVD), is a novel technique for depositing polymer and organosilicate glass (OSG) thin films. HFCVD is a one-step, solvent-free deposition technique by means of thermal decomposition of precursor gases. Thermal decomposition is achieved using resistively-heated filament wires, around which radical species are generated and then undergo or initiate polymerization reactions to form a film on a backside-cooled substrate. The cooled substrate promotes adsorption of the species necessary for film growth. HFCVD has been used to deposit poly(tetrafluoroethylene),¹⁸ polyoxymethylene,¹⁹ and poly(glycidyl methacrylate)¹⁷ (PGMA) thin films that are spectroscopically equivalent to their conventionally-polymerized counterparts. It has also been used to deposit OSG thin films composed of linear and cyclic siloxane repeat units.²⁰ iCVD differs from conventional HFCVD on one main count—an initiating species in addition to the monomer (or the building block species) is also introduced into the reactor. The use of initiators in iCVD has been shown to provide good compositional and rate control.^{17,21,22}

Free-radical polymerizations usually involve initiation, propagation, and termination. Initiation involves net generation of free radicals. In the case of conventional HFCVD, in which the monomer is the only ingredient, free radicals have to originate from the monomer. This origination requires a filament temperature sufficient to scission a particular bond in the monomer molecule. The introduction of an initiator that contains a weak bond relative to those present in the monomer allows initiation at a lower temperature and simultaneously enhances growth rate.^{17,21,22} Low filament temperatures promote selective chemistry by avoiding undesired chemical reactions such as the loss of pendant functional groups from the monomers and/or the polymers. No longer being initiation-limited by the generation of radicals from the monomer, the iCVD process allows control of molecular weight through adjustment of the monomer/initiator ratio.¹⁷

The initiator serves to provide a specific chemical group to start a chain to which multiple monomer units add spontaneously. Radicals are annihilated through termination. Both disproportionation and coupling reactions eliminate radicals and halt the addition of monomer units to the chains. The elimination of radicals avoids the presence of dangling-bond defects²³ in the resulting polymeric film.

The goal of this work is to use iCVD to produce linear PMMA without using solvents. Plasma-enhanced CVD (PECVD) is a well-established dry method for depositing a wide variety of polymer thin films. It is versatile because both saturated and unsaturated precursors, even those of low reactivity in bulk polymerizations, can be used.^{1,2,24,25} Although PECVD introduces cross-links, the degree of cross-linking can be controlled.²⁵ The electric discharge in PECVD can lead to loss of functionalities, but retention of pendant functional groups can be improved via pulsation of the plasma.²⁶ iCVD can be positioned as a complementary method to PECVD in depositing polymer thin films. In contrast to PECVD, there is no UV irradiation or ion bombardment in the iCVD process, so the resulting films have lower densities of dangling bonds and cross-links than films grown using plasma excitation.²⁷ The lack of cross-linking facilitates the characterization of iCVD films because they are readily soluble and thus can be characterized by solution-state nuclear magnetic resonance (NMR) spectroscopy and gel permeation chromatography.

This chapter reports the deposition of PMMA thin films using iCVD from MMA as a precursor. MMA, $\text{CH}_2=\text{C}(\text{CH}_3)\text{COOCH}_3$, is a vinyl ester containing five carbon and two oxygen atoms. Polymerization occurs via successive additions of monomer units across the vinyl bond. The resulting polymer chains therefore have the same carbon to oxygen atomic ratio (2.50) as the monomer. The effects of iCVD conditions on the retention of functionalities will be discussed. Films with high structural resemblance to conventional straight-chain PMMA can be produced.

This result positions iCVD as a novel vapor-phase technique that allows structural retention with little or no cross-linking.

6.2 EXPERIMENTAL METHODS

Depositions were performed in a custom-built vacuum chamber (Sharon Vacuum). The reactor was cylindrical with a height of 3.3 cm and a radius of 12 cm. The inlet of precursor gases and the exhaust were at opposite ends of the reactor. The top of the reactor was covered by a quartz plate (~15 cm radius and 2.5 cm thick), allowing visual inspection and laser interferometry. The chamber was equipped with a Nichrome filament array and a backside-cooled stage maintained at 25 °C. The Nichrome filaments (80% Ni/20% Cr, AWG 26, Omega Engineering), were resistively heated to approximately 550 °C, as measured by a thermocouple (Type K, AWG 36, Omega Engineering) directly attached to one of them. The clearance between the filaments and the stage was approximately 1.5 cm. Silicon wafers of 10 cm in diameter were used as substrates for the depositions. The pressure of the chamber was controlled by a throttling butterfly valve (Intellisys, Nor-Cal) connected to an auto-tuned proportional-integral-derivative digital controller (Intellisys, Nor-Cal). The pressure was measured using a capacitance diaphragm gauge (Nor-Cal) and was maintained at 9 Torr.

MMA (99.0%, Aldrich) and triethylamine (TEA, 99.5%, Aldrich) were used without further purification. MMA and TEA were volatilized in separate glass jars maintained at room temperature and were metered into the chamber through mass-flow controllers (1152C for MMA, 1479A for TEA, both MKS). Flow rates of 30 sccm and 9 sccm of MMA were used in two sets of experiments, in which the flow rate of TEA was kept constant at 1 sccm. The two species were thoroughly mixed in transfer lines before entering the chamber. Depositions were monitored

by measuring the reflectance of a 633-nm HeNe laser beam off the substrate (interferometry). The laser source and the detector were from JDS Uniphase and Metrologic, respectively.

Fourier-transform infrared (FTIR) measurements were performed on a Nicolet Nexus 870 ESP spectrometer in normal transmission mode using a DTGS KBr detector over the range of 400 to 4000 cm^{-1} at a 4- cm^{-1} resolution averaged over 64 scans. As a comparison, a PMMA standard (Alfa Aesar) was dissolved in tetrahydrofuran (THF), and the solution was cast onto a silicon wafer. XPS was done on a Kratos Axis Ultra spectrometer equipped with a monochromatized Al $K\alpha$ source. Room-temperature proton nuclear magnetic resonance (NMR) spectra were taken at 300 MHz using a Varian Unity 300 spectrometer. The iCVD polymer films were dissolved in deuterated chloroform (99.8% D, 0.03% (v/v) tetramethylsilane, Aldrich), and chemical shifts were determined by reference to the tetramethylsilane peak.

6.3 RESULTS AND DISCUSSION

In this work, attempts were made to use TBPO as an initiator for the polymerization of MMA using the same filament temperatures specified by Mao and Gleason. Films formed at a deposition pressure of 9 Torr but were volatile and did not survive a final reactor evacuation to below 100 mTorr at the end of the experiments. Even though no films were available for characterization, the hypothesis that the films were comprised of low molecular weight oligomers would account for the volatility. Solution-phase pulsed-laser polymerization experiments have shown that the rate of propagation of radical polymerization of MMA is approximately half of that of GMA radical polymerization.²⁸ Therefore, the propagation kinetics at the temperatures of the iCVD trials might not favor the

production of long PMMA chains. Increasing the filament temperature will increase the rate of propagation and enable long-chain PMMA to be made. Peroxide-type initiators, however, would not be suitable because of high conversions and additional undesirable reactions such as beta-scission at elevated temperatures. Use of such initiators would require very fine metering of flow rate, which is beyond the capability of the mass-flow controller in use. TEA was chosen as a potential initiator. TEA, like peroxides, also fragments into radicals when heated but only at substantially higher temperatures. It is split into a diethylamino radical and an ethyl radical at above 450 °C.²⁹ Depositions without TEA were attempted initially, but they were too slow (~1 nm/min) to yield sufficient materials for characterization in a reasonable time period. The addition of TEA to the process increased the deposition rate significantly to approximately 20 nm/min.

6.3.1 X-RAY PHOTOELECTRON SPECTROSCOPY

Figure 6-1 shows the X-ray photoelectron spectroscopy (XPS) survey scans of two iCVD samples, made using different flow rates of MMA. Both the low-flow and the high-flow samples contain nitrogen, as represented by the peak at approximately 402 eV. The atomic percent of nitrogen decreased from 5.54% to 0.87% as the MMA flow rate increased from 9 to 30 sccm while the TEA flow rate was fixed at 1 sccm. This decrease in atomic percent indicates that more MMA repeat units per nitrogen atom were incorporated when a higher MMA/TEA ratio was used. Both the incorporation of nitrogen and its trend, in addition to the increased rate in the presence of TEA, provide evidence that the dimethylamino radical was initiating the polymerization but do not preclude that the ethyl radical was doing the same. Assuming all the nitrogen is at the end groups of the chains, the molecular weights of the low-flow sample and the high-flow sample are

approximately 500 and 3300 g/mol. These numbers, however, should be used as a comparative measure instead of an absolute one. First, the calculation method does not take into account the possible initiating action of the ethyl radical nor does it consider other means of nitrogen incorporation due to side-group scission (to be discussed). It also does not account for the termination mechanism and the possible retention of free TEA. The atomic ratios between carbon and oxygen are 2.52 for the high-MMA-flow sample and 2.71 for the low-MMA-flow one. The large discrepancy between the ratio of the low-flow sample and the ideal ratio (2.50) indicates that the ester functional group or part thereof most likely was lost due longer exposure to the high filament temperature. It has been reported^{30,31} that, at elevated temperatures, the C–C bond connecting the ester group to the α -carbon is prone to breakage. Such events would increase the carbon/oxygen ratio, consistent with the XPS measurements. This problem was not manifested in the high-flow sample, most likely due to the shorter residence time (11 s) of species in the chamber compared to 33 s for the low-flow sample.

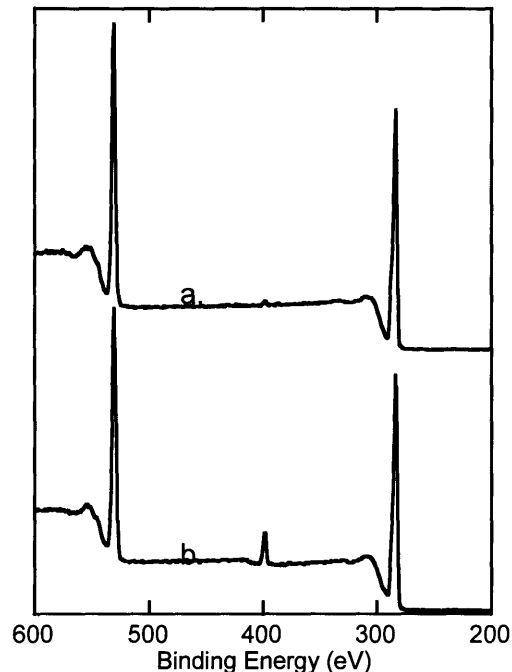


Figure 6-1. XPS survey scans of a) film deposited from 30 sccm MMA and b) film deposited from 9 sccm MMA. The peaks at 531 eV, 402 eV, and 287 eV correspond to O 1s, N 1s, and C 1s photoelectrons, respectively. The ratios between the carbon and the oxygen atoms are 2.52 and 2.71 for Samples a) and b), respectively. The ideal ratio for standard PMMA is 2.50.

Figure 6-2 shows the C 1s and the O 1s high-resolution XPS scans of the samples. The high-flow sample contains four different carbon moieties and two different oxygen moieties, consistent with the structure of PMMA. Table 6-1 shows excellent agreement of both the binding energies and peak area ratios of the high-flow sample with the previously-reported results for solution-polymerization PMMA.³² The low-flow sample, however, contains more than five different carbon moieties and more than two different oxygen moieties. Specifically, in the C 1s spectrum, there is one extra peak at 287.84 eV, corresponding to the presence of the O-C-O or the C=O carbon moiety. This result is in accordance with the existence of Peak 2 at 533.19 eV in the O 1s spectrum, which is also a proof of the presence of the particular moiety. The scission of the OC-O bond within the ester group would explain the dramatic imbalance between Peaks 1 (the methoxy

oxygen) and 2 (the carbonyl oxygen) and the presence of Peak 3 in the O 1s spectrum. This scission would also increase the carbon/oxygen ratio. Peak X in the O 1s spectrum, having a low binding energy, is likely due to the presence of the N–(C=O) moiety. Such a moiety can arise from the coupling between a diethylamino radical and a carbonyl radical, formed from the scission of the OC–O bond.

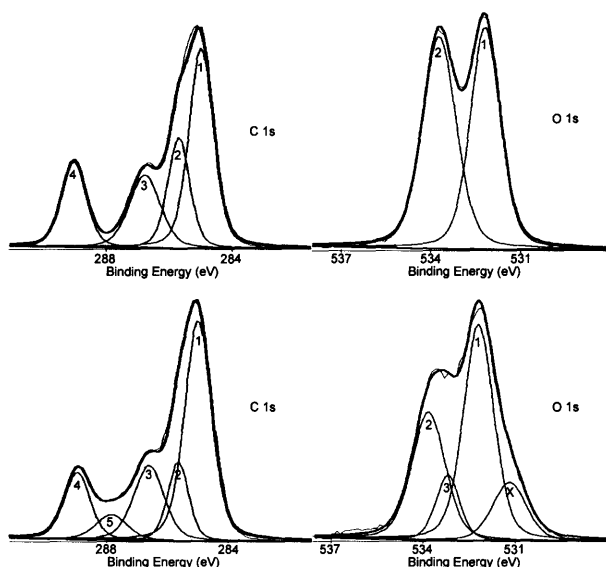


Figure 6-2. High-resolution C 1s (left) and O 1s (right) XPS scans of iCVD films. The spectra on the top are from the 30-sccm sample; those on the bottom are from the 9-sccm sample. Peak X in the bottom right spectrum is likely due to the presence of the N–C=O moiety.

Table 6-1. High-resolution XPS scan data of the PMMA film deposited from iCVD.

Core/level	Peak	Origin	HFCVD film		PMMA reference ^[32]	
			Binding energy (eV)	Area (%)	Binding energy (eV)	Area (%)
C 1s	1	–C*H ₃ , –C–C*H ₂ –C–	285.00	42	285.00	42
	2	–C*(CH ₃)–CO–	285.72	19	285.72	21
	3	–OC*H ₃	286.79	21	286.79	21
	4	–C*=O	289.03	18	289.03	16
O 1s	1	–C=O*	532.20	48	532.21	51
	2	–O*CH ₃	533.73	52	533.77	49

6.3.2 FOURIER–TRANSFORM INFRARED SPECTROSCOPY

Figure 6–3 shows the FTIR spectra of the PMMA standard obtained from Alfa Aesar, the high–flow sample, and the low–flow sample. Table 6–2 lists the major peak assignments from the literature.³³ Both the low– and the high–flow samples show C–H stretching, C=O stretching, C–H bending, and C–O stretching, characteristic of PMMA. As seen in Figure 6–3, the C=O intensity relative to the C–H intensity is approximately the same among all three spectra, indicating conservation of the carbonyl group. The low–flow sample, however, has an extra peak at approximately 1560 cm⁻¹ (Figure 6–3c). This peak could arise from the rupture of the bond between the polymer backbone and the carbonyl carbon (as discussed in Section 6.3.1) and the subsequent formation of a conjugated C=C system. Holland and Hay³¹ analyzed the decomposition of PMMA and suggested that elimination of the methoxycarbonyl side group (–COOCH₃) occurred during decomposition, creating an unsaturated conjugated system. Such a conjugated system absorbs at a lower wavenumber (~1550 cm⁻¹)³¹ than an unconjugated one (normally 1680–1620 cm⁻¹).^{31,34,35} The presence of the peak at 1560 cm⁻¹ in Figure 6–3c is most likely due to side–group elimination from PMMA chains in the gas phase. The XPS results support this argument, as such an elimination would certainly increase the carbon/oxygen ratio. The high–flow sample has very little C=C incorporation as seen from Figure 6–3b, as the shorter residence time reduced side–group elimination. Apart from having the extra peak, the low–flow sample also shows broadening in the C=O stretching, C–H bending, and C–O stretching regions. Such increases in line widths of FTIR peaks are indicative of a loss of homogeneity in bonding environments,³⁶ which is also a consequence of loss of functional groups. For the high–flow sample, retention of the α -methyl and the ester functionalities is evident through inspection of the C–H stretching and the

C–H bending regions. As seen in Figure 6–4, the high–flow sample and the standard have the same pattern in the C–H stretching region, within which the characteristic modes at 2995, 2948, 2920 (shoulder), and 2835 cm^{-1} were resolved. Similarly, in the C–H bending region shown in the same figure, the high–flow sample and the standard also have the same pattern; the characteristic modes at 1483, 1465 (shoulder), 1452, 1438, and 1388 cm^{-1} were resolved. It can also be seen in Figure 6–3 that, in the C–O stretching region, characteristic peaks at 1270 and 1240 cm^{-1} were resolved. Based on these detailed FTIR analyses, the retention of the functional groups is clearly evident in the high–flow sample. Compared to plasma films deposited from MMA^{6,8,11,12,37–39} based on FTIR results, the high–flow iCVD sample in this work exemplifies much more structural resemblance to conventional PMMA than the plasma samples. FTIR studies of plasma films have shown broadened peaks,^{8,11,38} diminished C=O peaks,^{8,39} and weakened C–O and C–H peaks.⁸

Table 6-2. FTIR assignments from the literature.³³

Wavenumber [cm ⁻¹]	Relative intensity	Assignment
2995	medium	$\nu_a(\text{CH}_3\text{-O}) + \nu_a(\text{CH}_2)$
2948	medium	$\nu_s(\text{CH}_3\text{-O}) + \nu_a(\alpha\text{-CH}_3)$ $+ \nu_s(\alpha\text{-CH}_3) + \nu_s(\text{CH}_2)$
2920	shoulder	combination band
2835	very weak	associated with CH ₃ -O
1730	very strong	$\nu(\text{C=O})$
1483	medium	$\delta_a(\alpha\text{-CH}_3)$
1465	shoulder	$\delta_a(\text{CH}_3\text{-O})$
1452	strong	$\delta(\text{CH}_2)$
1438	strong	$\delta_s(\text{CH}_3\text{-O})$
1388	medium	$\delta_a(\alpha\text{-CH}_3)$
1370	weak shoulder	$\delta_a(\alpha\text{-CH}_3)$ (amorphous)
1270	strong	$\nu_a(\text{C-C-O})$ coupled with
1240	strong	$\nu(\text{C-O})$
1190	very strong	internal C-H deformation vibration coupled with
1150	very strong	skeletal stretching
1063	weak	intramolecular interaction

ν_a - asymmetric stretching

ν_s - symmetric stretching

ν - stretching

δ_a - asymmetric bending

δ_s - symmetric bending

δ - bending

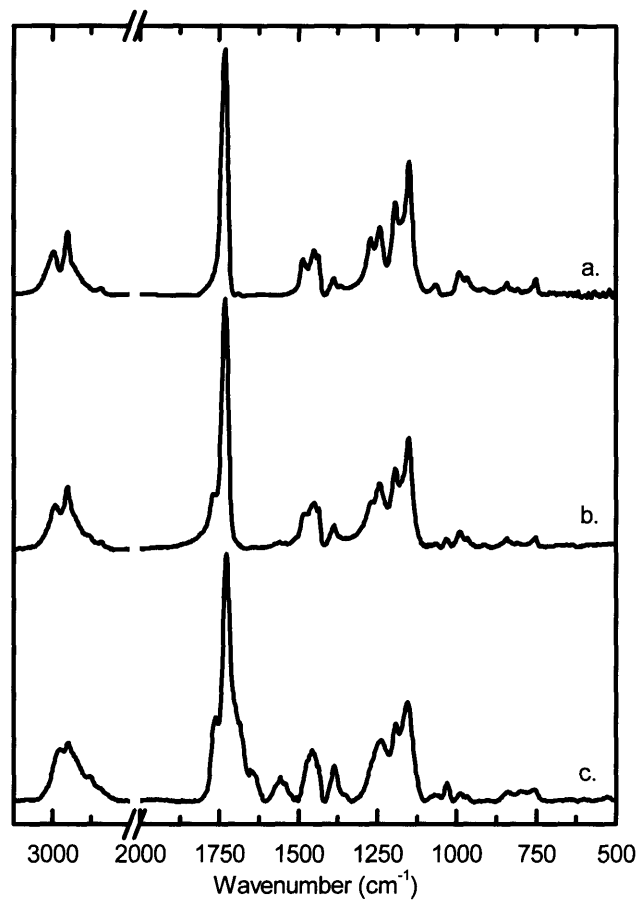


Figure 6-3. FTIR spectra of a) PMMA standard obtained from Alfa Aesar, b) iCVD film deposited from 30 sccm MMA, and c) iCVD film deposited from 9 sccm MMA.

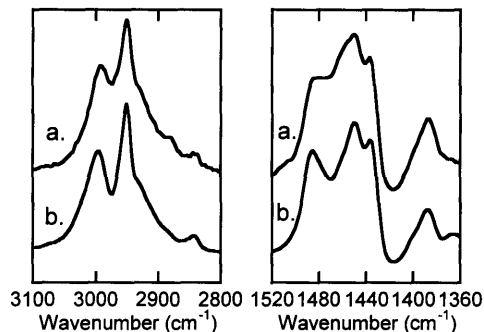


Figure 6-4. Details of the C–H stretching (left) and the C–H bending (right) regions showing the structural similarity between a) the 30-sccm iCVD sample and b) the standard.

6.3.3 PROTON NUCLEAR MAGNETIC RESONANCE SPECTROSCOPY

Proton nuclear magnetic resonance (NMR) measurements were performed only for the high-flow sample because XPS and FTIR results showed that it bore structural resemblance to conventional PMMA, as the main objective of this work was to create a thin-film polymer that was as similar to traditional PMMA as possible. The high degree of solubility of the iCVD PMMA films in chloroform-*d* (CDCl₃) for ¹H NMR precludes that they are cross-linked to any significant degree. The iCVD films are also completely soluble in acetone and tetrahydrofuran. This observation affirms iCVD's ability in producing linear polymer chains.

Table 6-3 lists the literature assignments of the chemical shifts.⁴⁰ There are three regimes: the α -methyl protons, the β -methylene protons, and the ester methyl protons. Figure 6-5 shows the NMR spectrum of the high-flow sample. The strong, sharp peak at approximately 3.6 ppm clearly indicates the presence of the ester methyl protons and thus the retention of the ester group. The strong peaks upfield (below 1.5 ppm) also signify the presence of the α -methyl protons and thus the retention of the α -methyl functional group. The complexity of the spectrum rules out the possibility that the sample is isotactic or syndiotactic; isotactic samples have only two doublets⁴¹⁻⁴³ and syndiotactic samples have only a

singlet for the β -methylene protons.⁴¹ In the iCVD spectrum (inset in Figure 6-5), the β -methylene proton signals were resolved into multiple groups assigned to *mmr*, *rmr*, *mrm*, *mrr*, and *rrr* pentads,^{41,44} respectively, from lower magnetic field. Multiple α -methyl proton peaks also indicate that the iCVD sample is atactic; three groups of α -methyl proton signals were resolved and are assigned to *mm*, *mr*, and *rr* triads,^{41,44} respectively, from lower magnetic field. Isotactic and syndiotactic PMMA have only a single α -methyl proton peak.^{41,42} It is evident from the relative intensities of the peaks within each of the regimes that the sample is comprised of mostly *rrr* pentads and *rr* triads, which means that the sample is atactic but with more racemo (*r*) than meso (*m*) diads. This interpretation is in accordance with the hypothesis that free-radical polymerization occurred in the iCVD process, as free-radical polymerization tends to produce atactic chains with a predominantly syndiotactic signature.^{41,42} Using the areas under the α -methyl proton peaks, the tacticity was calculated to be 62.7% *rr*, 31.4% *mr*, and 5.8% *mm* (signal-to-noise ratio is ~300 with respect to the weakest peak). These numbers are close to the values reported in the literature for radically-prepared PMMA samples,⁴¹ whose *rr* contents are in the range of 60–63%. In addition, resemblance of the spectrum in Figure 6-5 to those of PMMA samples prepared using organolanthanide complexes as catalysts,⁴⁵ which produced atactic chains with approximately 60% *rr* triads, supports the tacticity argument and thus the free-radical nature of the iCVD process.

Table 6-3. Literature assignments of PMMA proton peaks.⁴⁰

δ [ppm]	Proton assignment
3.625	OCH ₃
1.45–2.11	H _{β}
1.23–0.935	α -CH ₃

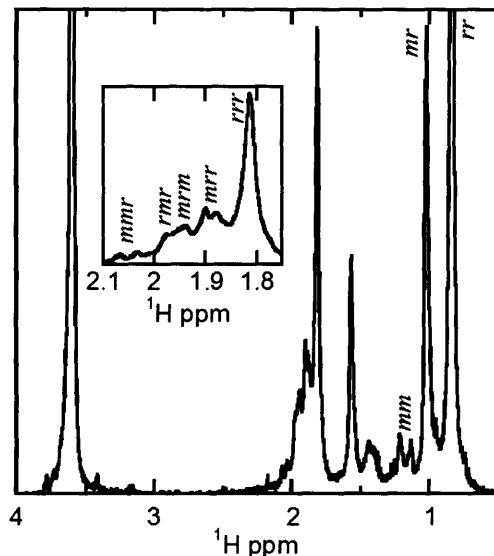


Figure 6–5. NMR spectrum of iCVD PMMA deposited from 30 sccm MMA. The inset details the β -methylene proton region. The peak assignments are based on those from the literature.^{39,42}

6.4 CONCLUSIONS

This work demonstrates that iCVD can be used to deposit PMMA by feeding a mixture of the initiator TEA and the vinyl monomer MMA into a vacuum chamber containing heated filament wires and a substrate maintained at room temperature. The iCVD method avoids the use of solvents and prevents cross-linking typically associated with PECVD.²⁵

Higher growth rates can be achieved in the presence of the initiator (~20 nm/min) compared to rates of approximately 1 nm/min achievable with the monomer alone. The rate enhancement of 20 times due to the initiator supports the hypothesis of a free-radical mechanism and motivates the technological application of the iCVD method.

The high structural resemblance of iCVD PMMA to conventional linear PMMA is evident in the FTIR, XPS, NMR, and solubility test results. The C–H stretching, C=O stretching, C–H bending, and C–O stretching modes were clearly resolved in

the FTIR spectrum, in which details within each of the regions further confirm structural resemblance. XPS survey scan shows a carbon/oxygen atomic ratio of 2.52, compared to the ideal value of 2.50, and the high-resolution scans show four carbon and two oxygen moieties of which all have binding energies and area percentages close to those in the literature for conventional PMMA. NMR spectroscopy identified all the protons expected for PMMA. All these spectroscopic results in addition to the solubility test results confirm that the iCVD process is capable of producing linear PMMA without significant cross-linking.

The tacticity analysis based on the NMR results provides strong evidence that the polymerization undergoes a free-radical mechanism. The percentages of *rr*, *mr*, and *mm* diads compare closely to those reported in the literature for radically-prepared polymer samples.

The difference between using TEA and TBPO as the initiator proves in this case that the filament temperature is important for the propagation kinetics as well as the breakdown of the initiator. A low filament temperature would be sufficient for the scission of the peroxy bond but not so for the propagation reaction. A high filament temperature is therefore necessary owing to the intrinsic propagation kinetics of the monomer. TBPO, however, needs to be replaced with TEA, which fragments at a higher temperature, to avoid excess breakdown of the initiator. This result demonstrates the need to match the optimal thermal decomposition range initiator to that for the rapid propagation of the monomer.

The loss of functionality in the low-flow sample shows the need of avoidance long exposure times to high filament temperatures. If indeed a monomer would propagate fast enough to produce long chains at low filament temperatures, such temperatures should be used and the initiator should be chosen accordingly. In the case of MMA, lowering filament temperature is not an option, but the loss of functionality can be countered by using a shorter residence time, which reduces

exposure of species in the gas phase to the heat from the filament wires. As indicated by the spectroscopy results, iCVD with a reduced residence time is able to produce films with better structural retention than PECVD.

This work will assist the choice of filament temperatures and the corresponding initiators for the iCVD of other vinyl monomers. The difference in the rates of propagation of MMA and GMA in bulk phase guided the use of a high filament temperature. The filament temperatures required for other monomers may therefore be estimated using a similar approach with bulk-phase kinetic data. This work has shown that iCVD, a dry process, is able to produce thin films with high structural resemblance to conventional, linear PMMA.

REFERENCES

- (1) Yasuda, H., Plasma Polymerization. In Academic: Orlando, FL, 1985.
- (2) Hollahan, J. R.; Bell, A. T., Techniques and Applications of Plasma Chemistry. In Wiley: New York, 1974.
- (3) Kramer, P. W.; Yeh, Y. S.; Yasuda, H. *J. Membr. Sci.* 1989, 46, 1.
- (4) Russell, S. P.; Weinkauf, D. H. *Polymer* 2001, 42, 2827.
- (5) Ralston, A. R. K.; Tobin, J. A.; Bajikar, S. S.; Denton, D. D. *Sens. Actuator B-Chem.* 1994, 22, 139.
- (6) Li, G. F.; Tobin, J. A.; Denton, D. D. *Appl. Phys. Lett.* 1993, 62, 1582.
- (7) Capan, R.; Ray, A. K.; Hassan, A. K.; Tanrisever, T. *J. Phys. D-Appl. Phys.* 2003, 36, 1115.
- (8) Zhang, C.; Wyatt, J.; Weinkauf, D. H. *Polymer* 2004, 45, 7665.
- (9) Teh, W. H.; Liang, C. T.; Graham, M.; Smith, C. G. *J. Microelectromech. Syst.* 2003, 12, 641.
- (10) Tamano, J.; Hattori, S.; Morita, S.; Yoneda, K. *Plasma Chem. Plasma Proc.* 1981, 1, 261.
- (11) Morita, S.; Tamano, J.; Hattori, S.; Ieda, M. *J. Appl. Phys.* 1980, 51, 3938.
- (12) Yamada, M.; Tamano, J.; Yoneda, K.; Morita, S.; Hattori, S. *Jpn. J. Appl. Phys. Part 1 - Regul. Pap. Short Notes Rev. Pap.* 1982, 21, 768.
- (13) Martinu, L.; Biederman, H. *Vacuum* 1983, 33, 253.
- (14) Tobin, J. A.; Denton, D. D. *Appl. Phys. Lett.* 1992, 60, 2595.
- (15) Zhao, Y.; Wang, F.; Cui, Z. C.; Zheng, J.; Zhang, H. M.; Zhang, D. M.; Liu, S. Y.; Yi, M. B. *Microelectron. J.* 2004, 35, 605.
- (16) Pierson, H. O. *Handbook of Chemical Vapor Deposition*, 2nd ed.; Noyes Publications: Norwich, NY, 1999.
- (17) Mao, Y.; Gleason, K. K. *Langmuir* 2004, 20, 2484.
- (18) Lau, K. K. S.; Gleason, K. K. *J. Fluor. Chem.* 2000, 104, 119.
- (19) Loo, L. S.; Gleason, K. K. *Electrochem. Solid State Lett.* 2001, 4, G81.
- (20) Pryce Lewis, H. G.; Casserly, T. B.; Gleason, K. K. *J. Electrochem. Soc.* 2001, 148, F212.
- (21) Pryce Lewis, H. G.; Caulfield, J. A.; Gleason, K. K. *Langmuir* 2001, 17, 7652.
- (22) Murthy, S. K.; Olsen, B. D.; Gleason, K. K. *Langmuir* 2002, 18, 6424.
- (23) Limb, S. J.; Labelle, C. B.; Gleason, K. K.; Edell, D. J.; Gleason, E. F. *Appl. Phys. Lett.* 1996, 68, 2810.
- (24) Inagaki, N., Plasma Surface Modification and Plasma Polymerization. In Technomic: Lancaster, PA, 1996.

- (25) Morosoff, N. In *Plasma Deposition, Treatment, and Etching of Polymers*; d'Agostino, R., Ed. Academic Press: Boston, MA, 1990; pp xiii.
- (26) Burkey, D. D.; Gleason, K. K. *Chem. Vapor Deposition* 2003, 9, 65.
- (27) Limb, S. J.; Lau, K. K. S.; Edell, D. J.; Gleason, E. F.; Gleason, K. K. *Plasmas Polym.* 1999, 4, 21.
- (28) Beuermann, S.; Buback, M.; Davis, T. P.; Garcia, N.; Gilbert, R. G.; Hutchinson, R. A.; Kajiwara, A.; Kamachi, M.; Lacik, I.; Russell, G. T. *Macromol. Chem. Phys.* 2003, 204, 1338.
- (29) Taylor, H. A.; Juterbock, E. E. *J. Phys. Chem.* 1935, 39, 1103.
- (30) Manring, L. E. *Macromolecules* 1991, 24, 3304.
- (31) Holland, B. J.; Hay, J. N. *Polymer* 2001, 42, 4825.
- (32) Beamson, G.; Briggs, D., High Resolution XPS of Organic Polymers: the Scienta ESCA300 Database. In Wiley: Chichester, West Sussex, England, 1992; p 295 p.
- (33) Nagai, H. *J. Appl. Polym. Sci.* 1963, 7, 1697.
- (34) Lin-Vien, D.; Colthup, N. B.; Fateley, W. G.; Grasselli, J. G., The Handbook of Infrared and Raman Characteristic Frequencies of Organic Molecules. In Academic Press: San Diego, CA, 1991; pp xvi.
- (35) Pretsch, E.; Bühlmann, P.; Affolter, C. *Structure Determination of Organic Compounds: Tables of Spectral Data*, 3rd ed.; Springer-Verlag: Berlin, 2000; p xv.
- (36) Cox, J. N. In *Encyclopedia of Materials Characterization: Surfaces, Interfaces, Thin Films*; Brundle, C. R., Evans, C. A., Wilson, S., Eds.; Butterworth-Heinemann: Stoneham, MA, 1992; pp 416.
- (37) Pan, Y. V.; Barrios, E. Z.; Denton, D. D. *J. Polym. Sci. Pol. Chem.* 1998, 36, 587.
- (38) Pan, Y. V.; Barrios, E. Z.; Denton, D. D. *Appl. Phys. Lett.* 1996, 68, 3386.
- (39) Jeon, H. S.; Wyatt, J.; Harper-Nixon, D.; Weinkauff, D. H. *J. Polym. Sci., Part B: Polym. Phys.* 2004, 42, 2522.
- (40) Pham, Q. T.; Pétiard, R. *Proton and Carbon NMR Spectra of Polymers*, 5th ed.; John Wiley & Sons: Chichester, West Sussex, England, 2003.
- (41) Hatada, K.; Kitayama, T., NMR Spectroscopy of Polymers. In Springer-Verlag: Berlin, 2004.
- (42) McCord, E. F.; Anton, W. L.; Wilczek, L.; Ittel, S. D.; Nelson, L. T. J.; Raffell, K. D.; Hansen, J. E.; Berge, C. *Macromol. Symp.* 1994, 86, 47.
- (43) Ramey, K. C. *J. Polym. Sci., Polym. Lett.* 1967, 5, 859.
- (44) Bovey, F. A., High Resolution NMR of Macromolecules. In Academic Press: New York, 1972.

(45) Bala, M. D.; Huang, J. L.; Zhang, H.; Qian, Y. L.; Sun, J. Q.; Liang, C. F. *J. Organomet. Chem.* 2002, 647, 105.



CHAPTER SEVEN

CONCLUSIONS & FUTURE DIRECTIONS

7.1 CONCLUSIONS

The first three technical chapters represent the core of this thesis. CHAPTERS TWO and THREE demonstrate the uniqueness of initiated CVD (iCVD) in making application-specific polymeric thin films. They do not only contain structural and physical characterizations but also demonstrate the applications of the thin films. The ability to synthesize such films with well-defined structural and physical properties in one step differentiates iCVD from spin-on deposition (SOD) and plasma-enhanced CVD (PECVD). It would be difficult, if not impossible, to achieve the same results in one step using SOD and PECVD. iCVD is the only chemical vapor deposition (CVD) technique that offers systematic control of film composition on the molecular level. Yet, this systematic control is easily implemented with flow-rate manipulation. CHAPTER FOUR shows that iCVD is analogous to bulk- and solution-phase polymerization processes with the exception that iCVD polymerization occurs on the surface with adsorbed monomers. This surface mechanism allows tuning of film composition with control of partial pressures of species in the chamber, corroborating the results from CHAPTER TWO. iCVD, however, is by no means limited to a two-component system and can be extended to making films composed of three or more monomers, based on the results in these first few chapters.

CHAPTER FIVE brings iCVD to a new level by introducing a novel combination of UV irradiation and a volatile photoinitiator. This method, photo-initiated CVD (piCVD), eliminates the need of a filament array, simplifying chamber design. piCVD can be used in place of iCVD when the use of a filament array is inconvenient. Complex geometries can be coated evenly with the use of UV irradiation of uniform intensity. This work also shows that iCVD is not limited to

using heat as the energy source and that radical generation can be separately engineered to achieve thin-film deposition.

iCVD is a powerful yet easy-to-use tool for depositing polymeric thin films. The engineering of an application-specific polymeric thin film starts from its target application. The application dictates the selection of monomer(s), while the choice of the initiation system is at the convenience of the engineer. With iCVD, film composition, growth rate, and molecular weight can all be controlled, as demonstrated in this thesis work. Fine tuning of microscopic properties allows optimization of macroscopic properties, leading to films not only suited for their target applications but with maximum performances.

7.2 FUTURE DIRECTIONS

The author believes that no research is ever complete. Things can always get better, no matter what. This statement is certainly true for iCVD, which has only experienced its initial success.

The goal of future iCVD research is to convince people that iCVD can replace existing methods and will perform better. The author believes that this goal can drive future researchers to produce a wider spectrum of application-specific polymers and to refine the process and its equipment. Demonstration of applicability in a larger interest would be a start toward the goal. For instance, the iCVD of hydrogels can be used to coat drug particles to accomplish controlled release for advanced drug delivery. The coatings can be made to have a graded degree of cross-linking to achieve zeroth-order delivery. On the other hand, the actual integration of the sacrificial material into integrated-circuit fabrication would demonstrate its real applicability to make low-k air gaps. In addition, with proper

photomasks, microfluidic channels, bragg mirrors, and microelectromechanical systems can be fabricated using the iCVD sacrificial polymer.

For piCVD, masked deposition should be feasible based on author's experience with the method, although the author has not collected sufficient evidence to prove so scientifically.

Further studies on the kinetics and the mechanism of iCVD would warrant better understanding of the process. This thesis has documented five monomers (three monofunctional and two difunctional), but there are many more others that may potentially be used in iCVD. As CHAPTER FOUR has projected, the rate constants of propagation, k_p , and termination, k_t , and the surface monomer concentration, $[M]$, are crucial parameters. The parameter k_p^2/k_t is the important parameter in determining viability, although termination kinetic data are not readily available for most monomers. Monomers that have bulky pendant groups, a signature of slow termination kinetics, tend to have more success in iCVD. Determination of k_p^2/k_t for a number of monomers and comparing these values to existing data in the literature would suggest if literature data are applicable to iCVD. If so, one would be able to predict *a priori* the viability of a particular monomer. Determination of k_p^2/k_t can be performed by fixing all parameters in Equations 4-5 and 4-6, including surface concentration. In order to keep the surface concentrations the same for different monomers, one must know the relationship between surface concentration and monomer partial pressure, which can be determined using the quartz-crystal microbalance. Measurements of deposition rates and molecular weights would be an indication of the quantity k_p^2/k_t . The flux of radicals can be calculated by computing the number of chains formed per a certain period of time, assuming a certain termination mechanism. In addition, reactivity-ratio study for a copolymer system based on surface concentrations would serve as a groundwork for modeling film composition and a

comparison to bulk-/solution-phase results. Such a comparison would suggest if direct use of kinetic data from traditional system for iCVD is acceptable.

The terminating action of the initiating radicals should also be investigated. Primary termination occurs when the chains are terminated by initiating radicals. This mode of termination occurs when there is a high concentration of initiating radicals or when chain-chain termination is difficult (e.g., chain mobility on surface is low for chains to come together). The rate and molecular-weight expressions in CHAPTER FOUR would have to be modified to account for primary termination. When primary termination occurs, increasing the number of radicals decreases the rate of polymerization, which is currently not reflected in CHAPTER FOUR. Sterically-hindered radical centers should have more difficulty terminating chains. The rate and molecular weight therefore are not functions of only the number of radicals but also the structure of the radicals.